THE UNIVERSITY OF CHICAGO

RATIONAL DESIGN AND SYNTHESIS OF VACCINE ADJUVANTS USING A COMBINATORIAL APPROACH: MULTI-PRR TRI-AGONISTS AND IMMUNOSTIMULANT-IMMUNOMODULATOR CONJUGATES

A DISSERTATION SUBMITTED TO

THE FACULTY OF THE PRITZKER SCHOOL OF MOLECULAR ENGINEERING

IN CANDIDACY FOR THE DEGREE OF

DOCTOR OF PHILOSOPHY

BY

NAOREM NIHESH

CHICAGO, ILLINOIS

JUNE 2022

This is dedicated to family and friends.

Table of Contents

List of Figures

List of Schemes

Acknowledgments

Over the past five years, my life has been made easier by the support of a small group of people. This includes my friends Teerath, Sangeeth, and Bushra, who have always been there to lend their ears and support when I have felt the lowest. My co-workers Jainu, Jorge, Britteny, and Jun, have been my fun and work partners. Without you all, graduate school would have been incredibly lonely. I am excited to see where your roads take you next.

To my sisters, Nidhi and Emila, thank you for never letting me feel guilty about leaving home. To my parents, who never expected me to do anything other than what I have always wanted, thank you for your trust and the responsibility.

I am also grateful to Dr. Saikat Manna and Dr. Flora Kimani for guiding me during my early graduate school days. Finally, I would like to thank my advisor Dr. Aaron Esser-Kahn who gave me the freedom to explore various exciting questions at the interface of chemistry and immunology. He has provided me with valuable insights at every step of my research.

Abstract

The research discussed here enables vaccinologists to choose from a large panel of adjuvants and formulate them in combinations that act cooperatively, resulting in optimal protection. We have developed adjuvants, rationally designed based on the current understanding of the immune response, particularly the molecular mechanism of the innate immune response.

The term adjuvant is often interchangeable with immunostimulant. Whereas immunostimulants are generally single compounds with intrinsic immunogenicity, adjuvants can be a mixture of different components. These components can have different functions and activities, including carrier or targeting functions and immunostimulant and immunomodulatory properties. The current challenge facing adjuvant development is finding the optimal combination of the different components that act synergistically and induce the desired immune response. Recent advances in biochemical tools have enabled us to design and develop such adjuvants. This study explores two new ways of designing and developing adjuvants. First, we demonstrate that combining multiple PRR ligands (three) into a single molecule using chemical conjugation amplified the immune response compared to the soluble mixture of ligands. Secondly, we showed that incorporating immunomodulators and immunostimulants into the same molecular scaffold improves the molecule's safety profile and the protection it affords.

1. Introduction

1.1 Adjuvant

Vaccine adjuvants are components that can increase and modulate an antigen's intrinsic immunogenicity, leading to the enhancement of the magnitude, breadth, and longevity of the immune response. The term adjuvant means to help. Vaccines, mainly subunit vaccines, need help as these have a more defined composition which results in lower immunogenicity than whole-cell or virus-based vaccines. Therefore, adjuvants are used to induce potent and durable immune responses, with the added benefit that a lesser dose of antigens is needed. Moreover, vaccine often requires the generation of strong cellular responses (T cell response) and antibodies. Aluminum salts, the most used adjuvants in human vaccines, predominantly induce antibody responses. Hence, for vaccines requiring a cell-mediated response, new adjuvants need to be developed. [1,2] Many licensed adjuvants other than alum, such as MF59, AS01, AS04, AS03, and CpG 1018, have given rise to potent and valuable vaccines. However, we do not entirely understand the molecular mechanism of these adjuvants. Hence, there is a need to develop a new generation of more focused adjuvants, that are rationally designed based on the recent developments made by researchers in innate immunity. Such adjuvants will induce a safe and durable protective immune response.

1.2 Pattern recognition receptors as molecular targets of adjuvants

Pattern recognition receptors are found on immune cells called antigen-presenting cells (APCs). The function of Pattern recognition receptors (PRRs) is to recognize pathogen-associated molecular patterns (PAMPs) in microorganisms.[3–5] This activates the APCs which then stimulate T and B cells.[6–8] Toll-like receptors (TLRs), retinoic acid-inducible gene I (RIG-I))[9], stimulator of interferon genes (STING) protein)[10], C-type lectins[11], nucleotide-binding oligomerization domain

(NOD)-like receptors (NLRs)[12,13] are some of the PRRs that impact adaptive immunity. Researchers are currently investigating the molecules that target these receptors as potential vaccine adjuvants[14].

The innate immune system is the first line of defense against invasion by pathogens. It provides early, non-specific inflammatory signals which act as a cue for the adaptive immune response to develop. Moreover, it is now understood that the magnitude and quality of the adaptive immune response mainly depend on the initial microbial signals sensed by innate immune cells following infection or vaccination. For instance, T_H1-cell polarization and subsequent interferon (IFN)-γ expression by T cells is driven by the secretion of pro-inflammatory cytokine interleukin (IL)-12 [15]. The secretion of IL-4, IL-5, and IL-6 is characteristic of T_H2 response, which provides B-cell help[16].

Toll-like receptors are transmembrane proteins expressed on the surface (TLR1, TLR2, TLR4, TLR5, and TLR6) or in the endosomes (TLR3, TLR7, TLR8, and TLR9) of different antigen-presenting cells (APC)[17,18]. They sense bacterial, viral, fungal, or protozoan signals. Which TLR or combination of TLRs gets activated determines the nature of the adaptive response. This activation of a single TLR or multiple TLRs can shift the balance towards T_H1 or T_H2 cells[19,20]. TLRs also play a crucial role in antigen presentation. For optimal antigen presentation, it is required that both antigen and TLR are colocalized in the same cellular compartment. By controlling the generation of ligands for T cell receptors, TLRs ensure that the microbial antigens are preferentially presented to T cells by the activated APC.[21, 22]

Additionally, direct TLR stimulation has been shown to be a requirement for the complete activation of B- cells [23,24]. Also, TLR stimulation regulates Treg activity. This occurs either directly through TLR activation on Treg cells or indirectly through APC–Treg interactions.[25-29]. This

indicates that TLR activation not only induces inflammatory responses but also regulates these responses by triggering the expansion of Treg cells. Finally, it has been demonstrated that TLR recognition is essential for the generation of memory CD4+ T cells but not for their activation[30]. These fundamental discoveries have been translated into practical applications in adjuvant research.

TLRs sense extracellular pathogens and cytosolic counterparts such as NODs, NLRs, RLRs, and STING, sense cytosolic bacteria and viruses, respectively[31]. NOD1 and NOD2 recognize bacterial peptidoglycans substructures.[32-34] NLRs sense danger-related signals such as uric acid crystals[31]. RLR proteins like retinoic acid-inducible gene I (RIG-I) and melanoma-differentiation-associated gene 5 (MDA5) sense viral invasion. RIG-I responds to RNA viruses, whereas MDA5 detects picornaviruses[35]. Cytosolic DNA from microbes also induces the expression of type I interferons (IFNs). Cytosolic protein, stimulator of interferon genes (STING), regulates the production of IFNs[36]. Intracellular cytosolic self-DNA or microbial DNA generates cyclic dinucleotides (CDNs) which start the STING pathway. The importance of STING signaling in the immune system is clearly illustrated by numerous strategies developed by pathogens to stop STING function[37]. C-type lectin receptors (CLRs) and scavenger receptors are extracellular receptors like TLRs, which are involved in pathogen capture and recognition. Scavenger receptors internalize pathogens and apoptotic cells by binding polyanionic ligands and modified low-density lipoproteins[38]. CLRs, like mannose receptors, interact with pathogens by binding sugar moieties such as mannose on the microbes[39].

1.3 Innate immune stimulation and crosstalk

Different PRR agonists stimulate the innate immune response in a synergistic manner and balance each other's immunostimulatory activity[40]. Combinations such as TLR2–TLR4[41], TLR3–TLR4–TLR7/8[42], TLR4–TLR7/8, TLR4–TLR9, or TLR3–TLR7/8[43] are known to show synergy. Some of these combinations (TLR4–TLR7/8, TLR4–TLR9, or TLR3–TLR7/8) increased the expression of the T_H1 bias cytokines like IL-12 and IL-23 in humans and mice DCs. The mRNA levels of the subunits IL-12p35 and IL-23p19 increased by 50 times compared to those induced by single agonists[43]. A recent study has shown that synergy is observed if the one of TLR pathways is MyD88 dependent and the other is MyD88 independent. However, activating TLRs which are dependent on the same path induced tolerance.[44]. Yellow fever vaccine, YF17D, stimulates complementary immune pathways.[45] It is not absurd to correlate its efficacy to the combination of PRRs it stimulates. This study demonstrated that whole-cell-based vaccines (attenuated or inactivated), with multiple endogenous PRR activating PAMPs, can induce broader and more robust immune responses without exogenous adjuvants. Crosstalk also exists between TLRs and NODs[46]. The synergy between NOD1/2 and TLR4 agonists[47], and between NOD2 and TLR9 agonists have been well established and studied. In Crohn's disease, the synergy between TLR9 and NOD2 is lost due to NOD2 mutations[48]. The explanation for this loss of synergy has been accredited to the impaired development of Treg cells in inflammatory diseases such as Crohn's[49]. Thus, the engagement of member(s) of different PRR families could be the answer to a complete immune response. To date in clinical adjuvant research, only single TLR agonists-carrier/depot combinations have been explored. [50] Combinations of TLR agonists with NLR or RLR or CLR or STING agonists should be investigated, and all the consequences of such associations documented.

There are only a handful of adjuvants used in licensed vaccines. But it is now clear that many whole-cell-based vaccines (attenuated or inactivated) that have been administered over a billion times contain endogenous adjuvants. Researchers have realized that many live vaccines that are widely used, activate specific PRRs[51]. These vaccines trigger innate immunity through their endogenous PAMPs. An example is the yellow fever vaccine (YF-17D). It is one of the most efficient vaccines ever developed and it activates multiple TLRs (TLR2, TLR3, and TLR7–TLR9) and other PRRs like RIG-I and MDA5[45]. This indicates that multiple PRR signaling is a key factor in the immunogenicity of YF-17D[45,52]. However, we should acknowledge that live attenuated virus is constantly replicating, and as a result, the antigen expression is sustained. Similarly, the Bacillus Calmette–Guérin (BCG) engages TLR2, TLR4, TLR9, and DC-SIGN[53,54]. Additionally, other inactivated vaccines such as the seasonal flu vaccine also trigger the innate immune system through the TLR7 and MyD88 signaling pathways[55]. These findings have further strengthened the case for PRR agonists to be developed and explored as targets for vaccine adjuvants, especially in endogenous adjuvant-less subunit vaccines. Numerous studies in mice and non-human primates (NHPs) have demonstrated that TLR ligands can be used as adjuvants. They boost the magnitude and durability of the antibody responses to vaccination with pure protein antigens [56,57].

It is reasonable to expect that, with adjuvants, inactivated vaccines could induce persistent and strong immune responses like live attenuated viral vaccines.[58,59]. Inspired by the yellow fever vaccine that stimulates multiple TLRs[45] pathways, Bali Pulendran's lab developed synthetic nanoparticles that contain TLR4 and TLR7/8 ligands as adjuvants, in combination with soluble protein antigens such as ovalbumin, or haemagglutinin[60,61]. They observed that these nanoparticles that targeted multiple TLRs induced stronger and more durable antibody responses compared to the nanoparticle that stimulated only one TLR[60]. Also, these particles could drive the generation

of long-lived plasma cells (LLPCs). Multiple DC subsets B cells could be activated by this combinatorial strategy. This resulted in robust immune responses that lasted a lifetime in mice [60]. Subsequent studies on NHPs showed similar results.[57,62,63] The key to generating durable antibody response seems to be LLPCs. Hence adjuvants inducing the proliferation of LLPCs should be explored further.[63,64] Recently it was shown that sustained-release carrier systems that maintain the antigen release over a long period can boost the magnitude, breadth, and durability of antibody responses [65,66]. Moreover, it has been shown that 3M-052, a TLR7/8 agonist that is slowly released from the site of injection [67], results in the activation of monocytes and DCs that lasts for 3–4 weeks[57]. This results in persistent antibody responses and LLPCs much greater than those observed with alum.[57,61]

1.4 Immune modulation

Owing to safety concerns, many adjuvants that have shown promise in preclinical models have not achieved human licensure. Safety and tolerability remain a primary challenge in adjuvant development. Adjuvants can often induce unwanted side effects, which can last up to a few days. The side effects can range from swelling, or pain to fever, headache, and flu-like symptoms[68,69]. In addition to such minor uneasiness, adjuvants can cause adverse events such as anaphylactic reactions [70].

The Esser-Kahn lab has recently shown that co-administering immunostimulants with immunomodulators improve the vaccine's safety while maintaining the protection it provides[71,72]. This was accomplished by combining selective NF-kb modulators with TLR agonists. This vaccine formulation reduced systemic inflammation and enhanced antibody response. The decrease in inflammation is separate from the increase in the humoral response. This observation was constant

across a broad range of antigens and adjuvants, implying that this can be a general strategy for improving vaccination response while minimizing side effects associated with inflammation. Moreover, this approach improved the vaccine's protective response in an influenza model. These modulators can range from peptides (SN50) to small molecules like honokiol, capsaicin, and catechol[71,72]. The addition of NF-kb modulators decreases pro-inflammatory cytokine expression while boosting cell-surface co-stimulatory receptors. This results in better antigen presentation in mice. There are hundreds of NF-kb modulators; some FDA approved, that can be used with different TLR agonists to provide safe vaccines. This strategy enables different PRRs to be used safely, resulting in wider adaptive immune response profiles.

1.5 Better adjuvants through chemistry

1.5.1 Synthetic PRR agonists.

The adjuvants in licensed vaccines mainly consist of components derived from natural sources such as alum salts or saponin. Their availability and potency drove their widespread use in vaccines even though their molecular mechanism was poorly understood. Now that there is a greater understanding of the innate immune system, researchers have shifted focus to synthetic chemistry to develop novel molecules for specific adjuvants. Such efforts have resulted in the development of small molecule immune potentiators (SMIPs).[73–76]. Although initially, the focus was on discovering and developing TLR agonists, the search for novel agonists of other innate immune pathways is underway[77–79]. The newly developed immunostimulants are primarily small molecules with a precise molecular mechanism that can also be modified to allow modulation of the level of interaction with the receptor to control activation signals. Also, the identification of

natural TLR agonists has helped in the development of synthetic ligands that can target various TLRs precisely and safely unlike pathogen-derived ligands[80].

Immunostimulants that were previously used as adjuvants without a clear understanding of their molecular mechanism have been identified to be TLR agonists. For example, unmethylated CpG DNA is recognized by TLR9; lipopeptides by TLR2; LPS and its derivatives by TLR4; poly (I: C) by TLR3; and imidazoquinolines by TLR7/8[81]. More TLR agonists have been synthesized, characterized, and tested in different experimental models. Examples include different TLR9 agonists for different species, better TLR7/8 agonists[67,76,82,83], TLR4 agonists[84,85], and TLR3 agonists[86].

Most of the focus of adjuvant research has been around TLRs. But now that is changing as other PRRs are also getting attention as possible adjuvant targets. New-generation adjuvants should target NLRs[87], RLRs[88], CLRs[89], and STING[78] pathways. Most PRRs signaling induces some local damage to the tissue or cell. This damage induces the release of danger-associated molecular patterns (DAMPs) which is a critical component of adjuvanticity. For instance, NLRs recognize multiple cellular products like ATP, uric acid, and K+ efflux, suggesting that cellular damage potentially mediated this activation[90,91]. Ligands of STING pathways are potential adjuvants that stimulate robust CD8+ T cell responses in mice[92]. Stimulation of RIG-I and RLRs offers another possible way to induce CD8+ T cell responses[93–95].

1.5.2 Immune stimulation through PRR agonist conjugation

The discovery of synergistic interactions between multiple types of PRRs has led to the development of new multi-agonist adjuvants via covalent conjugation. This has improved vaccine immunogenicity. Although unconjugated mixtures of multiple PRR agonists elicit synergistic

immune activity, this approach does not mimic the spatial component of PRR activation by a pathogen. Adjuvants mixtures of unconjugated agonists can diffuse through the immune system and may be cleared more readily.

Developing more potent and effective immunostimulants *via* covalent conjugation has led to applying these tools as adjuvants in vaccination models. The first example of this was CL429, a chimeric molecule containing the agonists Pam2C (2,3-dipalmitoyl-S-glyceryl cysteine) and murabutide (muramyl dipeptide (MDP) derivative), which stimulate TLR2 and NOD2, respectively.[96] CL429 was used as an adjuvant in an HIV-1 subunit vaccine and increased HIV-1 p- 24 antigen-specific IgG and IgA antibody titers compared to the individual agonists or a mixture of the unconjugated TLR2 and NOD2 agonists.

In addition to covalent localization of multi-agonist adjuvants, particulate vaccine delivery systems have been synthesized those mimic pathogens in size and spatial organization. Particulate systems, including nanoparticles, nanodiscs, and liposomes that range in diameter from sub- to low-micron size, provide cargo delivery at sizes similar to a virus or bacteria.[97,98] These delivery systems have shown enhanced antigen uptake by antigen-presenting cells (APCs), which can lead to increased antigen presentation and immune activation.[82,99] Biodegradable PLGA [poly(lactic-co-glycolic acid)] particles (~300nm in diameter) have been developed to encapsulate or adsorb dual or triple combinations of TLR agonists, imitating the size and composition of a pathogen.[60,100] These latter studies have shown that multi-TLR agonist adjuvant formulations induce distinct immune response in mice compared to the use of one agonist or antigen alone. These immune responses include the production of the highest avidity antibody titers against the target antigen and balanced T_H1/T_H2 responses via increased IgG1 and IgG2c levels.[100] Although targeting the antigen and adjuvant to the same endosome increases antigen presentation, more robust humoral

responses were observed when the antigen and adjuvant were in separate nanoparticles, requiring more mechanistic investigation.[60] Nanodiscs are another adjuvant delivery system which targets dual TLR pathways.[98] Immunizations with this scaffold led to a reduction in plasma cholesterol levels and potent antitumor activity in two different model systems, presenting another efficacious platform that can easily combine synergistic adjuvants with a range of antigens. In addition, synergistic TLR agonist combinations have been conjugated to whole tumor cells and exhibited enhanced activation marker and cytokine responses upon incubation with immune cells.[101] This study demonstrates that TLR synergy can also be helpful for cancer immunotherapy applications.

In an *in vivo* ovalbumin (OVA) immunization model, NOD2 and TLR9 agonist-loaded mesoporous silica particles exhibited synergistic increases in cytokine production and enhanced $CD4^+$ and humoral T_H1 responses compared to either NOD2 or TLR9 agonist-loaded particles.[102] Tukhvatulin and colleagues adsorbed TLR4 (MPLA) and NOD2 (MDP) agonists to alum particles.[103] By activating TLR4 instead of TLR9, both T_H1 and T_H2 responses were enhanced as well as OVA-specific IgG antibodies across multiple subsets (IgG1, IgG2, and IgG3), demonstrating an increase in the breadth of the immune response. These results show that by activating multiple PRRs, one can tune the immune response. depending on the activated PRRs.

Particulate delivery vehicles traffic to specific locations in vivo and create a depot in tissues to provide slow drug release have significantly impacted vaccine efficacy. Lynn and colleagues synthesized a nanoparticulate adjuvant that exemplified targeted biodistribution.[82] A TLR7/8 agonist was conjugated to a polymer scaffold at different densities and with varying polymer attributes, such as linker length and composition. The particulate nature of the adjuvant led to limited systemic toxicity and higher localized immune activation in the lymph nodes which

promoted APC uptake and enhanced T cell responses. They have expanded the application of this approach to several proteins and adjuvants.[104,105] Applying this technology to multiple PRR agonists and immune synergy studies may provide targeted delivery, specific biodistribution, and mechanistic insight into immune activation.

In our previous work, we have shown that linking multi-TLR agonists alter immune responses. Covalently linked agonists induced higher immune activation compared to a mixture of unlinked agonists and are dependent on the conjugation method. A library of dimeric TLR agonists containing combinations of TLR2, TLR4, and TLR9 agonists was synthesized. The two agonists were separated by polyethylene glycol linkers – PEG_6, PEG_{12}, and PEG_{24} linkers.[106,107] These single molecular entities aimed to mimic the spatial proximity of immunostimulatory components in natural pathogens with initial inspiration from the herpes simplex virus.[108] Evaluation of the immunostimulatory activity of these compounds provided evidence that the immunogenicity was dependent on the linker length, the specific combination of conjugated TLR agonists, and the sizes of the agonists due to possible steric interactions, all critical considerations for adjuvant development.

Recently, we explored covalently linked TLR tri-agonist as an adjuvant because many pathogens contain agonists for three to five different PRRs. [45,101,109,110] The trimeric molecule is composed of TLR4, 7, and 9 agonists linked to a triazine core. The tri-agonist increased antibody breadth and depth against vaccinia virus antigens in a vaccinia model vaccination study and elicited a more balanced T_H1/T_H2 immune response than its unconjugated counterparts or the corresponding conjugated counterparts di-agonists. This balanced response may induce potentially protective cellular, and antibody immune responses compared to just a T_H1 or T_H2 response. Now

we have increased the library of TLR tri-agonists to five trimers. The immune response to these combinations was evaluated and documented by measuring immune-stimulatory genes, cytokine expression, sera cytokine levels, and weight loss after model vaccinations *in vivo*. The linked TLR tri-agonists and the unlinked agonist combination produced completely different immune responses. Despite these promising results, this was only five of over 300 potential hetero-trimeric TLR combinations. The synthetic systems discussed are modular, so PRR agonists can be exchanged to test different immune synergies. The specific combination of covalently linked agonists is crucial to obtaining the desired immune response because each agonist stimulates distinct immune signaling pathways and cytokine production. However, to date, no one has studied a combination of covalently conjugated three different PRR agonists.

Here, chapter 2 discuss the design and synthesis of a multi-PRR tri-agonist that stimulates TLR2, NOD2, and NLRP3 inflammasome. This molecule amplified the cytokine expression compared to the unlinked mix of ligands. Moreover, when used as an adjuvant with OVA, it induced higher T cell response and antibody response compared to the unlinked mixture.

Chapters 3 and 4 discuss our approach to increasing the safety profile while maintaining or enhancing the protective response of vaccines. Although most of the adjuvant research has focused on enhancing the protective response, less effort has been devoted to the study of toxicity mechanisms and how to eliminate or reduce them to the tolerable limit. Here, we investigated two strategies for reducing the reactogenicity of small molecule TLR7/8 agonist while maintaining its intrinsic immunogenicity. First, we covalently conjugated innate immune modulators directly to the small molecule agonist (chapter 3) which gave small dimer molecules. Secondly, we loaded multiple units of the immunostimulant and the immunomodulator on a peptide scaffold. This improved the PK and PD property of the molecule compared to the small dimer molecules.

1.6 Conclusion

Developing efficient and safe vaccine adjuvants is a challenge. Traditional approaches have been predominantly empirical wherein a single component, such as aluminum salts or emulsions has been used. However, with the fast emergence of new diseases and the increasing risk of pandemics, new immunostimulants inducing T-cell responses in addition to antibodies, are needed. Recent progress in basic immunology has illustrated that the type of adaptive responses is shaped by early innate immune signals. This has led researchers to create more specific synthetic adjuvants whose molecular mechanisms are well understood. Moreover, researchers can now identify, characterize and rationally combine these immunostimulants and formulations that will give the right immune response. The nature of protection required should decide which adjuvant to be used in a vaccine. However, there is a lot more research required to identify the optimal combination of ligands that will give the safest and most effective protection against a particular pathogen.

1.7 REFERENCES

1. Ulmer, J. B.; Valley, U.; Rappuoli, R. Vaccine Manufacturing: Challenges and Solutions. *Nat Biotechnol* **2006**, *24* (11), 1377–1383.

2. Hunter, R. L. Overview of Vaccine Adjuvants: Present and Future. *Vaccine* **2002**, *20*, S7–S12.

3. Beutler, B. Inferences, Questions and Possibilities in Toll-like Receptor Signalling. *Nature* **2004**, *430* (6996), 257–263.

4. Kawai, T.; Akira, S. The Role of Pattern-Recognition Receptors in Innate Immunity: Update on Toll-like Receptors. *Nat Immunol* **2010**, *11* (5), 373–384.

5. Medzhitov, R. Toll-like Receptors and Innate Immunity. *Nat Rev Immunol* **2001**, *1* (2), 135–145.
6. Coffman, R. L.; Sher, A.; Seder, R. A. Vaccine Adjuvants: Putting Innate Immunity to Work. *Immunity* **2010**, *33* (4), 492–503

7. Reed, S. G.; Orr, M. T.; Fox, C. B. Key Roles of Adjuvants in Modern Vaccines. *Nat Med* **2013**, *19* (12), 1597–1608.

8. Steinman, R. M.; Banchereau, J. Taking Dendritic Cells into Medicine. *Nature* **2007**, *449* (7161), 419–426.

9. Chow, K. T.; Gale, M.; Loo, Y.-M. RIG-I and Other RNA Sensors in Antiviral Immunity. *Annu Rev Immunol* **2018**, *36*, 667–694.

10. Barber, G. N. Chapter 3 - Cytosolic DNA-Sensing and the STING Pathway. In *Biological DNA Sensor*; Ishii, K. J., Tang, C. K., Eds.; Academic Press: Amsterdam, 2014; pp 67–81.

11. Brown, G. D.; Willment, J. A.; Whitehead, L. C-Type Lectins in Immunity and Homeostasis. *Nat Rev Immunol* **2018**, *18* (6), 374–389.

12. Christgen, S.; Kanneganti, T.-D. Inflammasomes and the Fine Line between Defense and Disease. *Curr Opin Immunol* **2020**, *62*, 39–44.

13. Mangan, M. S. J.; Olhava, E. J.; Roush, W. R.; Seidel, H. M.; Glick, G. D.; Latz, E. Targeting the NLRP3 Inflammasome in Inflammatory Diseases. *Nat Rev Drug Discov* **2018**, *17* (8), 588–606.

14. Kwissa, M.; Pai Kasturi, S.; Pulendran, B. The Science of Adjuvants. *Expert Review of Vaccines* **2007**, *6* (5), 673–684.

15. Schijns, V. E. Induction and Direction of Immune Responses by Vaccine Adjuvants. *Crit Rev Immunol* **2001**, *21* (1–3), 75–85.

16. Koyasu, S.; Moro, K. Type 2 Innate Immune Responses and the Natural Helper Cell. *Immunology* **2011**, *132* (4), 475–481.

17. Flacher, V.; Bouschbacher, M.; Verronèse, E.; Massacrier, C.; Sisirak, V.; Berthier-Vergnes, O.; de Saint-Vis, B.; Caux, C.; Dezutter-Dambuyant, C.; Lebecque, S.; Valladeau, J. Human Langerhans Cells Express a Specific TLR Profile and Differentially Respond to Viruses and Gram-Positive Bacteria. *J Immunol* **2006**, *177* (11), 7959–7967.

18. Jarrossay, D.; Napolitani, G.; Colonna, M.; Sallusto, F.; Lanzavecchia, A. Specialization and Complementarity in Microbial Molecule Recognition by Human Myeloid and Plasmacytoid Dendritic Cells. *Eur J Immunol* **2001**, *31* (11), 3388–3393.

19. Agrawal, S.; Agrawal, A.; Doughty, B.; Gerwitz, A.; Blenis, J.; Van Dyke, T.; Pulendran, B. Cutting Edge: Different Toll-like Receptor Agonists Instruct Dendritic Cells to Induce Distinct Th Responses via Differential Modulation of Extracellular Signal-Regulated Kinase-Mitogen-Activated Protein Kinase and c-Fos. *J Immunol* **2003**, *171* (10), 4984–4989.

20. Dillon, S.; Agrawal, A.; Van Dyke, T.; Landreth, G.; McCauley, L.; Koh, A.; Maliszewski, C.; Akira, S.; Pulendran, B. A Toll-like Receptor 2 Ligand Stimulates Th2 Responses in Vivo, via Induction of Extracellular Signal-Regulated Kinase Mitogen-Activated Protein Kinase and c-Fos in Dendritic Cells. *J Immunol* **2004**, *172* (8), 4733–4743.

21. Blander, J. M.; Medzhitov, R. Toll-Dependent Selection of Microbial Antigens for Presentation by Dendritic Cells. *Nature* **2006**, *440* (7085), 808–812.

22. Yarovinsky, F.; Kanzler, H.; Hieny, S.; Coffman, R. L.; Sher, A. Toll-like Receptor Recognition Regulates Immunodominance in an Antimicrobial CD4+ T Cell Response. *Immunity* **2006**, *25* (4), 655–664.

23. Ruprecht, C. R.; Lanzavecchia, A. Toll-like Receptor Stimulation as a Third Signal Required for Activation of Human Naive B Cells. *Eur J Immunol* **2006**, *36* (4), 810–816.

24. Pasare, C.; Medzhitov, R. Control of B-Cell Responses by Toll-like Receptors. *Nature* **2005**, *438* (7066), 364–368.

25. Sakaguchi, S. Control of Immune Responses by Naturally Arising CD4+ Regulatory T Cells That Express Toll-like Receptors. *Journal of Experimental Medicine* **2003**, *197* (4), 397–401.

26. Sutmuller, R. P. M.; den Brok, M. H. M. G. M.; Kramer, M.; Bennink, E. J.; Toonen, L. W. J.; Kullberg, B.-J.; Joosten, L. A.; Akira, S.; Netea, M. G.; Adema, G. J. Toll-like Receptor 2 Controls Expansion and Function of Regulatory T Cells. *J Clin Invest* **2006**, *116* (2), 485–494.

27. Caramalho, I.; Lopes-Carvalho, T.; Ostler, D.; Zelenay, S.; Haury, M.; Demengeot, J. Regulatory T Cells Selectively Express Toll-like Receptors and Are Activated by Lipopolysaccharide. *J Exp Med* **2003**, *197* (4), 403–411.

28. Peng, G.; Guo, Z.; Kiniwa, Y.; Voo, K. S.; Peng, W.; Fu, T.; Wang, D. Y.; Li, Y.; Wang, H. Y.; Wang, R.-F. Toll-like Receptor 8-Mediated Reversal of CD4+ Regulatory T Cell Function. *Science* **2005**, *309* (5739), 1380–1384.

29. Pasare, C.; Medzhitov, R. Toll Pathway-Dependent Blockade of CD4+CD25+ T Cell-Mediated Suppression by Dendritic Cells. *Science* **2003**, *299* (5609), 1033–1036.

30. Pasare, C.; Medzhitov, R. Toll-Dependent Control Mechanisms of CD4 T Cell Activation. *Immunity* **2004**, *21* (5), 733–741.

31. Meylan, E.; Tschopp, J.; Karin, M. Intracellular Pattern Recognition Receptors in the Host Response. *Nature* **2006**, *442* (7098), 39–44.

32. Traub, S.; von Aulock, S.; Hartung, T.; Hermann, C. Invited Review: MDP and Other Muropeptides — Direct and Synergistic Effects on the Immune System. *Journal of Endotoxin Research* **2006**, *12* (2), 69–85.

33. Lemesre, J.-L.; Holzmuller, P.; Cavaleyra, M.; Gonçalves, R. B.; Hottin, G.; Papierok, G. Protection against Experimental Visceral Leishmaniasis Infection in Dogs Immunized with Purified Excreted Secreted Antigens of Leishmania Infantum Promastigotes. *Vaccine* **2005**, *23* (22), 2825–2840.

34. Nardin, A.; Lefebvre, M.-L.; Labroquère, K.; Faure, O.; Abastado, J.-P. Liposomal Muramyl Tripeptide Phosphatidylethanolamine: Targeting and Activating Macrophages for Adjuvant Treatment of Osteosarcoma. *Curr Cancer Drug Targets* **2006**, *6* (2), 123–133.

35. Kato, H.; Takeuchi, O.; Sato, S.; Yoneyama, M.; Yamamoto, M.; Matsui, K.; Uematsu, S.; Jung, A.; Kawai, T.; Ishii, K. J.; Yamaguchi, O.; Otsu, K.; Tsujimura, T.; Koh, C.-S.; Reis e Sousa, C.; Matsuura, Y.; Fujita, T.; Akira, S. Differential Roles of MDA5 and RIG-I Helicases in the Recognition of RNA Viruses. *Nature* **2006**, *441* (7089), 101–105.

36. Ishikawa, H.; Ma, Z.; Barber, G. N. STING Regulates Intracellular DNA-Mediated, Type I Interferon-Dependent Innate Immunity. *Nature* **2009**, *461* (7265), 788–792.

37. Ahn, J.; Barber, G. N. STING Signaling and Host Defense against Microbial Infection. *Exp Mol Med* **2019**, *51* (12), 1–10.

38. Peiser, L.; Mukhopadhyay, S.; Gordon, S. Scavenger Receptors in Innate Immunity. *Curr Opin Immunol* **2002**, *14* (1), 123–128.

39. Robinson, M. J.; Sancho, D.; Slack, E. C.; LeibundGut-Landmann, S.; Sousa, C. R. e. Myeloid C-Type Lectins in Innate Immunity. *Nat Immunol* **2006**, *7* (12), 1258–1265.

40. Trinchieri, G.; Sher, A. Cooperation of Toll-like Receptor Signals in Innate Immune Defence. *Nat Rev Immunol* **2007**, *7* (3), 179–190.
41. Sato, S.; Nomura, F.; Kawai, T.; Takeuchi, O.; Mühlradt, P. F.; Takeda, K.; Akira, S. Synergy and Cross-Tolerance Between Toll-Like Receptor (TLR) 2- and TLR4-Mediated Signaling Pathways. *J Immunol* **2000**, *165* (12), 7096–7101.

42. Roelofs, M. F.; Joosten, L. a. B.; Abdollahi-Roodsaz, S.; van Lieshout, A. W. T.; Sprong, T.; van den Hoogen, F. H.; van den Berg, W. B.; Radstake, T. R. D. J. The Expression of Toll-like Receptors 3 and 7 in Rheumatoid Arthritis Synovium Is Increased and Costimulation of Toll-like Receptors 3, 4, and 7/8 Results in Synergistic Cytokine Production by Dendritic Cells. *Arthritis Rheum* **2005**, *52* (8), 2313–2322.

43. Napolitani, G.; Rinaldi, A.; Bertoni, F.; Sallusto, F.; Lanzavecchia, A. Selected Toll-like Receptor Agonist Combinations Synergistically Trigger a T Helper Type 1-Polarizing Program in Dendritic Cells. *Nat Immunol* **2005**, *6* (8), 769–776.

44. Bagchi, A.; Herrup, E. A.; Warren, H. S.; Trigilio, J.; Shin, H.-S.; Valentine, C.; Hellman, J. MyD88-Dependent and MyD88-Independent Pathways in Synergy, Priming, and Tolerance between TLR Agonists. *J Immunol* **2007**, *178* (2), 1164–1171.

45. Querec, T.; Bennouna, S.; Alkan, S.; Laouar, Y.; Gorden, K.; Flavell, R.; Akira, S.; Ahmed, R.; Pulendran, B. Yellow Fever Vaccine YF-17D Activates Multiple Dendritic Cell Subsets via TLR2, 7, 8, and 9 to Stimulate Polyvalent Immunity. *J Exp Med* **2006**, *203* (2), 413–424.

46. Takada, H.; Uehara, A. Enhancement of TLR-Mediated Innate Immune Responses by Peptidoglycans through NOD Signaling. *Curr Pharm Des* **2006**, *12* (32), 4163–4172.

47. Fritz, J. H.; Girardin, S. E.; Fitting, C.; Werts, C.; Mengin-Lecreulx, D.; Caroff, M.; Cavaillon, J.-M.; Philpott, D. J.; Adib-Conquy, M. Synergistic Stimulation of Human Monocytes and Dendritic Cells by Toll-like Receptor 4 and NOD1- and NOD2-Activating Agonists. *Eur J Immunol* **2005**, *35* (8), 2459–2470.

48. van Heel, D. A.; Ghosh, S.; Hunt, K. A.; Mathew, C. G.; Forbes, A.; Jewell, D. P.; Playford, R. J. Synergy between TLR9 and NOD2 Innate Immune Responses Is Lost in Genetic Crohn's Disease. *Gut* **2005**, *54* (11), 1553–1557.

49. Watanabe, T.; Kitani, A.; Strober, W. NOD2 Regulation of Toll-like Receptor Responses and the Pathogenesis of Crohn's Disease. *Gut* **2005**, *54* (11), 1515–1518.

50. O'Hagan, D. T.; Lodaya, R. N.; Lofano, G. The Continued Advance of Vaccine Adjuvants – 'We Can Work It Out.' *Seminars in Immunology* **2020**, *50*, 101426.

51. Pulendran, B.; Ahmed, R. Immunological Mechanisms of Vaccination. *Nat Immunol* **2011**, *12* (6), 509–517.

52. Querec, T. D.; Akondy, R. S.; Lee, E. K.; Cao, W.; Nakaya, H. I.; Teuwen, D.; Pirani, A.; Gernert, K.; Deng, J.; Marzolf, B.; Kennedy, K.; Wu, H.; Bennouna, S.; Oluoch, H.; Miller, J.; Vencio, R. Z.; Mulligan, M.; Aderem, A.; Ahmed, R.; Pulendran, B. Systems Biology Approach Predicts Immunogenicity of the Yellow Fever Vaccine in Humans. *Nat Immunol* **2009**, *10* (1), 116–125.

53. Tsuji, S.; Matsumoto, M.; Takeuchi, O.; Akira, S.; Azuma, I.; Hayashi, A.; Toyoshima, K.; Seya, T. Maturation of Human Dendritic Cells by Cell Wall Skeleton of Mycobacterium Bovis Bacillus Calmette-Guérin: Involvement of Toll-like Receptors. *Infect Immun* **2000**, *68* (12), 6883–6890.

54. Moliva, J. I.; Turner, J.; Torrelles, J. B. Immune Responses to Bacillus Calmette-Guérin Vaccination: Why Do They Fail to Protect against Mycobacterium Tuberculosis? *Front Immunol* **2017**, *8*, 407.

55. Koyama, S.; Ishii, K. J.; Kumar, H.; Tanimoto, T.; Coban, C.; Uematsu, S.; Kawai, T.; Akira, S. Differential Role of TLR- and RLR-Signaling in the Immune Responses to Influenza A Virus Infection and Vaccination. *J Immunol* **2007**, *179* (7), 4711–4720.

56. Francica, J. R.; Zak, D. E.; Linde, C.; Siena, E.; Johnson, C.; Juraska, M.; Yates, N. L.; Gunn, B.; De Gregorio, E.; Flynn, B. J.; Valiante, N. M.; Malyala, P.; Barnett, S. W.; Sarkar, P.; Singh, M.; Jain, S.; Ackerman, M.; Alam, M.; Ferrari, G.; Salazar, A.; Tomaras, G. D.; O'Hagan, D. T.; Aderem, A.; Alter, G.; Seder, R. A. Innate Transcriptional Effects by Adjuvants on the Magnitude, Quality, and Durability of HIV Envelope Responses in NHPs. *Blood Adv* **2017**, *1* (25), 2329–2342.

57. Petitdemange, C.; Kasturi, S. P.; Kozlowski, P. A.; Nabi, R.; Quarnstrom, C. F.; Reddy, P. B. J.; Derdeyn, C. A.; Spicer, L. M.; Patel, P.; Legere, T.; Kovalenkov, Y. O.; Labranche, C. C.; Villinger, F.; Tomai, M.; Vasilakos, J.; Haynes, B.; Kang, C. Y.; Gibbs, J. S.; Yewdell, J. W.; Barouch, D.; Wrammert, J.; Montefiori, D.; Hunter, E.; Amara, R. R.; Masopust, D.; Pulendran, B. Vaccine Induction of Antibodies and Tissue-Resident CD8+ T Cells Enhances Protection against Mucosal SHIV-Infection in Young Macaques. *JCI Insight* **2019**, *4* (4), 126047.

58. Crotty, S.; Felgner, P.; Davies, H.; Glidewell, J.; Villarreal, L.; Ahmed, R. Cutting Edge: Long-Term B Cell Memory in Humans after Smallpox Vaccination. *J Immunol* **2003**, *171* (10), 4969–4973.

59. Hammarlund, E.; Lewis, M. W.; Hansen, S. G.; Strelow, L. I.; Nelson, J. A.; Sexton, G. J.; Hanifin, J. M.; Slifka, M. K. Duration of Antiviral Immunity after Smallpox Vaccination. *Nat Med* **2003**, *9* (9), 1131–1137.

60. Kasturi, S. P.; Skountzou, I.; Albrecht, R. A.; Koutsonanos, D.; Hua, T.; Nakaya, H. I.; Ravindran, R.; Stewart, S.; Alam, M.; Kwissa, M.; Villinger, F.; Murthy, N.; Steel, J.; Jacob, J.; Hogan, R. J.; García-Sastre, A.; Compans, R.; Pulendran, B. Programming the Magnitude

and Persistence of Antibody Responses with Innate Immunity. *Nature* **2011**, *470* (7335), 543–547.

61. Kasturi, S. P.; Rasheed, M. A. U.; Havenar-Daughton, C.; Pham, M.; Legere, T.; Sher, Z. J.; Kovalenkov, Y.; Gumber, S.; Huang, J. Y.; Gottardo, R.; Fulp, W.; Sato, A.; Sawant, S.; Stanfield-Oakley, S.; Yates, N.; LaBranche, C.; Alam, S. M.; Tomaras, G.; Ferrari, G.; Montefiori, D.; Wrammert, J.; Villinger, F.; Tomai, M.; Vasilakos, J.; Fox, C. B.; Reed, S. G.; Haynes, B. F.; Crotty, S.; Ahmed, R.; Pulendran, B. 3M-052, a Synthetic TLR-7/8 Agonist, Induces Durable HIV-1 Envelope-Specific Plasma Cells and Humoral Immunity in Nonhuman Primates. *Sci Immunol* **2020**, *5* (48), eabb1025.

62. Kasturi, S. P.; Kozlowski, P. A.; Nakaya, H. I.; Burger, M. C.; Russo, P.; Pham, M.; Kovalenkov, Y.; Silveira, E. L. V.; Havenar-Daughton, C.; Burton, S. L.; Kilgore, K. M.; Johnson, M. J.; Nabi, R.; Legere, T.; Sher, Z. J.; Chen, X.; Amara, R. R.; Hunter, E.; Bosinger, S. E.; Spearman, P.; Crotty, S.; Villinger, F.; Derdeyn, C. A.; Wrammert, J.; Pulendran, B. Adjuvanting a Simian Immunodeficiency Virus Vaccine with Toll-Like Receptor Ligands Encapsulated in Nanoparticles Induces Persistent Antibody Responses and Enhanced Protection in TRIM5α Restrictive Macaques. *J Virol* **2017**, *91* (4), e01844-16.

63. Slifka, M. K.; Ahmed, R. Long-Lived Plasma Cells: A Mechanism for Maintaining Persistent Antibody Production. *Curr Opin Immunol* **1998**, *10* (3), 252–258.

64. Slifka, M. K.; Antia, R.; Whitmire, J. K.; Ahmed, R. Humoral Immunity Due to Long-Lived Plasma Cells. *Immunity* **1998**, *8* (3), 363–372.

65. Cirelli, K. M.; Carnathan, D. G.; Nogal, B.; Martin, J. T.; Rodriguez, O. L.; Upadhyay, A. A.; Enemuo, C. A.; Gebru, E. H.; Choe, Y.; Viviano, F.; Nakao, C.; Pauthner, M. G.; Reiss, S.; Cottrell, C. A.; Smith, M. L.; Bastidas, R.; Gibson, W.; Wolabaugh, A. N.; Melo, M. B.; Cossette, B.; Kumar, V.; Patel, N. B.; Tokatlian, T.; Menis, S.; Kulp, D. W.; Burton, D. R.; Murrell, B.; Schief, W. R.; Bosinger, S. E.; Ward, A. B.; Watson, C. T.; Silvestri, G.; Irvine, D. J.; Crotty, S. Slow Delivery Immunization Enhances HIV Neutralizing Antibody and Germinal Center Responses via Modulation of Immunodominance. *Cell* **2019**, *177* (5), 1153-1171.e28.

66. Tam, H. H.; Melo, M. B.; Kang, M.; Pelet, J. M.; Ruda, V. M.; Foley, M. H.; Hu, J. K.; Kumari, S.; Crampton, J.; Baldeon, A. D.; Sanders, R. W.; Moore, J. P.; Crotty, S.; Langer, R.; Anderson, D. G.; Chakraborty, A. K.; Irvine, D. J. Sustained Antigen Availability during Germinal Center Initiation Enhances Antibody Responses to Vaccination. *Proc Natl Acad Sci U S A* **2016**, *113* (43), E6639–E6648.

67. Smirnov, D.; Schmidt, J. J.; Capecchi, J. T.; Wightman, P. D. Vaccine Adjuvant Activity of 3M-052: An Imidazoquinoline Designed for Local Activity without Systemic Cytokine Induction. *Vaccine* **2011**, *29* (33), 5434–5442

68. Hervé, C.; Laupèze, B.; Del Giudice, G.; Didierlaurent, A. M.; Tavares Da Silva, F. The How's and What's of Vaccine Reactogenicity. *NPJ Vaccines* **2019**, *4*, 39.

69. Batista-Duharte, A.; Martínez, D. T.; Carlos, I. Z. Efficacy and Safety of Immunological Adjuvants. Where Is the Cut-Off? *Biomed Pharmacother* **2018**, *105*, 616–624.
70. Nanishi, E.; Dowling, D. J.; Levy, O. Toward Precision Adjuvants: Optimizing Science and Safety. *Curr Opin Pediatr* **2020**, *32* (1), 125–138.

71. Moser, B. A.; Escalante-Buendia, Y.; Steinhardt, R. C.; Rosenberger, M. G.; Cassaidy, B. J.; Naorem, N.; Chon, A. C.; Nguyen, M. H.; Tran, N. T.; Esser-Kahn, A. P. Small Molecule NF-KB Inhibitors as Immune Potentiators for Enhancement of Vaccine Adjuvants. *Frontiers in Immunology* **2020**, *11*.

72. Moser, B. A.; Steinhardt, R. C.; Escalante-Buendia, Y.; Boltz, D. A.; Barker, K. M.; Cassaidy, B. J.; Rosenberger, M. G.; Yoo, S.; McGonnigal, B. G.; Esser-Kahn, A. P. Increased Vaccine Tolerability and Protection via NF-KB Modulation. *Science Advances 6* (37), eaaz8700.

73. Ericsson, D. J.; Nurbo, J.; Muthas, D.; Hertzberg, K.; Lindeberg, G.; Karlén, A.; Unge, T. Identification of Small Peptides Mimicking the R2 C-Terminus of Mycobacterium Tuberculosis Ribonucleotide Reductase. *J Pept Sci* **2010**, *16* (3), 159–164.

74. Guan, Y.; Omueti-Ayoade, K.; Mutha, S. K.; Hergenrother, P. J.; Tapping, R. I. Identification of Novel Synthetic Toll-like Receptor 2 Agonists by High Throughput Screening. *J Biol Chem* **2010**, *285* (31), 23755–23762.

75. Wu, T. Y.-H. Strategies for Designing Synthetic Immune Agonists. *Immunology* **2016**, *148* (4), 315–325.

76. Wu, T. Y.-H.; Singh, M.; Miller, A. T.; De Gregorio, E.; Doro, F.; D'Oro, U.; Skibinski, D. A. G.; Mbow, M. L.; Bufali, S.; Herman, A. E.; Cortez, A.; Li, Y.; Nayak, B. P.; Tritto, E.; Filippi, C. M.; Otten, G. R.; Brito, L. A.; Monaci, E.; Li, C.; Aprea, S.; Valentini, S.; Calabró, S.; Laera, D.; Brunelli, B.; Caproni, E.; Malyala, P.; Panchal, R. G.; Warren, T. K.; Bavari, S.; O'Hagan, D. T.; Cooke, M. P.; Valiante, N. M. Rational Design of Small Molecules as Vaccine Adjuvants. *Sci Transl Med* **2014**, *6* (263), 263ra160.

77. Brito, L. A.; O'Hagan, D. T. Designing and Building the next Generation of Improved Vaccine Adjuvants. *J Control Release* **2014**, *190*, 563–579.

78. Ramanjulu, J. M.; Pesiridis, G. S.; Yang, J.; Concha, N.; Singhaus, R.; Zhang, S.-Y.; Tran, J.-L.; Moore, P.; Lehmann, S.; Eberl, H. C.; Muelbaier, M.; Schneck, J. L.; Clemens, J.; Adam, M.; Mehlmann, J.; Romano, J.; Morales, A.; Kang, J.; Leister, L.; Graybill, T. L.; Charnley, A. K.; Ye, G.; Nevins, N.; Behnia, K.; Wolf, A. I.; Kasparcova, V.; Nurse, K.; Wang, L.; Puhl, A. C.; Li, Y.; Klein, M.; Hopson, C. B.; Guss, J.; Bantscheff, M.; Bergamini, G.; Reilly, M. A.; Lian, Y.; Duffy, K. J.; Adams, J.; Foley, K. P.; Gough, P. J.;

Marquis, R. W.; Smothers, J.; Hoos, A.; Bertin, J. Design of Amidobenzimidazole STING Receptor Agonists with Systemic Activity. *Nature* **2018**, *564* (7736), 439–443.

79. Salyer, A. C. D.; Caruso, G.; Khetani, K. K.; Fox, L. M.; Malladi, S. S.; David, S. A. Identification of Adjuvantic Activity of Amphotericin B in a Novel, Multiplexed, Poly-TLR/NLR High-Throughput Screen. *PLoS One* **2016**, *11* (2), e0149848.

80. Dougan, G.; Hormaeche, C. How Bacteria and Their Products Provide Clues to Vaccine and Adjuvant Development. *Vaccine* **2006**, *24 Suppl 2*, S2-13–19.

81. Kaisho, T.; Akira, S. Toll-like Receptors as Adjuvant Receptors. *Biochim Biophys Acta* **2002**, *1589* (1), 1–13.

82. Lynn, G. M.; Laga, R.; Darrah, P. A.; Ishizuka, A. S.; Balaci, A. J.; Dulcey, A. E.; Pechar, M.; Pola, R.; Gerner, M. Y.; Yamamoto, A.; Buechler, C. R.; Quinn, K. M.; Smelkinson, M. G.; Vanek, O.; Cawood, R.; Hills, T.; Vasalatiy, O.; Kastenmüller, K.; Francica, J. R.; Stutts, L.; Tom, J. K.; Ryu, K. A.; Esser-Kahn, A. P.; Etrych, T.; Fisher, K. D.; Seymour, L. W.; Seder, R. A. In Vivo Characterization of the Physicochemical Properties of Polymer-Linked TLR Agonists That Enhance Vaccine Immunogenicity. *Nat Biotechnol* **2015**, *33* (11), 1201–1210.

83. Wilson, D. S.; Hirosue, S.; Raczy, M. M.; Bonilla-Ramirez, L.; Jeanbart, L.; Wang, R.; Kwissa, M.; Franetich, J.-F.; Broggi, M. A. S.; Diaceri, G.; Quaglia-Thermes, X.; Mazier, D.; Swartz, M. A.; Hubbell, J. A. Antigens Reversibly Conjugated to a Polymeric Glyco-Adjuvant Induce Protective Humoral and Cellular Immunity. *Nature Materials* **2019**, *18* (2), 175–185.

84. Chan, M.; Kakitsubata, Y.; Hayashi, T.; Ahmadi, A.; Yao, S.; Shukla, N. M.; Oyama, S.; Baba, A.; Nguyen, B.; Corr, M.; Suda, Y.; Carson, D. A.; Cottam, H. B.; Wakao, M. Structure–Activity Relationship Studies of Pyrimido [5,4- *b*] Indoles as Selective Toll-Like Receptor 4 Ligands. *Journal of Medicinal Chemistry* **2017**, *60* (22), 9142–9161.

85. Dowling, D. J. Recent Advances in the Discovery and Delivery of TLR7/8 Agonists as Vaccine Adjuvants. *IH* **2018**, *2* (6), 185–197.

86. Komal, A.; Noreen, M.; El-Kott, A. F. TLR3 Agonists: RGC100, ARNAX, and Poly-IC: A Comparative Review. *Immunol Res* **2021**, *69* (4), 312–322.

87. Manna, S.; Howitz, W. J.; Oldenhuis, N. J.; Eldredge, A. C.; Shen, J.; Nihesh, F. N.; Lodoen, M. B.; Guan, Z.; Esser-Kahn, A. P. Immunomodulation of the NLRP3 Inflammasome through Structure-Based Activator Design and Functional Regulation via Lysosomal Rupture. *ACS Cent. Sci.* **2018**, *4* (8), 982–995.

88. Yong, H. Y.; Luo, D. RIG-I-Like Receptors as Novel Targets for Pan-Antivirals and Vaccine Adjuvants Against Emerging and Re-Emerging Viral Infections. *Front Immunol* **2018**, *9*, 1379.

89. Decout, A.; Silva-Gomes, S.; Drocourt, D.; Barbe, S.; André, I.; Cueto, F. J.; Lioux, T.; Sancho, D.; Pérouzel, E.; Vercellone, A.; Prandi, J.; Gilleron, M.; Tiraby, G.; Nigou, J. Rational Design of Adjuvants Targeting the C-Type Lectin Mincle. *Proceedings of the National Academy of Sciences* **2017**, *114* (10), 2675–2680.

90. Maisonneuve, C.; Bertholet, S.; Philpott, D. J.; De Gregorio, E. Unleashing the Potential of NOD- and Toll-like Agonists as Vaccine Adjuvants. *Proc Natl Acad Sci U S A* **2014**, *111* (34), 12294–12299.

91. Muñoz-Planillo, R.; Kuffa, P.; Martínez-Colón, G.; Smith, B. L.; Rajendiran, T. M.; Núñez, G. K^+ Efflux Is the Common Trigger of NLRP3 Inflammasome Activation by Bacterial Toxins and Particulate Matter. *Immunity* **2013**, *38* (6), 1142–1153.

92. Gutjahr, A.; Papagno, L.; Nicoli, F.; Kanuma, T.; Kuse, N.; Cabral-Piccin, M. P.; Rochereau, N.; Gostick, E.; Lioux, T.; Perouzel, E.; Price, D. A.; Takiguchi, M.; Verrier, B.; Yamamoto, T.; Paul, S.; Appay, V. The STING Ligand CGAMP Potentiates the Efficacy of Vaccine-Induced CD8+ T Cells. *JCI Insight* **2019**, *4* (7), 125107.

93. Probst, P.; Grigg, J. B.; Wang, M.; Muñoz, E.; Loo, Y.-M.; Ireton, R. C.; Gale, M.; Iadonato, S. P.; Bedard, K. M. A Small-Molecule IRF3 Agonist Functions as an Influenza Vaccine Adjuvant by Modulating the Antiviral Immune Response. *Vaccine* **2017**, *35* (15), 1964–1971.

94. Kandasamy, M.; Suryawanshi, A.; Tundup, S.; Perez, J. T.; Schmolke, M.; Manicassamy, S.; Manicassamy, B. RIG-I Signaling Is Critical for Efficient Polyfunctional T Cell Responses during Influenza Virus Infection. *PLoS Pathog* **2016**, *12* (7), e1005754.

95. Suthar, M. S.; Ramos, H. J.; Brassil, M. M.; Netland, J.; Chappell, C. P.; Blahnik, G.; McMillan, A.; Diamond, M. S.; Clark, E. A.; Bevan, M. J.; Gale, M. The RIG-I-like Receptor LGP2 Controls CD8(+) T Cell Survival and Fitness. *Immunity* **2012**, *37* (2), 235–248.

96. Pavot, V.; Rochereau, N.; Rességuier, J.; Gutjahr, A.; Genin, C.; Tiraby, G.; Perouzel, E.; Lioux, T.; Vernejoul, F.; Verrier, B.; Paul, S. Cutting Edge: New Chimeric NOD2/TLR2 Adjuvant Drastically Increases Vaccine Immunogenicity. *J.I.* **2014**, *193* (12), 5781–5785.

97. Fox, C. B.; Sivananthan, S. J.; Duthie, M. S.; Vergara, J.; Guderian, J. A.; Moon, E.; Coblentz, D.; Reed, S. G.; Carter, D. A Nanoliposome Delivery System to Synergistically Trigger TLR4 AND TLR7. *J Nanobiotechnology* **2014**, *12*, 17.

98. Kuai, R.; Sun, X.; Yuan, W.; Ochyl, L. J.; Xu, Y.; Hassani Najafabadi, A.; Scheetz, L.; Yu, M.-Z.; Balwani, I.; Schwendeman, A.; Moon, J. J. Dual TLR Agonist Nanodiscs as a Strong Adjuvant System for Vaccines and Immunotherapy. *J Control Release* **2018**, *282*, 131–139.

99. Junkins, R. D.; Gallovic, M. D.; Johnson, B. M.; Collier, M. A.; Watkins-Schulz, R.; Cheng, N.; David, C. N.; McGee, C. E.; Sempowski, G. D.; Shterev, I.; McKinnon, K.; Bachelder, E. M.; Ainslie, K. M.; Ting, J. P.-Y. A Robust Microparticle Platform for a STING-Targeted Adjuvant That Enhances Both Humoral and Cellular Immunity during Vaccination. *J Control Release* **2018**, *270*, 1–13.

100. Madan-Lala, R.; Pradhan, P.; Roy, K. Combinatorial Delivery of Dual and Triple TLR Agonists via Polymeric Pathogen-like Particles Synergistically Enhances Innate and Adaptive Immune Responses. *Sci Rep* **2017**, *7* (1), 2530.

101. Tom, J. K.; Dotsey, E. Y.; Wong, H. Y.; Stutts, L.; Moore, T.; Davies, D. H.; Felgner, P. L.; Esser-Kahn, A. P. Modulation of Innate Immune Responses *via* Covalently Linked TLR Agonists. *ACS Cent. Sci.* **2015**, *1* (8), 439–448.

102. Gause, K. T.; Yan, Y.; O'Brien-Simpson, N. M.; Cui, J.; Lenzo, J. C.; Reynolds, E. C.; Caruso, F. Codelivery of NOD2 and TLR9 Ligands via Nanoengineered Protein Antigen Particles for Improving and Tuning Immune Responses. *Advanced Functional Materials* **2016**, *26* (41), 7526–7536.

103. Tukhvatulin, A. I.; Dzharullaeva, A. S.; Tukhvatulina, N. M.; Shcheblyakov, D. V.; Shmarov, M. M.; Dolzhikova, I. V.; Stanhope-Baker, P.; Naroditsky, B. S.; Gudkov, A. V.; Logunov, D. Y.; Gintsburg, A. L. Powerful Complex Immunoadjuvant Based on Synergistic Effect of Combined TLR4 and NOD2 Activation Significantly Enhances Magnitude of Humoral and Cellular Adaptive Immune Responses. *PLoS One* **2016**, *11* (5), e0155650.

104. Zhu, G.; Lynn, G. M.; Jacobson, O.; Chen, K.; Liu, Y.; Zhang, H.; Ma, Y.; Zhang, F.; Tian, R.; Ni, Q.; Cheng, S.; Wang, Z.; Lu, N.; Yung, B. C.; Wang, Z.; Lang, L.; Fu, X.; Jin, A.; Weiss, I. D.; Vishwasrao, H.; Niu, G.; Shroff, H.; Klinman, D. M.; Seder, R. A.; Chen, X. Albumin/Vaccine Nanocomplexes That Assemble in Vivo for Combination Cancer Immunotherapy. *Nat Commun* **2017**, *8* (1), 1954.

105. Francica, J. R.; Lynn, G. M.; Laga, R.; Joyce, M. G.; Ruckwardt, T. J.; Morabito, K. M.; Chen, M.; Chaudhuri, R.; Zhang, B.; Sastry, M.; Druz, A.; Ko, K.; Choe, M.; Pechar, M.; Georgiev, I. S.; Kueltzo, L. A.; Seymour, L. W.; Mascola, J. R.; Kwong, P. D.; Graham, B. S.; Seder, R. A. Thermoresponsive Polymer Nanoparticles Co-Deliver RSV F Trimers with a TLR-7/8 Adjuvant. *Bioconjug Chem* **2016**, *27* (10), 2372–2385.

106. Ryu, K. A.; Slowinska, K.; Moore, T.; Esser-Kahn, A. Immune Response Modulation of Conjugated Agonists with Changing Linker Length. *ACS Chem Biol* **2016**, *11* (12), 3347–3352.

107. Mancini, R. J.; Tom, J. K.; Esser-Kahn, A. P. Covalently Coupled Immunostimulant Heterodimers. *Angew Chem Int Ed Engl* **2014**, *53* (1), 189–192.

108. Sato, A.; Linehan, M. M.; Iwasaki, A. Dual Recognition of Herpes Simplex Viruses by TLR2 and TLR9 in Dendritic Cells. *Proc Natl Acad Sci U S A* **2006**, *103* (46), 17343–17348.

109. Albin, T. J.; Tom, J. K.; Manna, S.; Gilkes, A. P.; Stetkevich, S. A.; Katz, B. B.; Supnet, M.; Felgner, J.; Jain, A.; Nakajima, R.; Jasinskas, A.; Zlotnik, A.; Pearlman, E.; Davies, D. H.; Felgner, P. L.; Burkhardt, A. M.; Esser-Kahn, A. P. Linked Toll-Like Receptor Triagonists Stimulate Distinct, Combination-Dependent Innate Immune Responses. *ACS Cent. Sci.* **2019**, *5* (7), 1137–1145.

110. Mogensen, T. H.; Paludan, S. R.; Kilian, M.; Ostergaard, L. Live Streptococcus Pneumoniae, Haemophilus Influenzae, and Neisseria Meningitidis Activate the Inflammatory Response through Toll-like Receptors 2, 4, and 9 in Species-Specific Patterns. *J Leukoc Biol* **2006**, *80* (2), 267–277.

2. A Synthetic Pathogen Mimetic Molecule Induces a Highly Amplified Synergistic Immune Response via Activation of Multiple Signaling Pathways

2.1 Summary

The current understanding of how the immune system processes complex information during natural infections is yet to be exploited for the molecular design of potent immune activators. Here, we address this challenge by the design and synthesis of a pathogen-mimetic molecule that simultaneously co-stimulates cell-surface, endosomal, and cytosolic immune receptors. The co-activation of TLR2, NOD2, and NLRP3 resulted in synergistic enhancement of the innate immune response and the downstream adaptive immune response.

2.2 Introduction

The immune system has evolved to identify complex combinations of microbial patterns and exploit the interdependencies of various microbial signals to generate an effective response during infections.[1] Whole-cell vaccine derived from live pathogens can mimic such responses, thereby generating robust lifelong immunity.[2,3] However, the generation of a robust response has remained elusive with subunit vaccines that consist of protein antigens. A major roadblock is the rational design of efficacious immunostimulants, or adjuvants employed in these vaccines. For instance, traditionally employed aluminum salt adjuvants primarily induce T-helper cell 2 (Th2) biased responses and fail to generate robust antigen-specific cellular responses.[4–7] Furthermore, adjuvants developed by targeting pathogen-sensing pathways such as MPLA and CpG, only activate a single immune signaling pathway, thereby poorly mimicking the mechanisms of pathogen recognition. Thus, the design and development of molecules that integrate complex

mechanisms of pathogen signaling, to generate robust immune activation remains both a challenge and necessity.

2.3 Results and Discussion

2.3.1 Design and Synthesis

In our attempt to explore pathogen sensing through molecular design, we previously demonstrated the development of multi-Toll-like receptor (TLR) agonist adjuvants by covalently linking three TLR agonists.[8-10] These studies employed the use of a triazine scaffold to install unique combinations of three TLR-agonists using sequential orthogonal conjugation chemistry. The TLR tri-agonists synthesized include TLR2/6_4_7, TLR2/6_4_9, TLR1/2_4_9, TLR1/2_4_7, and TLR4_7_9.[8,9] Each tri-agonist combination elicited unique cytokine responses and generated tailored immune response when applied in vaccines.[9,10] However, recent studies of various immune signaling pathways during infections have demonstrated the critical importance of crosstalk between different classes of pathogen sensing pathways involving various cellular compartments.[11–15] For instance, a study by Mellman and coworkers demonstrated that bacterial sensing by cell-surface TLR receptors in innate immune cells leads to the overexpression of endo-lysosomal peptide transporters, and the generation of endosomal membrane tubules. This serves to prime cells for any subsequent detection of bacterial NOD2 ligands at the endosomal membrane.[16] Furthermore, studies on NLRP3 inflammasome activation - which plays a critical role in pathogen clearance - has demonstrated that a TLR dependent priming signal is necessary for robust NLRP3 activation. This indicates the interdependencies of these two signaling responses.[17–21]

However, such mechanistic findings are yet to be exploited in the design of molecular systems that induce co-operativity and synergism between multiple pathogen-sensing pathways to

generate robust immune responses. Hence, the critical question is: can well-known pairwise synergistic immune activation be effectively combined in a synthetic system to generate higher-order interactions similar to microbial sensing? To understand the dynamics of such cellular

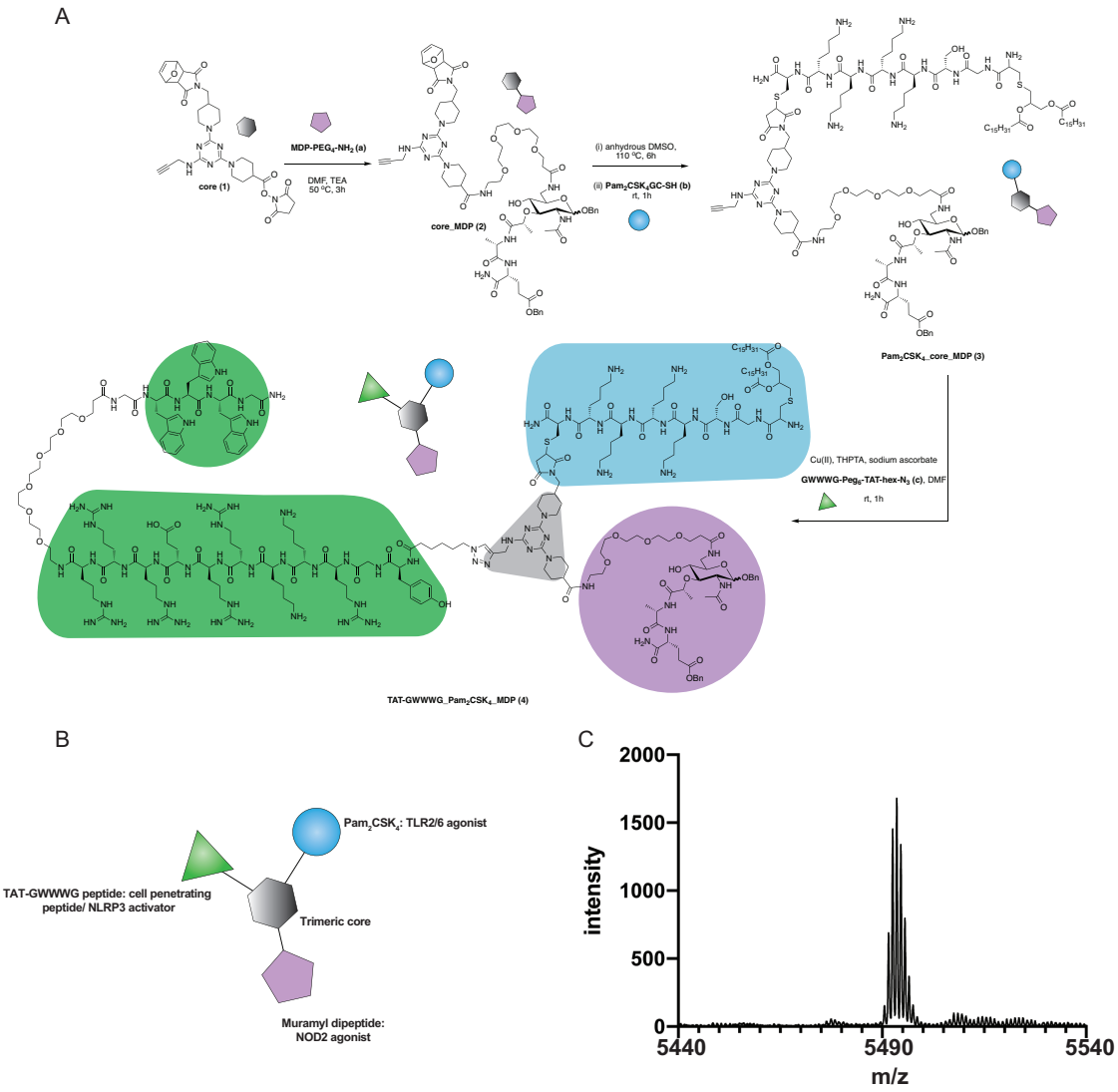

Figure 2.1. Synthesis of TAT-GWWWG_Pam2CSK4_MDP tri-agonist (4). (A) Synthesis Scheme (B): Schematic presentation of the linked tri-agonist. (C): MALDI trace of the linked tri-agonist.

signaling processes at a molecular level, here we report a new class of immunomodulators that elicits activation of three distinct classes of pathogen-sensing pathways involving distinct cellular compartments like a pathogen.

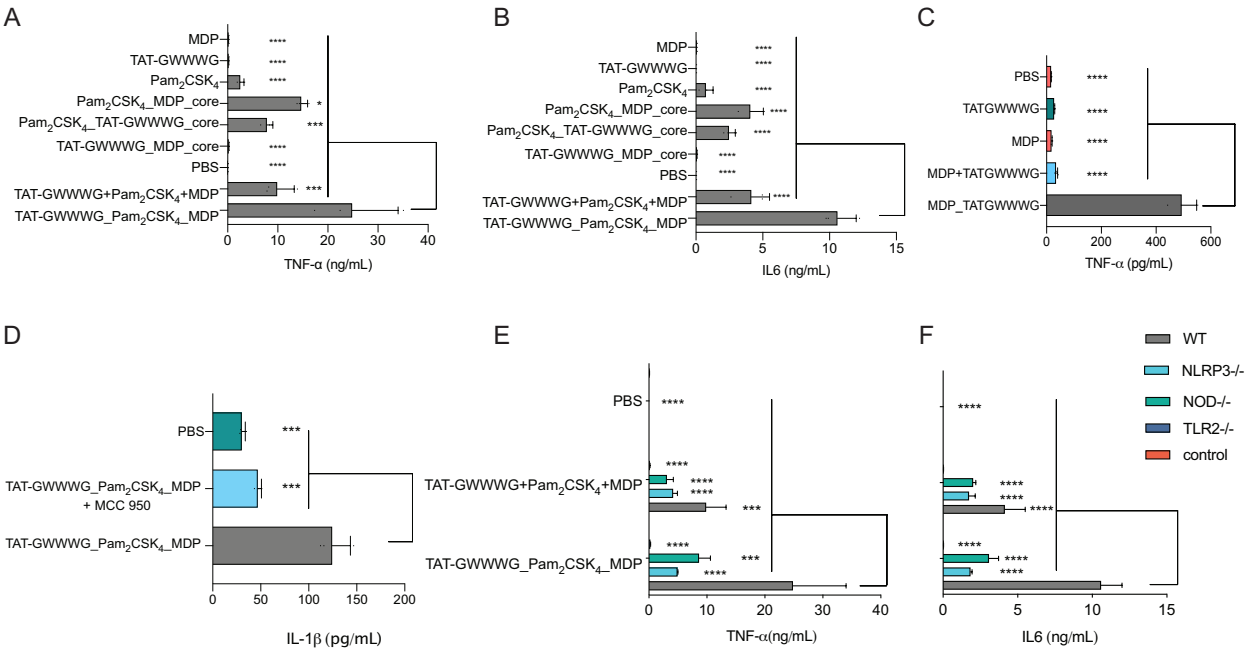

Figure 2.2. In vitro cytokine expression from BMDCs. (A), (B): Cells were incubated with linked PRR tri-agonist, a 1:1:1 (molar ratio) mixture of unlinked PRR agonists, various linked di-agonist combinations and single agonists (100 nM each) at 37ºC for 6 h. TNF-a (A) and IL-6 (B) measured by CBA. (C): In vitro TNF-a expression from BMDCs as measured by ELISA. Cells were incubated with MPD_TATGWWWG (25 μM) or a 1:1 (molar ratio) mixture of the analogous unlinked agonists for 24 h at 37 °C. (D): Analysis of NLRP3 activity (IL-1b secretion) by ELISA. Cells were preincubated with NLRP3 inhibitor MCC-950 (10 mM) for 1 h and then stimulated with linked PRR tri-agonist (10 mM) at 37ºC for 24 h. Inhibition of NLRP3 via MCC-950 results in loss of IL-1b activity. (E), (F): Analysis of TNF-a and IL-6 with WT, TLR2-/-, NOD2 -/- and NLRP3-/- cells treated with linked PRR tri-agonist or unlinked agonists (100 nM). Samples were run in triplicate, where * $p < 0.05$, *** $p < 0.001$, ****$p < 0.0001$. Statistical analysis performed using ANOVA with Turkey's multiple comparison test.

The design of our pathogen-mimetic immunomodulator incorporated a surface-active TLR2, an endosomal-membrane active NOD2 and cytosolic NLRP3 inflammasome activating

ligands. We thereby assembled Pam_2CSK_4[22] (TLR2/6 agonist, synthetic analogue of bacterial lipoprotein), Muramyl dipeptide[23] (MDP, NOD2 agonist: the minimal immunomodulatory structure of bacterial cell wall peptidoglycan), and TAT-GWWWG peptide[24] (cell-penetrating peptide, NLRP3 activator) on a trimeric scaffold (**Figure 2.1**).

The motivation behind this design was to induce crosstalk between each component and enhance NOD2 and NLRP3 inflammasome activation following initial cellular priming by cell-surface TLR2 stimulation.[16,24]Additionally, we hypothesized that MDP when chemically conjugated to TAT-GWWWG would result in enhanced NOD2 activation and this proved to be true (Figure **2.2C**). We conjecture that this enhancement in response is the result of increased cytosolic delivery of MDP mediated by TAT-GWWWG.[25–27]

The synthesis of our tri-agonist molecule (4) employed sequential conjugation chemistry used previously in the synthesis of TLR tri-agonists.[8,9] The synthesis started with development of a triazine core (1) with three orthogonal conjugation handles consisting of an NHS ester, an alkyne, and a protected maleimide (Appendix A, **Scheme S1**).[8,9,28] Following this, amine-functionalized MDP (a, Appendix A **Scheme S2**)[29] was conjugated to core (1) using NHS chemistry to give core_MDP (2). The core_MDP was then heated to 110ºC for 6 h to reveal active maleimide via furan deprotection, following which cysteine-modified Pam_2CSK_4 (b) was conjugated via thiol-maleimide reaction give Pam_2CSK_4_core_MDP (3). This was followed by conjugation of azide-functionalized TAT-GWWWG peptide (c) to Pam_2CSK_4_core_MDP (3) via Cu(I) catalyzed cycloaddition chemistry to afford the final tri-agonist molecule (4, SI for synthetic details, purification & characterization).

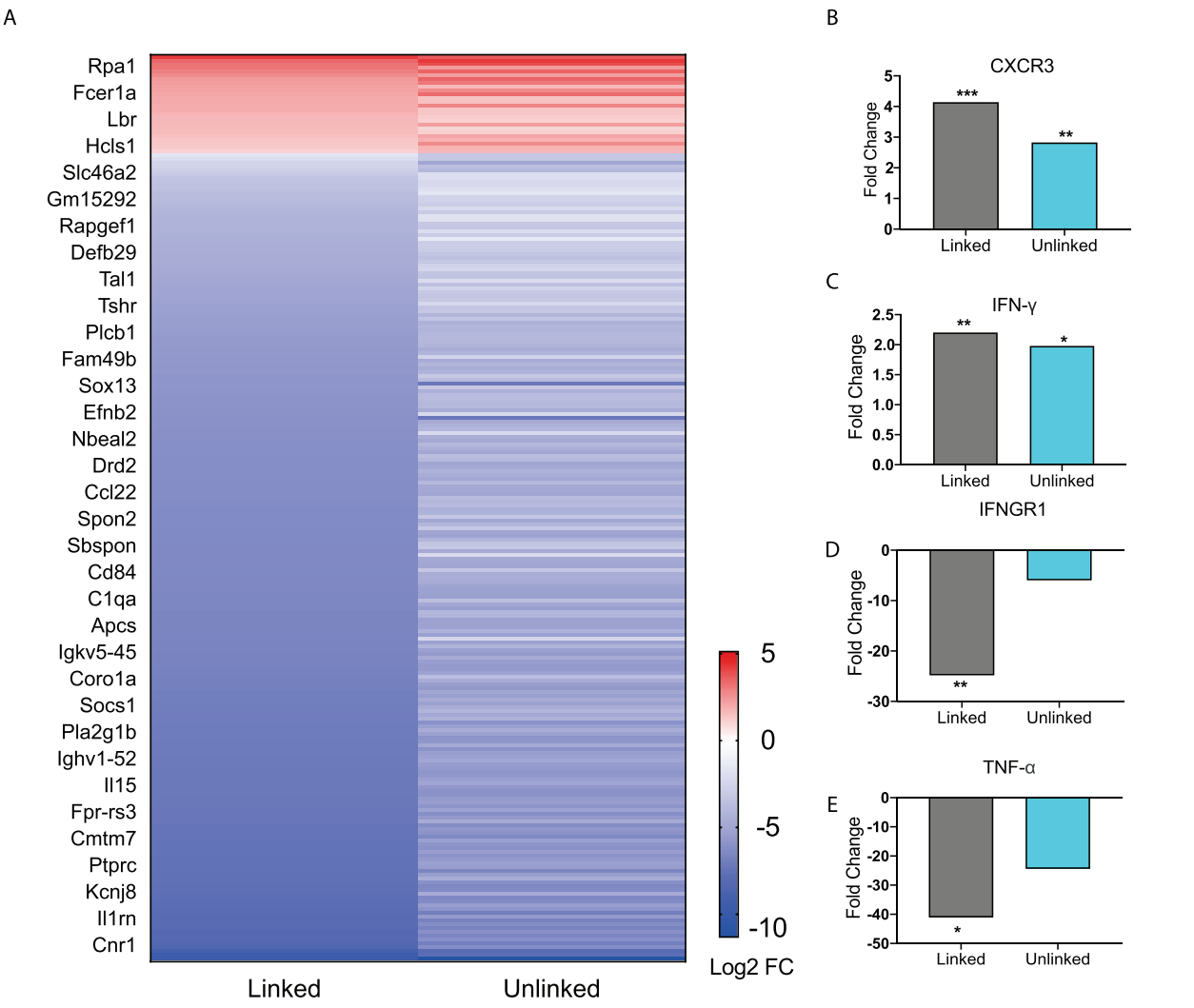

Figure 2.3. BMDC gene expression profile data. (A) Heat map of immune function related genes. Each figure represents the average of three independent experiments. BMDCs were incubated as untreated, or with either the linked or unlinked tri-agonist combination for 6 h at 37 °C. RNA was then extracted and sequenced on a NextSeq550. The gene expression of the BMDCs in response to unlinked and linked tri-agonist stimulation was compared to unstimulated BMDCs to determine the differential gene expression profiles. Included in the heatmap are only immune-associated genes with p value < 0.05 for either the linked or unlinked tri-agonists relative to unstimulated BMDCs and a 2-fold change in expression. (B), (C), (D), (E): Fold change in gene expression for CXCR3, IFN-γ, TNF-α, IFNGR1 in BMDCs in response to linked and unlinked tri-agonist combination where *p < 0.05, **p < 0.01, and ***p<0.001. P-values are calculated relative to unstimulated BMDCs.

Additionally, all the dimeric agonist compounds, PAM_2CSK_4_MDP (3, Appendix A, **Scheme S3**), PAM_2CSK_4_TAT-GWWWG (7, SI **Scheme S4**) and MDP_TAT-GWWWG (8, Appendix A, **Scheme S5**) were also synthesized to measure the contribution of di-agonist components to the immune response.

2.3.2 *In vitro* experiments

Following synthesis, we next proceeded to analyze the immunological properties of the tri-agonist. We analyzed the cytokine profile elicited by murine bone marrow-derived dendritic cells (BMDCs) *in vitro* on stimulation with the tri- agonist (100 nM) or equivalent amount of unlinked agonists mixture for 6 h. Parallel studies were performed by incubating equivalent quantities of linked di-agonists and single agonists as well. Analysis of levels of cytokines secreted by agonist stimulation indicated that the linked tri-agonist combination elicited at least 70%±60% (95% Confidence interval, CI) higher TNF-a and 160%±53% higher IL-6 production compared to the most potent di-agonist combination (**Figure 2.2A**, **2.2B**). Most notably, compared to an equivalent mixture of unlinked agonists, linking the three ligands boosted the synergistic IL-6 secretion by 155%±52% and TNF-a secretion by 151%±95% (**Figure 2.2A, 2.2B**). These results indicated that synergistic cellular co-activation by localization of these microbial signals induced crosstalk to enhance immune activation.[30] With these exciting results, we next proceeded to analyze whether the tri-agonist activated all the target pathogen sensing pathways. We thereby analyzed cytokine secretion elicited by the tri-agonist stimulation on wild type (WT) BMDCs along with TLR2, NOD2 and NLRP3 knockout BMDCs (**Figure 2.2D, 2.2E**). It was observed that TLR2 knockout BMDCs expressed near background level cytokines indicating that TLR signaling orchestrates the

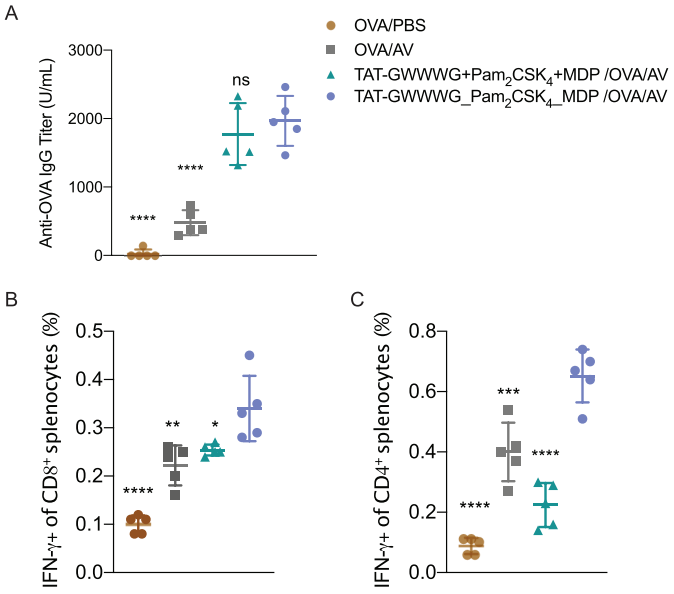

Figure 2.4. *In-vivo* Vaccination studies. Mice (n=5) were vaccinated on day 0 with OVA (100 mg) adjuvanted with PBS (vehicle control), or Addavax (25 mL), or 5 nmole each of unconjugated multi-PRR agonist, in Addavax (AV, 25 mL), or 5 nmole of linked tri-agonist in Addavax (25 mL). Final volume of each formulation was made 50 mL with PBS. Mice were given a vaccine boost on day 14. On day 24, sera, spleens were collected from mice. Antibody titer was measured by ELISA and T cell response was measured by intracellular cytokine staining. ns = non-significant, * $p < 0.05$, ** $p < 0.01$, *** $p < 0.001$, **** $p < 0.0001$. Statistical analysis is performed between the linked tri-agonist and indicated groups using ANOVA by the Turkey's multiple comparison test.

immune activation and primes other signaling pathways. Intriguingly, the NOD2 knockout BMDCs expressed 65%±54% lower TNF-a and 70%±20% lower IL-6 levels compared to the WT BMDCs implying a significant enhancement in immune response due to crosstalk between NOD2 and TLR2 receptors. Similarly, NLRP3 knockout BMDCs elicited lower cytokine responses (TNF-a, IL-6) compared to WT BMDCs (**Figure 2.2D, 2.2E**). However, such effects might also be the result of reduction in MDP activity observed in NLRP3 -/- cells. To further validate NLRP3-infllammasome activation by the tri-agonist, we analyzed for secretion of IL-1b, a common marker of inflammasome activation.[19,21] Stimulation with the tri-agonist resulted in 600%±130% higher

levels of IL-1b compared to an equivalent mixture of unlinked agonists (Appendix A, **Figure S1**). Additionally, studies with the tri-agonist with WT BMDCs along with MCC-950, a NLRP3 specific inhibitor displayed a 62%±20% reduction in IL-1b activity, thereby validating NLRP3 activation (**Figure 2.2C**).[31,32]

Our studies indicated complex dynamics of cellular co-activation. To further analyze these responses, we studied the transcriptional response in BMDCs upon stimulation with unlinked agonists and linked tri-agonist. The RNA of BMDCs was extracted after 6 h of stimulation with the agonists or PBS and differential gene expression was compared. As seen in the heatmap (**Figure 2.3A**), we observed a similar trend in responses when the BMDCs were activated with the unlinked agonists or linked tri-agonist.

However, key differences exist in magnitude of this regulation. For instance, compared to the unlinked mixture, the linked tri-agonist generated higher expression of CXCR3, a key receptor for interferon induced chemo-attractants that helps differentiate naïve T cells into T_h1 effector T cells (**Figure 2.3B**).[33,34] Additionally, it induced greater differences in expression for both interferon-gamma (IFN-γ) and interferon gamma receptor 1 (IFNGR1) – which dimerizes with IFNGR2 to detect IFN-γ (**Figure 2.3C, 2.3D**). The greater upregulation of IFN-γ, along with the greater downregulation of IFNGR1, indicates the tri-agonist induces high levels of IFN-γ signaling. This can possibly be an effect of enhanced IL-18 secretion due to inflammasome activation by the linked tri-agonist.[35] We hypothesize this high expression of CXCR3 and IFN- γ with the linked tri-agonist would induce robust tailored T cell responses, specifically T_h1 polarized responses.

Although high cytokine levels of TNF-α was observed at 6 h, the transcriptional levels of TNF-α were strongly downregulated at the same time point. This difference in response is likely down to kinetics, as TNF-α is an inflammatory response gene that does not require new protein

synthesis (**Figure 2.3E**). As a result, TNF-α transcription is commonly upregulated at earlier timepoints and peaks within 2 h of stimulation, supporting this difference in the transcriptional levels compared to the cytokine levels.[36]

2.3.3 *In vivo* experiments

With promising *in vitro* results and the indication of robust tailored cellular responses, we proceeded to determine if amplified immune response from the linked tri-agonist would translate to its use as a vaccine adjuvant *in vivo*. Groups of five mice were immunized via IM injection with ovalbumin (OVA, 100 mg) adjuvanted with linked tri-agonist (5 nmol) or equivalent quantities of unlinked agonist mixture. Vaccines were formulated in Addavax (AV), an MF-59 like oil-in-water nano-emulsion.[37] Parallel studies were also performed with unadjuvanted OVA or OVA admixed with Addavax as controls. Mice were boosted in an identical fashion on day 14. On day 24 blood sera were collected to analyze for antibody titer (**Figure 2.4A**) and splenocytes were harvested to analyze for antigen-specific T cell responses (**Figure 2.4B, 2.4C)**. It was observed that the linked tri-agonist formulation enhanced IFN-g secreting $CD4^+$ T cells response by 200%±60% and IFN-g secreting $CD8^+$ T cells response by 40%±30% compared to unlinked combination of agonists (**Figure 2.4B, 2.4C)**. It also elicited 300%±115% higher antibody responses compared to OVA/Addavax formulation (**Figure 2.4A**). However, the antibody response to the linked and the unlinked combination was similar. There can be various reasons for this observation. Mainly, just as TLR2 activation was the main driver of the *in vitro* cytokine response **(Figure 2.2E, 2.2F),** it is possible that the antibody response is also primarily driven by TLR2 engagement. As a result of which there is not much difference between the linked and the unlinked combinations. Moreover, the most important find is that the linked combination enhances both $CD8^+$ and $CD4^+$ T cell

response relative to the unlinked combination. It can be envisioned that the adjuvanticity of the tri-agonist can be improved by making structural changes to the construct. We are currently exploring the use of D configuration amino acids instead of L amino acids for the synthesis of TAT-GWWWG which will possibly make it more resistant to proteolysis. Also, the potency of the tri-agonist maybe improved by using Murabutide, a more potent NOD2 activator compared to Muramyl dipeptide. These changes will likely improve the NOD2 and NLRP3 activation and improve humoral and cellular responses. Additionally, formulation development to enhance pharmacokinetics may improve the activity of the tri-agonist. Nevertheless, these results demonstrated that the tri-agonist served as a potent adjuvant *in vivo* which provides a unique immune stimulatory method with the potential to improve cellular responses in vaccine adjuvants.

2.4 Conclusions

In our previous work on polyvalent TLR agonist we demonstrated that TLR tri-agonist stimulate distinct, combination-dependent innate immune responses. Building on the understanding on dynamics of cellular co-activation of innate immune signaling pathways, here we developed a small-molecule tri-agonist inspired by the mechanisms of stimulation of multiple different pattern-sensing pathways by a pathogen. It gave us insight into how pathogen-sensing pathways respond to multiple input signals as is often the case with infections. Our data reveals that the complex combinatorial logic of pathogen sensing pathways can be incorporated in molecular design to modulate the innate immune system. Our studies also indicated that trimeric combinations of pairwise interactions between multiple pathogen sensing pathways can generate complex higher-order interactions that is not achieved in an unconstrained system or with dimeric interactions. This work thus provides a framework to harness complex pathogen sensing in

designing efficacious pathogen-mimetic immune therapies. This study thus provides a framework to rationally design other multi-agonist constructs with highly synergistic immune activation. We are currently expanding our toolkit and employing the tri-agonists for application in various infectious disease vaccines.

2.5 Materials and Methods

Reagents and Instrumentation. Unless otherwise stated all chemicals were purchased from commercial sources and were used as received. All chemical reactions were carried out in dried glassware using anhydrous solvents under Argon gas. Reagents were purchased from Sigma-Aldrich, Bachem, ThermoFisher, Quanta Biodesign, Anaspec, Broadpharm or Acros Organics. Buffers and media for cell culture were purchased from Fisher Life Technologies. Addavax was purchased from Invivogen. Absorbance for ELISA was measured on a Fisher Scientific MultiSkan FC. Cytometric bead array data was acquired on a Novocyte flow cytometer. ^{1}H and ^{13}C NMR spectra were taken on a Bruker 500 NMR spectrometer (500 MHz) or 400 NMR spectrometer (400 MHz) and analyzed using MestreNova software. Spectra are referenced to solvent peak for 1H NMR (CD3OD = 3.33 ppm, (CD3)2SO = 2.50 ppm, CDCl3 = 7.26 ppm) and 13C NMR (CD3OD = 49.00 ppm, (CD3)2SO = 39.52 ppm, CDCl3 = 77.16 ppm). Peptides were synthesized via solid phase peptide synthesis on an automated microwave peptide synthesizer (Liberty Bllue, CEM) Analytical high-performance liquid chromatography (HPLC) was performed using an Agilent 1260 Infinity HPLC with a Phenomenex Luna 3 μm C8 100 Å 150 x 4.6 mm LC column. Preparative HPLC was performed on a Gilson Preperative HPLC System with 333 HPLC Pumps and GX-271 liquid handler using a Phenomenex Luna 5 μm C8(2) 100 Å 150 x 21.2 mm LC column. Electrospray ionization – mass spectrometry (ESI-MS) was performed on an Agilent 6130

LC MS. MALDI-TOF was performed on Bruker ultraflextreme MALDI-TOF-TOF system. Silica Gel Chromatography was performed using RediSep Rf normal silica columns on a Teledyne-Isco CombiFlash Rf auto column instrument. Data were analyzed using one-way ANOVA in Graph Pad Prism software. All values were reported as mean ± SD, where error bars represent biological replicates.

BMDC activation studies: Bone marrow derived dendritic cells (BMDCs) were harvested from the femurs of 6-week-old C57BL/6 mice (Jackson Laboratory). BMDCs were cultured in BMDC primary medium: RPMI 1640 (Life Technologies), 10% heat inactivated fetal bovine serum (FBS), 20 ng/mL granulocyte-macrophage colony-stimulating factor (GM-CSF), 2 mM L-glutamine (Life Technologies), antibioticantimycotic (1×) (Life Technologies), and 50 μM betamercaptoethanol (all components were 0.2 μM sterile filtered together before use). For BMDC activation studies, 2×10^5 cells per well were seeded in round-bottom 48-well plates and treated with various concentrations of linked PRR tri-agonist or 1:1:1(molar ratio) mixture of the analogous unlinked PRR agonists or various linked di-agonist combination, then incubated at 37 °C. The supernatants were collected after 6 h or 24 h. Cytokine concentration in the media were measured either by mouse inflammation kit CBA (BD Biosciences) or ELISA kits (BioLegend) following manufacturer's instructions.

NLRP3 inhibition studies

For NLRP3 inhibition studies, 2×10^5 cells per well were seeded in round-bottom 48-well plates and treated with 10 μM of MCC-950 at 37 ^{o}C for 1 h followed by addition of 10 μM of PRR tri-agonist for 24 h. Samples were collected and analyzed for IL-1b by ELISA kit (BioLegend) as per manufacturer's instructions.

***In-vitro* cytokine analysis by cytometric bead array (CBA).** CBA mouse inflammation kit was purchased from BD Biosciences. BMDCs were plated in 48 well plates (4 x 10^5 cells in 400 µL) and stimulated with indicated sample for 6 h. The supernatant was transferred to Eppendorf tubes and centrifuged at 1000 x g for 10 minutes. The supernatant was removed and diluted by a factor of 2.5. The assay was then performed following manufacturers protocol and analyzed by a Novocyte flow cytometer. Data were analyzed using Graphpad Prism software.

***In-vitro* cytokine analysis by ELISA.** BMDCs were plated in 48 well plates (4 x 10^5 cells in 400 µL) and stimulated with indicated sample at 37 ^oC for 24 h. The supernatants were assessed by ELISA for IL-1b. ELISA kits were purchased from Biolegend and used according to instruction manual. Samples were undiluted.

RNA sequencing and analysis. BMDCs were incubated with the linked and unlinked tri-agonist combinations for 6 h. RNA was extracted using a Direct-zol RNA-Microprep kit (Zymo), prepped using SMARTer® Stranded Total RNA-Seq Kit v2 (Takara), and sequenced on a NextSeq550 (Illumina). RNA seq reads were mapped to GRCm38 mouse reference genome using STAR version 2.7.0b. The resulting files from the alignment step above were taken to evaluate transcriptional expression using subread::feature counts with gencode transcript annotation M19 by comparing BMDc's with linked or unlinked trimer activation to unstimulated BMDCs. The obtained count table was normalized and log fold change in expression was generated using the edgeR package. Immune genes with pval <.05 and 2-fold differential expression for at least one of the dosing conditions are considered in the analysis.

***In-vivo* studies.** All animal experiments were approved by Institutional Animal Care and Use Committee (IACUC), University of Chicago (72517). Mice (n=5) were vaccinated on day 0 with OVA (100 ug) adjuvanted with PBS (vehicle control), or Addavax (25 uL), or 5 nmole each of

unconjugated multi-PRR agonist (TAT-GWWWG+Pam_2CSK_4+MDP) in Addavax (AV, 25 uL), or 5 nmole of conjugated agonists (TAT-GWWWG_Pam_2CSK_4_MDP) in Addavax (25 uL). Final volume of each formulation was made 50 uL with PBS. Mice were given a vaccine boost on day 14. On day 24, sera and spleens were collected from mice. Antibody titer was measured by ELISA and T cell response was measured by intracellular cytokine staining.

T-cell recall assays: Spleens were collected from mice on day 24 and incubated in ice-cold RPMI until processing. Spleens were processed into a single-cell suspension via mechanical disruption and passaged through a 70 μm strainer. The splenocytes were washed with PBS and then treated with RBC lysis buffer for 3 min at room temperature. The single-cell suspension was washed with PBS and resuspended in RPMI. These single cell suspensions were then plated at a density of 10^7 cells/mL and treated with respective peptide epitopes (20 mg/mL). Following two hours of incubation, golgi plug (Brefeldin A) was added and the cells were additionally stimulated for 6 h more. Following incubation, cells were stained with viability stain and for appropriate cell surface markers (CD4, CD8) and intracellular cytokine staining was performed for IFN-g. Samples were analyzed on a NovoCyte 3000 flow using the NovoExpress software. Total numbers of spleen/LN lymphocytes were back-calculated from the number of marker-positive cells read and the total volume of sample processed by the NovoCyte 3000 flow cytometer.

Measurement of the anti-OVA IgG response: Blood was collected by cardiac puncture from mice on day 24 and serum was separated by centrifugation and stored at −20 °C. Sera was assayed for antibody levels against OVA using ELISA kit (Alpha Diagnostics) following manufacturer's protocol. The absorbance was measured at 450 nm in a microtiter-plate spectrophotometer using a blank measurement at 620 nm.

2.6 REFERENCES

1. Pandey, S.; Gruenbaum, A.; Kanashova, T.; Mertins, P.; Cluzel, P.; Chevrier, N. Pairwise Stimulations of Pathogen-Sensing Pathways Predict Immune Responses to Multi-Adjuvant Combinations. *cels* **2020**, *11* (5), 495-508.e10.

2. Pulendran, B. Learning Immunology from the Yellow Fever Vaccine: Innate Immunity to Systems Vaccinology. *Nature Reviews Immunology* **2009**, *9* (10), 741–747.

3. Querec, T.; Bennouna, S.; Alkan, S.; Laouar, Y.; Gorden, K.; Flavell, R.; Akira, S.; Ahmed, R.; Pulendran, B. Yellow Fever Vaccine YF-17D Activates Multiple Dendritic Cell Subsets via TLR2, 7, 8, and 9 to Stimulate Polyvalent Immunity. *J Exp Med* **2006**, *203* (2), 413–424.

4. Mount, A.; Koernig, S.; Silva, A.; Drane, D.; Maraskovsky, E.; Morelli, A. B. Combination of Adjuvants: The Future of Vaccine Design. *Expert Review of Vaccines* **2013**, *12* (7), 733–746.

5. Mutwiri, G.; Gerdts, V.; Hurk, S. van D. L. den; Auray, G.; Eng, N.; Garlapati, S.; Babiuk, L. A.; Potter, A. Combination Adjuvants: The next Generation of Adjuvants? *Expert Review of Vaccines* **2011**, *10* (1), 95–107.

6. Guy, B. The Perfect Mix: Recent Progress in Adjuvant Research. *Nat Rev Microbiol* **2007**, *5* (7), 396–397.

7. Seder, R. A.; Hill, A. V. S. Vaccines against Intracellular Infections Requiring Cellular Immunity. *Nature* **2000**, *406* (6797), 793–798.

8. Tom, J. K.; Dotsey, E. Y.; Wong, H. Y.; Stutts, L.; Moore, T.; Davies, D. H.; Felgner, P. L.; Esser-Kahn, A. P. Modulation of Innate Immune Responses *via* Covalently Linked TLR Agonists. *ACS Cent. Sci.* **2015**, *1* (8), 439–448.

9. Albin, T. J.; Tom, J. K.; Manna, S.; Gilkes, A. P.; Stetkevich, S. A.; Katz, B. B.; Supnet, M.; Felgner, J.; Jain, A.; Nakajima, R.; Jasinskas, A.; Zlotnik, A.; Pearlman, E.; Davies, D. H.; Felgner, P. L.; Burkhardt, A. M.; Esser-Kahn, A. P. Linked Toll-Like Receptor Triagonists Stimulate Distinct, Combination-Dependent Innate Immune Responses. *ACS Cent. Sci.* **2019**, *5* (7), 1137–1145.

10. Gilkes, A. P.; Albin, T. J.; Manna, S.; Supnet, M.; Ruiz, S.; Tom, J.; Badten, A. J.; Jain, A.; Nakajima, R.; Felgner, J.; Davies, D. H.; Stetkevich, S. A.; Zlotnik, A.; Pearlman, E.; Nalca, A.; Felgner, P. L.; Esser-Kahn, A. P.; Burkhardt, A. M. Tuning Subunit Vaccines with Novel TLR Triagonist Adjuvants to Generate Protective Immune Responses against *Coxiella Burnetii*. *J.I.* **2020**, *204* (3), 611–621.

11. Kawai, T.; Akira, S. Toll-like Receptors and Their Crosstalk with Other Innate Receptors in Infection and Immunity. *Immunity* **2011**, *34* (5), 637–650.

12. Ferwerda, G.; Girardin, S. E.; Kullberg, B.-J.; Le Bourhis, L.; de Jong, D. J.; Langenberg, D. M. L.; van Crevel, R.; Adema, G. J.; Ottenhoff, T. H. M.; Van der Meer, J. W. M.; Netea, M. G. NOD2 and Toll-Like Receptors Are Nonredundant Recognition Systems of Mycobacterium Tuberculosis. *PLoS Pathog* **2005**, *1* (3).

13. Oviedo-Boyso, J.; Bravo-Patiño, A.; Baizabal-Aguirre, V. M. Collaborative Action of Toll-Like and Nod-Like Receptors as Modulators of the Inflammatory Response to Pathogenic Bacteria. *Mediators of Inflammation* **2014**, *2014*, e432785.

14. van Heel, D. A.; Ghosh, S.; Hunt, K. A.; Mathew, C. G.; Forbes, A.; Jewell, D. P.; Playford, R. J. Synergy between TLR9 and NOD2 Innate Immune Responses Is Lost in Genetic Crohn's Disease. *Gut* **2005**, *54* (11), 1553–1557.

15. Pavot, V.; Rochereau, N.; Rességuier, J.; Gutjahr, A.; Genin, C.; Tiraby, G.; Perouzel, E.; Lioux, T.; Vernejoul, F.; Verrier, B.; Paul, S. Cutting Edge: New Chimeric NOD2/TLR2 Adjuvant Drastically Increases Vaccine Immunogenicity. *J.I.* **2014**, *193* (12), 5781–5785.

16. Nakamura, N.; Lill, J. R.; Phung, Q.; Jiang, Z.; Bakalarski, C.; de Mazière, A.; Klumperman, J.; Schlatter, M.; Delamarre, L.; Mellman, I. Endosomes Are Specialized Platforms for Bacterial Sensing and NOD2 Signalling. *Nature* **2014**, *509* (7499), 240–244.

17. Swanson, K. V.; Deng, M.; Ting, J. P.-Y. The NLRP3 Inflammasome: Molecular Activation and Regulation to Therapeutics. *Nature Reviews Immunology* **2019**, *19* (8), 477–489.

18. Yang, Y.; Wang, H.; Kouadir, M.; Song, H.; Shi, F. Recent Advances in the Mechanisms of NLRP3 Inflammasome Activation and Its Inhibitors. *Cell Death & Disease* **2019**, *10* (2), 1–11.

19. Schroder, K.; Tschopp, J. The Inflammasomes. *Cell* **2010**, *140* (6), 821–832.

20. Lamkanfi, M.; Dixit, V. M. Modulation of Inflammasome Pathways by Bacterial and Viral Pathogens. *The Journal of Immunology* **2011**, *187* (2), 597–602.

21. Guo, H.; Callaway, J. B.; Ting, J. P.-Y. Inflammasomes: Mechanism of Action, Role in Disease, and Therapeutics. *Nature Medicine* **2015**, *21* (7), 677–687.

22. Bessler, W. G.; Cox, M.; Lex, A.; Suhr, B.; Wiesmüller, K. H.; Jung, G. Synthetic Lipopeptide Analogs of Bacterial Lipoprotein Are Potent Polyclonal Activators for Murine B Lymphocytes. *The Journal of Immunology* **1985**, *135* (3), 1900–1905.

23. Girardin, S. E.; Boneca, I. G.; Viala, J.; Chamaillard, M.; Labigne, A.; Thomas, G.; Philpott, D. J.; Sansonetti, P. J. Nod2 Is a General Sensor of Peptidoglycan through Muramyl Dipeptide (MDP) Detection. *J. Biol. Chem.* **2003**, *278* (11), 8869–8872.

24. Manna, S.; Howitz, W. J.; Oldenhuis, N. J.; Eldredge, A. C.; Shen, J.; Nihesh, F. N.; Lodoen, M. B.; Guan, Z.; Esser-Kahn, A. P. Immunomodulation of the NLRP3 Inflammasome through

Structure-Based Activator Design and Functional Regulation via Lysosomal Rupture. *ACS Cent. Sci.* **2018**, *4* (8), 982–995.

25. Lönn, P.; Kacsinta, A. D.; Cui, X.-S.; Hamil, A. S.; Kaulich, M.; Gogoi, K.; Dowdy, S. F. Enhancing Endosomal Escape for Intracellular Delivery of Macromolecular Biologic Therapeutics. *Scientific Reports* **2016**, *6* (1).

26. Erazo-Oliveras, A.; Najjar, K.; Dayani, L.; Wang, T.-Y.; Johnson, G. A.; Pellois, J.-P. Protein Delivery into Live Cells by Incubation with an Endosomolytic Agent. *Nature Methods* **2014**, *11* (8), 861–867.

27. Derakhshankhah, H.; Jafari, S. Cell Penetrating Peptides: A Concise Review with Emphasis on Biomedical Applications. *Biomedicine & Pharmacotherapy* **2018**, *108*, 1090–1096.

28. Banerjee, R.; Pace, N. J.; Brown, D. R.; Weerapana, E. 1,3,5-Triazine as a Modular Scaffold for Covalent Inhibitors with Streamlined Target Identification. *J. Am. Chem. Soc.* **2013**, *135* (7), 2497–2500.

29. Grimes, C. L.; Podolsky, D. K.; O'Shea, E. K. Synthesis of Biologically Active Biotinylated Muramyl Dipeptides. *Bioorganic & Medicinal Chemistry Letters* **2010**, *20* (20), 6061–6063.

30. Lin, B.; Dutta, B.; Fraser, I. D. C. Systematic Investigation of Multi-TLR Sensing Identifies Regulators of Sustained Gene Activation in Macrophages. *Cell Systems* **2017**, *5* (1), 25-37. e3.

31. Coll, R. C.; Hill, J. R.; Day, C. J.; Zamoshnikova, A.; Boucher, D.; Massey, N. L.; Chitty, J. L.; Fraser, J. A.; Jennings, M. P.; Robertson, A. A. B.; Schroder, K. MCC950 Directly Targets the NLRP3 ATP-Hydrolysis Motif for Inflammasome Inhibition. *Nature Chemical Biology* **2019**, *15* (6), 556–559.

32. Coll, R. C.; Robertson, A. A. B.; Chae, J. J.; Higgins, S. C.; Muñoz-Planillo, R.; Inserra, M. C.; Vetter, I.; Dungan, L. S.; Monks, B. G.; Stutz, A.; Croker, D. E.; Butler, M. S.; Haneklaus, M.; Sutton, C. E.; Núñez, G.; Latz, E.; Kastner, D. L.; Mills, K. H. G.; Masters, S. L.; Schroder, K.; Cooper, M. A.; O'Neill, L. A. J. A Small-Molecule Inhibitor of the NLRP3 Inflammasome for the Treatment of Inflammatory Diseases. *Nature Medicine* **2015**, *21* (3), 248–255.

33. Maurice, N. J.; McElrath, M. J.; Andersen-Nissen, E.; Frahm, N.; Prlic, M. CXCR3 Enables Recruitment and Site-Specific Bystander Activation of Memory CD8 + T Cells. *Nature Communications* **2019**, *10* (1), 4987.

34. Yoon, S. H.; Yun, S. O.; Park, J. Y.; Won, H. Y.; Kim, E.-K.; Sohn, H.-J.; Cho, H.-I.; Kim, T.-G. Selective Addition of CXCR3 + CCR4 - CD4 + Th1 Cells Enhances Generation of Cytotoxic T Cells by Dendritic Cells in Vitro. *Experimental & Molecular Medicine* **2009**, *41* (3), 161–170.

35. Stober, D.; Schirmbeck, R.; Reimann, J. IL-12/IL-18-Dependent IFN-γ Release by Murine Dendritic Cells. *The Journal of Immunology* **2001**, *167* (2), 957–965.

36. Dual RNA Sequencing Reveals the Expression of Unique Transcriptomic Signatures in Lipopolysaccharide-Induced BV-2 Microglial Cells. *PLOS ONE* **2015**, *10* (3), e0121117.

37. Sahly, H. E. MF59™ as a Vaccine Adjuvant: A Review of Safety and Immunogenicity. *Expert Review of Vaccines* **2010**, *9* (10), 1135–1141.

3. Improving the adjuvanticity of small molecule immune potentiators using covalently linked NF-κB modulators

3.1 Summary

Small molecule immune potentiators (SMIPs) such as imidazoquinolinone derivatives that activate Toll-like receptor (TLR) 7/8 have immense potential as vaccine adjuvants and as anti-tumor agents. However, these molecules have high bioavailability that results in unacceptable levels of systemic inflammation due to adjuvant toxicity, thereby greatly limiting their use. To address this challenge, here we report the design and synthesis of novel imidazoquinolinone-NF-κB immuno-modulator dimers. Employing *in vitro* assays, we screened a select library of synthesized dimers and selected viable candidates for further *in vivo* experiments. With ovalbumin as a model antigen, we vaccinated mice and demonstrated that these dimers reduce the systemic toxicity associated with SMIPs to baseline levels while simultaneously maintaining the adjuvanticity in a vaccine formulation. Additionally, we showed that select dimers improved efficacy in a CT26 mouse colon carcinoma tumor model while eliciting minimal adjuvant toxicity.

3.2 Introduction

Toll-like receptor (TLR) activation in innate immune cells has been linked to the high immunogenicity and protective effects of vaccines.[1,2] The incorporation of TLR activating immunostimulants or adjuvants in subunit and epitope-based vaccine formulations has led to great improvements in both antibody and T-cell levels and antigen specificity.[3,4] Currently, the discovery of many small molecule adjuvants has demonstrated immense potential and opened up the possibility for new therapies.[5,6] However, their tolerability in preclinical and clinical studies have limited the use of many of these compounds requiring either reformulation or redesign.[7]

Historically, discovery of adjuvants has been empirical but with synthetic small molecule adjuvants, modern drug discovery techniques permitted optimized adjuvanticity. This opportunity has led to the development of a class of adjuvants collectively referred to as small molecule immune potentiators (SMIPs).[8,9] In this class, imidazoquinolinones that activate TLR 7/8 such as imiquimod (R837) and resiquimod (R848) have been extensively studied. Imiquimod is currently approved for clinical immunotherapy use in topical creams.[9–11] These SMIPs elicit antigen specific cellular responses when administered as adjuvants.[12–14] Additionally, activation of TLR7/8 by resiquimod can lead to anti-tumor activity facilitated by APC activation of CD8+ T cells and CD4+ Th cells due to IFN-γ and IL-2 production and hence enhanced proliferation.[15–17] Unfortunately, despite such tremendous potential the high bioavailability of imidazoquinolinone adjuvants and associated toxicity has primarily limited the use of TLR7/8 agonist formulations to topical applications and prevented their approval as injectable adjuvants in humans.[9,18,19] To address this challenge, here we report on an alternative method that links a TLR7/8 activating imidazoquinolinone to a NF-κB modulator, thereby modulating the response to the molecule directly elicited from immune cells (**Figure 3.1**).

Recently, we reported that small molecule NF-κB inhibitors can be used to modulate the activity of CpG (TLR 9 agonist) in vaccine formulations. In a screen, we showed that capsaicin and honokiol reduced pro-inflammatory systemic IL-6 and TNF-α levels while maintaining vaccination efficacy.[20] Unfortunately, we did not observe similar effects with *in vivo* experiments employing TLR7/8 agonist R848 as an adjuvant. We hypothesized that this was due to the high rate of diffusion of the small molecule adjuvant and the immune modulators from the injection site. Therefore, we designed hybrid molecules by covalently linking an imidazoquinoline

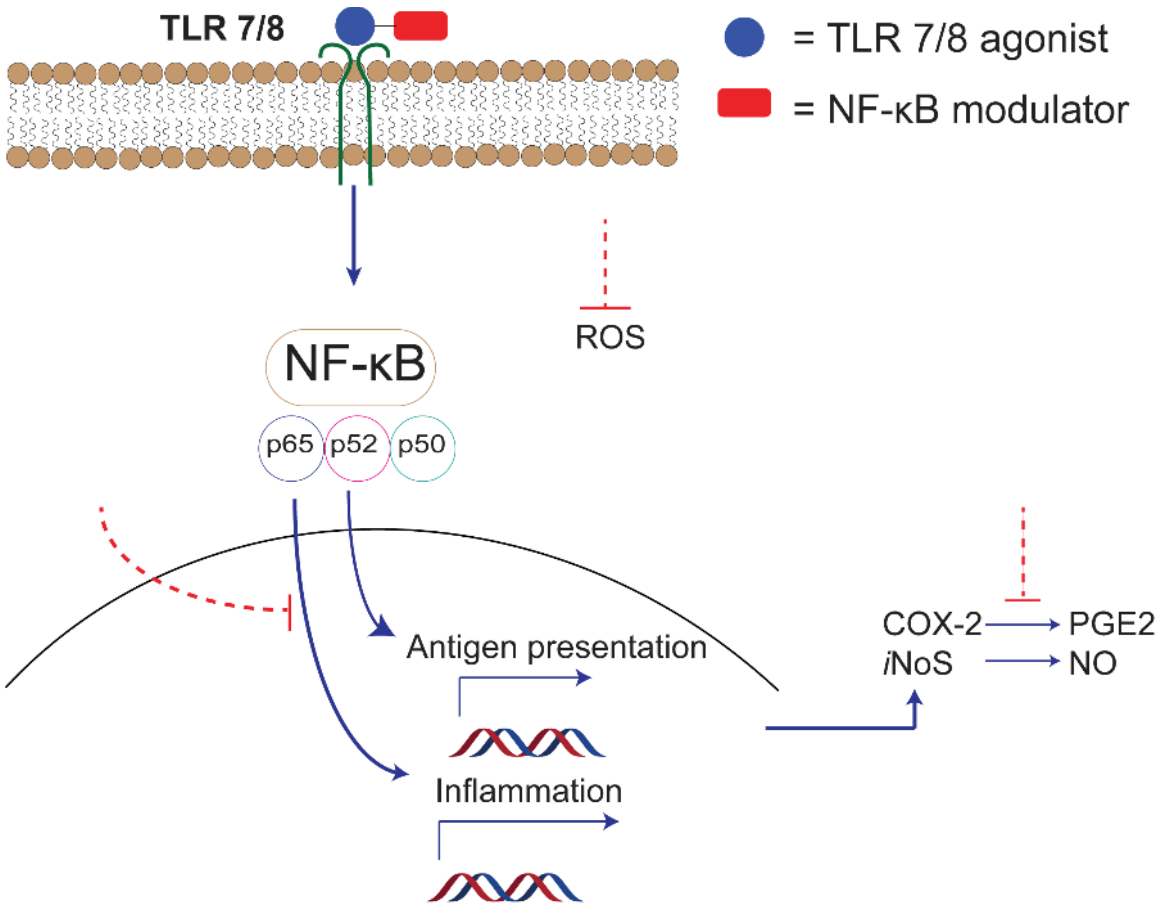

Figure 3.1. Comparing methods of small molecular immune potentiation. Traditional SMIP adjuvant NF-κB pathway. Activation of TLR7/8 with the agonist (blue) leads to downstream pro-inflammatory responses and responses associated with adaptive immunity (antigen presentation). In our work, the adjuvant contains an activation moiety and a direct modulation moiety that alters the NF-κB pathway. Activation of TLR7/8 with the dimers also results in activation of NF-κB pathway by the adjuvant (blue) while the tethered modulators (red) inhibit specific parts of the pathway resulting in lower pro-inflammatory immune response and enhanced or unchanged adaptive immune response

derivative[21] with a conjugatable amine handle to vanilloid catechol and honokiol[20] derivatives. We envisioned such a construct would lead to simultaneous cellular co-activation of TLR 7/8 receptors simultaneous with immunomodulation from the coupled NF-κB modulators. We ran *in vitro*

experiments using murine macrophages and identified candidates to test in *in vivo* experiments. Using ovalbumin (OVA) as a model antigen, we demonstrate that the imidazoquinolinone-immune modulator dimers significantly reduce systemic toxicity induced by the small molecule adjuvant while maintaining the adjuvanticity in vaccine formulation. We also investigated imidazoquinolinone anti-tumor activity by employing a CT26 mouse colon carcinoma tumor model and introduced the dimers through peritumoral injection. We showed that select dimers increased mouse survivability by inhibiting tumor proliferation while inducing low systemic inflammation and reducing adjuvant toxicity. With these results we show that by tethering NF-κB modulators s to SMIPs we improve their tolerability without affecting adjuvanticity and anti-tumor efficacy.

3.3 Results and discussion

3.3.1 Synthesis of imidazoquinoline -immune modulator dimers

In our previous studies using small molecule NF-κB modulatorss in vaccine formulations we screened various commercially available molecules both *in vivo* and *in vitro*. From this screen we identified vanillin and honokiol derivatives as the most effective small molecule modulators.[20] These anti-inflammatory and antioxidant molecules have been extensively studied in the literature for NF-κB. modulation through direct inhibition of the canonical NF-κB pathway or through scavenging pro-inflammatory mediators such as nitric oxide and other ROIs.[22–24] However, when we performed *in vivo* experiments using a mixture of R848 and capsaicin or honokiol modulators in vaccine formulations we observed high systemic cytokines 1 hour after vaccination (Appendix B, **Figure S1**). For this work, we designed and synthesized dimers by conjugating a TLR 7/8 imidazoquinolinone derivative with a conjugatable amine handle[21] to vanillin, catechol and

honokiol derivatives to yield IMD-ferulic (**1**), IMD-vanillin (**2**), IMD-catechol (**3**), IMD-biphenylA (**4**), IMD-biphenylB (**5**) and IMD-biphenylC (**6**) (**Figure 3.2**).

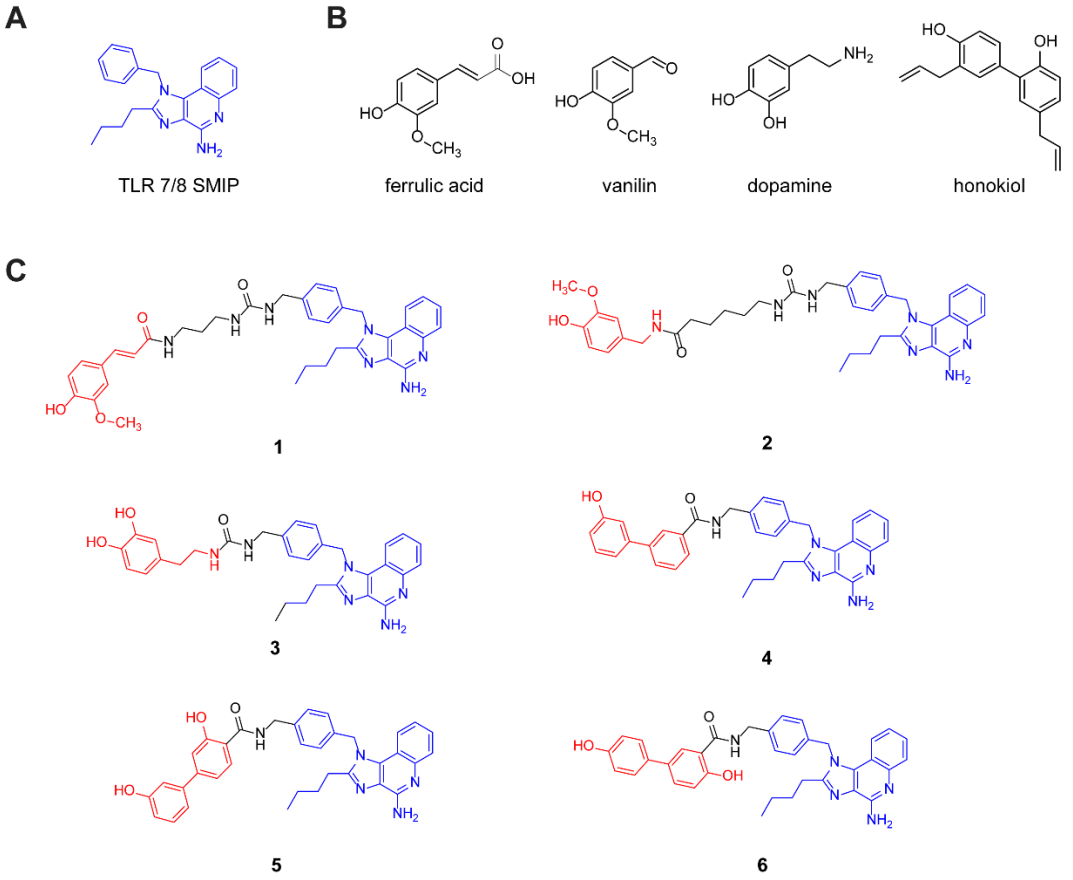

Figure 3.2. A) TLR 7/8 small molecule potentiator (SMIP) imidazoquinolinone B) NF-κB small molecule modulatorss C) Synthesized (blue) TLR 7/8_NF-κB modulators (red) dimers

3.3.2 *In vitro* analyses of synthesized dimers

Next, we designed an *in vitro* screen to test the synthesized dimers and identify promising candidates for further development in an *in vivo* model. Using a RAW macrophage NF-κB-SEAP (Secreted Alkaline Phosphatase) reporter cell line we measured the overall activity of the compounds. We saw a reduction in activity of the dimers compared to the imidazoquinolinone

agonist and equimolar mixtures of the agonist and NF-κB small molecule modulators (**Figure 3.3a**). We next proceeded to analyze if the reduction in activity is due to disruption of cellular uptake and receptor binding or due to selective modulation of NF-κB activity. To elucidate the activity of the dimers we ran pro-inflammatory cytokine and cell surface protein expression assays on murine bone marrow derived dendritic cells (BMDCs). After incubating the parent SMIP and the dimers with BMDCs for 8 h, we observed that dimer compounds IMD-ferulic (1), IMD-vanillin (2), IMD-catechol (3), IMD-biphenylA (4) reduced the levels of IL-6 secreted to almost baseline levels. Compounds IMD-biphenylB (5) and IMD-biphenylC (6) did not significantly change the IL-6 levels when compared to the parent SMIP. We also observed that the equimolar mixture of the SMIP and the small molecule NF-κB modulators did not lower the levels of IL-6 secreted (**Figure 3.3b**). In a similar BMDC experiment, we stained the BMDCs for cell surface expression of CD40, a well-characterized co-stimulatory molecule with an important role in adaptive immunity,[25] and quantified the expression levels using flow cytometry. Notably, we observed that the expression levels of CD40 remained unchanged for most of the compounds and were slightly lower for IMD-ferulic (1) (**Figure 3.3c**) Using this experiment we screened for dimers that would lower pro-inflammatory cytokines while maintaining or improving cell surface protein expression. This would indicate that the hybrid molecule was modulating the NF-κB response of the imidazoquinolinone as opposed to merely inhibiting the activity.

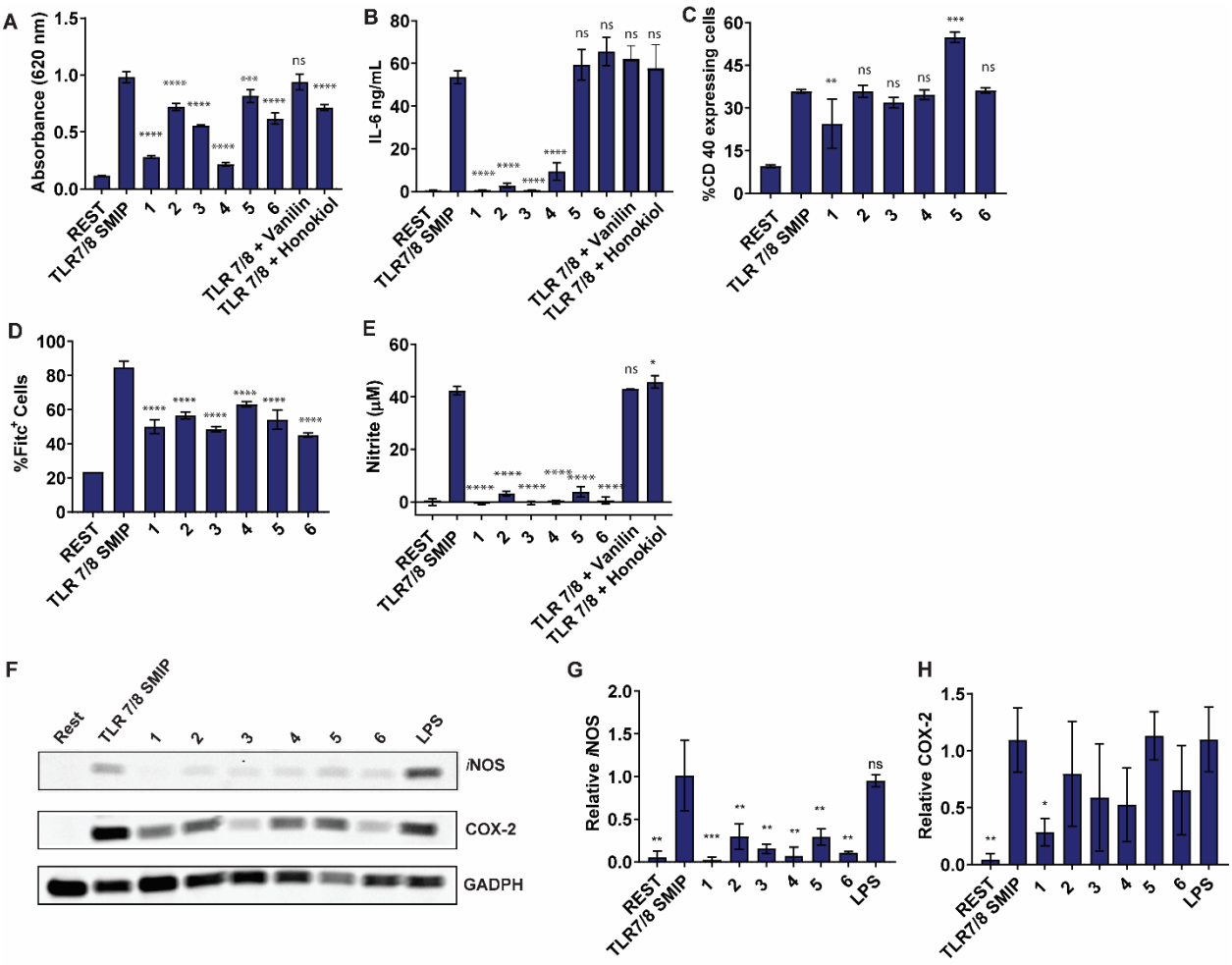

Figure 3.3. *In vitro* assays determining TLR 7/8 NF-κB activation and modulation of synthesized dimers. A) Immune activation measured by RAW-Blue activation *via* NF-κB stimulation after 24 h incubation with 500 nM of compounds at 37 °C. B) IL-6 expression (ELISA) and C) cell surface protein expression (FACS) measured 8 h after incubation with BMDCs. Compounds were assayed at 200 nm. D) Intracellular reactive oxygen species (ROS) measured by incubating RAW macrophages with 6-chloromethyl-2',7'-dichlorodihydrofluorescein diacetate, acetyl ester (CM-H2DCFDA), and fluorescence measured using flow cytometry. E) Nitrite levels in the supernatant of RAW macrophages incubated with 500 nM of compounds for 16h and measured using Griess reagent. F, G) Expression of COX-2 protein measured in the lysate of RAW macrophages incubated with 500 nM compounds for 16h. Samples run in triplicate. Statistical significance to TLR 7/8 SMIP, compared by the one-way ANOVA *p ≤ 0.05, **** p ≤ 0.0001 A+B denotes equimolar mixture. IMD-ferulic (1), IMD-vanillin (2), IMD-catechol (3), IMD-biphenylA (4), IMD-biphenylB (5) and IMD-biphenylC (6)

In addition to inhibition of the upstream events of NF-κB pathway, the small molecule modulators we selected to derivatize and synthesize the adjuvant dimers were previously described in the literature as downstream inhibitors of pro-inflammatory mediators such as nitric oxide and reactive oxygen species (ROS).[24]

We were interested in learning if the dimer adjuvants would have a similar effect on immune cells. To study the effect of the dimers on oxidative stress we incubated RAW macrophages with the compounds for 16 h and measured the levels of intracellular ROS using ROS-reactive fluorescent dye, CM-H2DCFDA and quantified the fluorescence using Flow cytometry. Here, we observed a nearly 50% reduction in intracellular ROS for all the dimer agonists suggesting that these compounds were ROS scavengers (**Figure 3.3d**). In a similar experiment we incubated RAW macrophages for 16 h with the dimer agonists and used Griess reagent to measure the levels of nitrite, a metabolite of nitric oxide in the cell supernatant. The nitrite levels were quantified by measuring absorbance using a plate reader. From this experiment we showed that the dimer adjuvants reduced the NO levels to baseline levels compared to the parent SMIP (**Figure 3.3e**) indicating that the dimers were potent inhibitors of nitric oxide either through scavenging or direct inhibition of the enzymatic pathway. Additionally, using western blot analysis of RAW macrophage cell lysate we observed that the molecules inhibited inducible nitric oxide synthase (*i*NOS) a pathway precusor of NO (**Figure 3.3f, 3.3g**)

Lastly, we wanted to investigate if the dimer agonists were Cyclooxygenase-2 (COX-2) inhibitors. COX-2 is a pro-inflammatory marker associated with the activation of both the NF-κB and MAPK pathways. After incubating RAW macrophages with the dimer agonists for 16 h, we lysed the cells and separated the proteins using SDS-PAGE after which we transferred the proteins to a membrane and probed the protein levels using an anti-COX-2 antibody. We observed low

relative expression levels of COX-2 protein with IMD-ferulic (1). However, IMD-vanillin (2), IMD-catechol (3), IMD-biphenylA (4), IMD-biphenylB (5) and IMD-biphenylC (6) did not significantly reduce COX-2 expression suggesting that these compounds were not inhibitors of the COX-2 pathway (**Figure 3.3f, 3.3h**).

3.3.3 *In vivo* analysis of synthesized dimers

With this promising *in vitro* analysis, we next set up *in vivo* experiments to see how these dimers would perform in a vaccine formulation. Using ovalbumin as a model antigen we vaccinated mice with the most promising dimers (IMD-vanillin (**2**), IMD-catechol (**3**) and IMD-biphenylA (**4**)) that reduced inflammation while maintaining CD40 expression in the *in vitro* assays. (**Figure 3.3b, 3.3c**) IMD-ferulic (**1**) was structurally similar to IMD-vanillin (**2**) and was slightly less effective at inducing expression of CD40 compared to the parent agonist (**Figure 3.3c**). Compounds IMD-biphenylB (**5**) and IMD-biphenylC (**6**)**,** while activating CD40, were not effective at reducing inflammation (**Figure 3.3b**) and were therefore excluded from further *in vivo* experimentation. We performed intramuscular injection (i.m) with 100 μg of OVA, 70 nmoles of imidazoquinolinone, potentiated dimers, and equimolar mixtures of imidazoquinolinone and NF-κB modulators in 50 μl of PBS. At the 1-hour mark post injection we collected serum from the mice and quantified systemic levels of TNF-α and IL-6. We observed that the dimers reduced these systemic cytokines to background levels comparable to the PBS, vanillin, and catechol controls (**Figure 3.4b, 3.4c**). On day 14 we performed a boost injection, then on day 28, we sacrificed the mice, collected sera, and analyzed anti-OVA antibodies. Notably, compounds IMD-vanillin (**2**) and IMD-catechol (**3**) induced significantly higher levels of anti-OVA Ig (A+G+M) and specific IgG compared to the TLR7/8 adjuvanted mice (**Figure 3.4d, 3.4e**) Comparing specific IgA antibodies, we saw that IMD-vanillin (**2**) induced statistically higher levels of these antibodies (**Figure 3.4f**).

Because activation of TLR 7/8 has been previously associated with increased CD8+ T cell function[17] we were interested in investigating this activity for these new compounds compared to

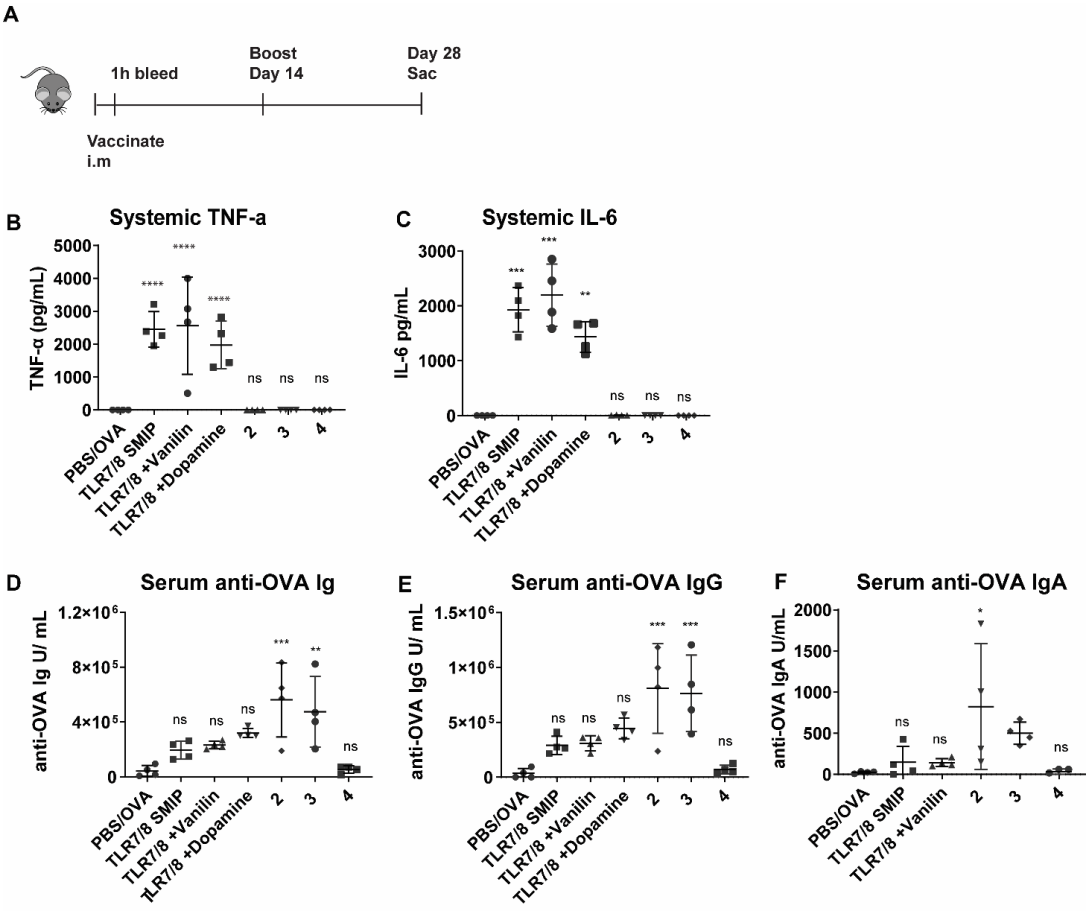

Figure 3.4. *In vivo* assays TLR 7/8_NF-κB modulator dimers. A) Outline of *in vivo* vaccination experiment. B) Serum levels of cytokines assayed 1h after injection. IL-6 and TNF- α levels of linked compounds not detected. C) Serum anti-OVA antibodies measured day 28. Statistical significance to PBS control, compared by the one-way ANOVA *p ≤ 0.05, **** p ≤ 0.0001 A+B denotes equimolar mixture. IMD-vanillin (**2**), IMD-catechol (**3**), IMD-biphenylA (**4**),

the parent TLR 7/8 agonist. On day 28 post OVA *in vivo* vaccination experiment we harvested the spleen of the mice and prepared a single cell splenocyte suspension. We then incubated the cells with a SINFEKL MHC specific tetramer and analyzed the cells using Flow cytometry. We did not observe increased activity with the agonist dimers compared to the vehicle control. (Appendix B,

Figure S3a). This result was expected because this route of administration, admixing OVA and the adjuvant in PBS and i.m injection has been reported to enhance antibody titers but not T-cell immunity.[26] In a separate experiment, we examined splenocyte proliferation with naïve splenocytes, incubating the cells for 48 h with the dimer agonists and parent adjuvant. We found that the dimer agonists promoted the proliferation of lymphocytes to comparable levels when compared to the parent agonist (Appendix B**, Figure S3b**). In summary, the attachment of the modulator slightly increased the activity of the parent compound to generate antibody responses while maintaining all other aspects of its innate immune stimulation except excess cytokine production.

3.3.4 Anti-tumor activity of dimer agonists

With the promising results from our preliminary vaccination experiments, we were further motivated to evaluate their efficacy as cancer immunotherapeutics. Imidazoquinoline SMIPs have shown great promise as anti-tumor immune-therapeutic agents, but their inflammation has often hindered effective therapeutic development. To examine how adding NF-κB modulation to a SMIP might alter this, we tested the anti-tumorigenic activity of the dimers. Previous studies have shown that intra-tumoral adjuvant introduction is effective in reducing tumor proliferation by enhancing T-cell anti-tumor activity.[27] Specifically, TLR 7/8 activation leads to enhanced innate immune cell activation propagated by increased secretion of IFNα, IL-12 and IFN-γ cytokines.[17,28] For most compounds used for this purpose, especially resiquimod (R848), systemic adjuvant toxicity is a major limiting factor. As our dimer agonist platform reduced systemic cytokines, we decided to test the compounds on a tumor model. In this *in vivo* model, we used the CT26 tumor models and administered the adjuvant and select adjuvant dimers (compounds IMD-ferulic (**1**), IMD-vanillin

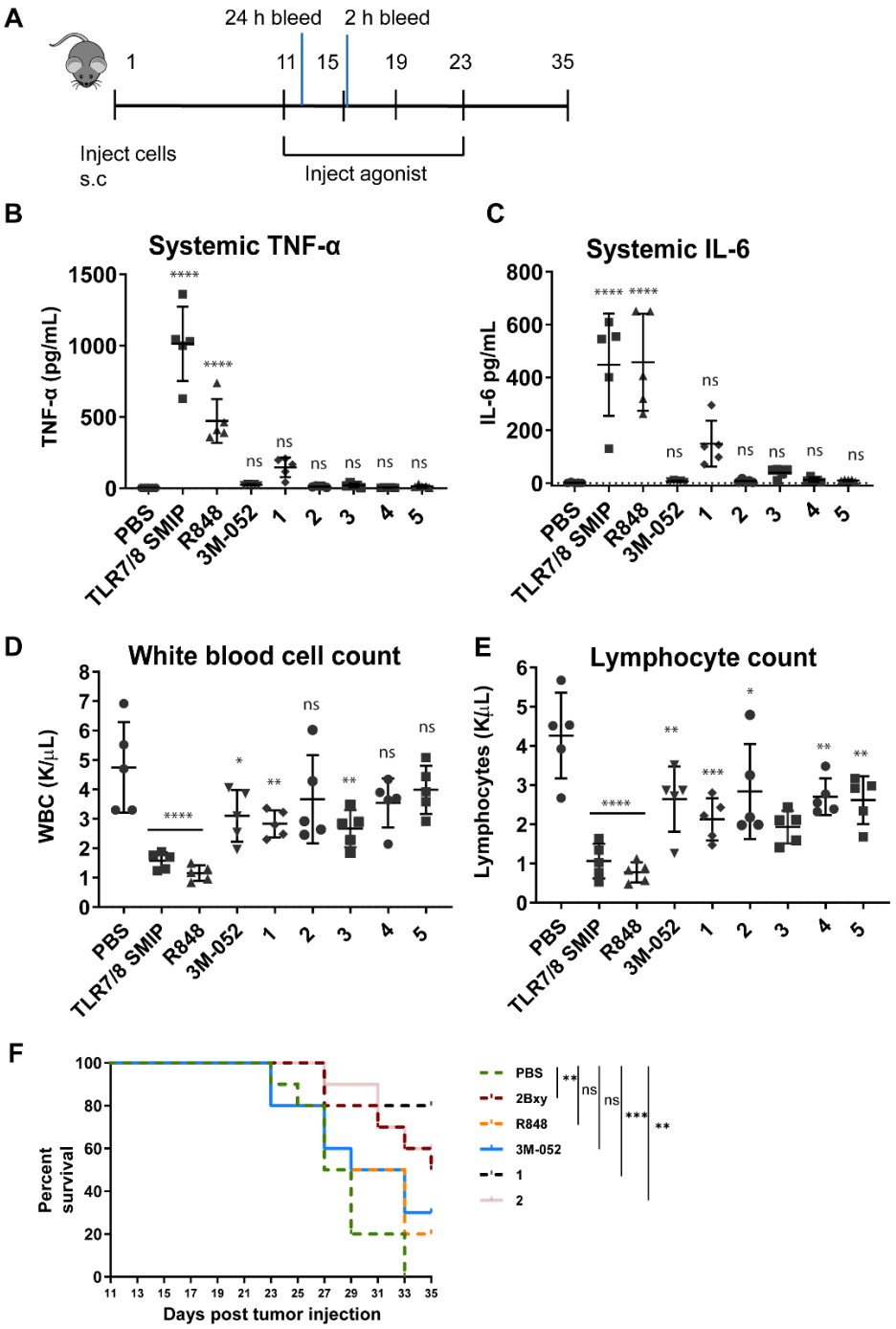

Figure 3.5. A) *In vivo* tumor model experiment using SMIP-modulator dimers with peritumoral injection into subcutaneous CT-26 tumor model.

Figure 3.5 continued. Agonists were injected when tumors were about 75 cc in size followed by three additional injection every four days. B) Systemic cytokine levels measured in the serum 2 h after peritumoral injection of compounds. D, E) Hematological analysis of peripheral blood measured 24 h after intertumoral injection of compounds. F) Kaplan−Meier survival analysis- Tumor size was measured every alternate day and animals were euthanized when the tumors reached 20 mm in any linear dimension. Measurement was performed till day 35. The tumor volume was measured using the formula 0.5*L*W*W. statistical analysis conducted using the logrank test with Bonferroni-correction. IMD-ferulic (**1**), IMD-vanillin (**2**), IMD-catechol (**3**), IMD-biphenylA (**4**), IMD-biphenylB (**5**)

(**2**), IMD-catechol (**3**), IMD-biphenylA (**4**) and IMD-biphenylB (**5**)) and a PBS control. Additionally, we included controls, resiquimod (R848) along with a resiquimod derivative 3M-052, that has been employed in clinical trials of cancer immunotherapy.[28]

After 11 days, the tumors were established, and we administered the adjuvants and adjuvant dimers via peritumoral injection. We collected serum and blood, at 2 h and 24 h after these injections, respectively to measure systemic cytokines in the serum and quantify adjuvant toxicity via a hematological analysis on the blood. Similar to the OVA vaccination model, we observed that the dimer adjuvants induced baseline levels of TNF-α and IL-6 as measured in the serum (**Figure 3.5b, 3.5c**). In contrast, the parent adjuvant and R848 induced high levels of these pro-inflammatory cytokines while 3M-052 was comparable to the vehicle control and the dimer adjuvants. Interestingly, IMD-ferulic (**1**) induced slightly elevated IL-6 and TNF-α when compared to the rest of the tested dimer adjuvants. Additionally, the hematological analysis of the blood showed that the molecules that induced higher systemic inflammatory cytokines led to lower white blood count and lymphocyte counts compared to the vehicle control (**Figure 3.5d, 3.5e**) These results suggest that the parent adjuvant and R848 upon peritumoral injection resulted in much higher adjuvant induced toxicity.

Observing promising tolerability with the adjuvant dimers, we continued the tumor model experiment, monitoring tumor proliferation. Since CT-26 is a highly aggressive murine carcinoma model, tumor proliferation was monitored till day 35. We observed that of the dimer adjuvants tested, two dimer molecules IMD-ferulic (**1**), IMD-vanillin (**2**) improved survivability with IMD-ferulic (**1**) providing 80 % survivability at day 35 which was higher than the parent adjuvant, 3M-052 and R848 (**Figure 3.5f,** see Appendix **Figure S.3.4** for tumor growth curves). We observed slightly elevated levels of IL-6 and TNF-α in the serum of mice injected with IMD-ferulic (**1**) suggesting moderate levels of systemic immune activation by these molecules might be necessary for efficacious responses. Because it has never been possible before to decouple the inflammatory response from the activity of a specific molecule, it is possible that the improvement we observe is the cumulative effect of reduced inflammation while maintaining identical T-cell responses. Overall, this study indicates that our di-agonists serve as a powerful platform to reduce toxicity of SMIP agonists while maintaining or enhancing efficacy.

3.4 Conclusion

Agonists that activate TLR7/8 receptors are promising as vaccine and cancer immunotherapy adjuvants. These receptors are broadly expressed on antigen-presenting cells and once activated lead to enhancement of APC maturation with increased expression of costimulatory markers and cytokine expression which causes both cellular and humoral immunity. SMIPs activating TLR 7/8 such as the imidazoquinolinone family are potent adjuvants whose major limitation is unfavorable systemic toxicity limiting their use. In this study we show that by the chimeric assembly of these adjuvants with NF-κB potentiating small molecule we can modulate these molecules, reducing the unfavorable toxicity. We show using an *in vitro* screen to identify

viable dimers and demonstrate their adjuvanticity in a vaccination model as well as anti-tumorigenic activity without systemic toxicity. Due to the large availability of molecules that modulate the NF-κB, IRF and MAPK inflammatory pathways, we envision this dimer strategy to broaden the use of SMIPs both as adjuvants and in immunotherapy formulations.

3.5 Materials and methods

Reagents and solvents were purchased from commercial sources and used without further purification. Vanillin, dopamine hydrochloride, 4-hydroxy-3-methoxybenzylamine hydrochloride and ferulic acid were commercially obtained. APC anti-mouse CD40, PE anti-mouse CD11c and purified anti-mouse CD16/32 were purchased from BioLegend. COX-2 (mouse) Polyclonal Antibody was purchased from Cayman Chemical. GAPDH (14C10) Rabbit mAb and iNOS (D6B6S) Rabbit mAb were purchased from Cell Signaling Technology. Spectroscopic characterization was done on Bruker Avance III HD 500 11.7 Tesla NMR (500 MHz) for ^{1}H and ^{13}C NMR. NMR spectra were analyzed using MestreNova software. Coupling on the spectra is expressed in hertz and abbreviations for multiplicities given as s = singlet, d = doublet, t = triplet, dd = doublet of doublets, and m = multiplet where applicable. Mass spectral analysis was performed on Agilent 6224 TOF-MS. Preparative reversed-phase HPLC purification was carried using Phenomenex Luna C18 or C8 Prep (150 X 21.2250 mm, 5 μm particle size) column with a flow rate of 21.2 mL/min on a Gilson 333/334 pump system and GX-271 liquid handler system. UV detection (214 nm, 254 nm, and 260 nm) was used for preparative HPLC. Flow Cytometry data was acquired on a NovoCyte Benchtop Flow Cytometer. Absorbance measurements were acquired on a Multiskan FC plate reader (Thermo Scientific). Data was analyzed using one-way ANOVA in Graph Pad Prism software. All values were reported as mean ± SD. Female C57/BL6

mice and male Balb/c mice were purchased from Jackson Laboratories and allowed to equilibrate for a minimum of 48 h before use. For all experiments, the mice were 6-10 wk old. All animal studies and mice maintenance were approved by the Institutional of Animal Care and Use (IACUC #2012-3048).

RAW264.7 Macrophage (RAW-Blue) NF-κB assay

RAW-Blue cells, (InvivoGen) were cultured as described by the manufacturer. Cells were grown in complete culture media composed of Dulbecco's Modified Eagle's Medium (DMEM) with 4.5 g/L glucose (Life Technologies), 2 mM L-glutamine, 10,000 U/mL penicillin, 10 mg/mL streptomycin, 25μg/mL amphotericin B, supplemented with 10% fetal bovine serum (FBS, Thermo Fisher Scientific). RAW-Blue cells (passage 5-15) were plated in a 96 well plate at a density of 100,000 cells/well in 180 μL DMEM containing 10% heat-inactivated FBS (HI-FBS) and selective antibiotics. The cells were treated with agonist and agonist dimers and LPS control (50 ng/mL) for 20 h at 37 °C and 5% CO_2. NF-κB activity was measured by a QUANTI-Blue (InvivoGen) assay and the absorbance was measured at 620 nm using a Multiskan FC plate reader (Thermo Scientific).

Bone Marrow-Derived Dendritic Cell Harvest and Culture.

Bone marrow-derived dendritic cells (BMDCs) were harvested from female C57Bl/6 mice as previously described.[1] Femur bones were aseptically removed from mice and the bone marrow was extracted into PBS buffer and the cell suspension centrifuged at 300 RCF for 10 min at RT to pellet the cells. ACK Lysing Buffer (3 mL, Lonza) was added to the cell pellet and incubated for 2 min at RT. PBS buffer (13 mL) was then added to the cell suspension, and the cell solution was centrifuged at 300 RCF for 10 min at RT. Next, the cell pellet was resuspended in BMDC complete media (RPMI 1640, 10% heat-inactivated FBS, 20 ng/mL granulocyte-macrophage colony-

stimulating factor (GM-CSF), 2 mM L-glutamine (Life Technologies), 10,000 U/mL penicillin, 10 mg/mL streptomycin, 25μg/mL amphotericin B, and 50 μM beta-mercaptoethanol). The cells were then plated at $1x10^6$ cells/mL in 100 mm petri dishes in 10 mL complete media and incubated at 37 °C in a CO_2 incubator. On day 3, 10 mL of fresh BMDC media was added to each petri dish. On day 6, BMDCs were released and plated in untreated 12-well plates at $1x10^6$ cells/mL for cell surface marker activation and cytokine secretion experiments.

Western blot analysis of pathway proteins

RAW264.7 Macrophage cells (InvivoGen) cultured in complete media were plated in 6 well plates at 1 $x10^6$ cells/mL and allowed to adhere for 12 h at 37 °C in a CO_2 incubator. The cells were then treated with agonist, agonist dimers, and LPS control for 16 h. The treated cells were washed and scraped into cold phosphate-buffered saline (PBS) and centrifuged at 400 × g at 4°C for 5 min. The cell pellets were resuspended in triple detergent lysis buffer (10 mL) containing one protease inhibitor cocktail (cOmplete™ ULTRA Tablets, Sigma) and centrifuged to yield whole cell lysate. The lysate was quantified using a Pierce™ BCA Protein Assay Kit. 50 μg of total protein was separated using 4-15% SDS–PAGE and blotted onto PVDF membranes (Bio-Rad). The membranes were probed using monoclonal antibodies for COX-2 at a dilution of 1:1000 (Cayman Chemicals, MI) GAPDH (14C10) at a dilution of 1:1000 and Rabbit mAb and at a dilution of 1:500 iNOS (D6B6S) Rabbit mAb Visualization was achieved using IRDye® 800CW (Abcam) at a dilution of 1:10000 and imaged on Azure biosystems imager. Densitometric analysis was done using Image J.

Flow Cytometry for Cell Surface Marker Upregulation and Cytokine secretion analysis.

BMDCs were plated in untreated 12-well plates at $1x10^6$ cells/mL and incubated with agonist and agonist dimers in culture media for 8 h at 37 °C with 5% CO2. The cells were released from the

plate by pipetting vigorously and centrifuged at 2500 RPM at 4 °C for 10 min. The cell culture media was saved for IL-6 cytokine quantification using ELISA (BioLegend). The cell pellet was resuspended in cold FACS buffer (PBS, 10% FBS, and 0.1% sodium azide) buffer (300 µL) and incubated with CD16/32 FcR blocking antibodies (1.0 µg/1x106 cells) on ice for 15 min. The cell suspension was pelleted, and the supernatant was removed. Next, the cell pellet was resuspended in cold FACS buffer (100 µL) and incubated with PE-CD11c (1.0µg/1x106 cells) and APC CD40 (1.0 µg/1x106 cells), on ice and in the dark for 30 min. The samples were then washed twice with 300 µL FACS buffer. The pelleted cells were resuspended in cold FACS buffer (200 µL) and kept on ice until being loaded onto the flow cytometer for analysis.

***In vivo* vaccination of mice**

Female C57/BL6 mice were briefly anesthetized with isoflurane and injected intramuscularly in the right hind leg with 50 µL containing ovalbumin (100 µg), adjuvant, adjuvant dimers, vanillin, and dopamine (0.07 µmoles) and a PBS vehicle control group.

Plasma cytokine analysis and Antibody quantification

Mouse blood was collected via the submandibular vein in 0.2 mL heparin-coated collection tubes (VWR Scientific) 1 h after vaccination. Serum was isolated by allowing blood to clot for 30 min RT and centrifugation at 2000 x g for 10 min. Supernatant was collected and stored at -80 °C until use. Serum was analyzed using BD Cytometric Bead Array Mouse Inflammation cytokine kit or LEGENDplex™ Mouse Inflammation Panel (Biolegend) according to manufacturer's protocol. For antibody quantification, mouse blood was collected via cardiac puncture 28 days after vaccination in 0.2 mL heparin-coated collection tubes (VWR Scientific). Serum was isolated by allowing blood to clot for 30 min RT and centrifuging at 2000 x g for 10 min. Serum was analyzed

using a quantitative anti-ovalbumin total Ig's, IgA, and IgG ELISA kits (Alpha Diagnostic International) according to the manufacture's protocol

Tumor studies

0.2×10^6 CT-26 cells were injected subcutaneously into the flank of 6-week-old Balb/c mice (n = 10 per group) in 100 µL of PBS. The tumor size was monitored on alternating days. Tumor volumes were measured using the equation V =1/2×L×W×W. When the tumors reached a size of approximately 75 mm^3 (day 11), treatment was started. Various formulations (20 nmols of each agonist or PBS) were injected peritumorally every 4 days (day 15, 19, and 23). Mice were euthanized when the tumors reached 20 mm in any linear dimension. Five mice for each group were used for blood analysis. Blood was collected two days post the first injection for hematological toxicity analysis and two hours post the second injection for systemic cytokine analysis.

Nitric oxide assay

RAW264.7 Macrophage (InvivoGen) cultured in complete media were plated in 12-well plates at 1 $x10^6$ cells/mL and treated with agonist and agonist dimers for 16 h at 37 °C in a CO_2 incubator. The cell supernatant was collected and the quantity of nitrite in the culture medium was measured as an indicator of NO production. Amounts of nitrite, a stable metabolite of NO, were measured using Griess reagent (1% sulfanilamide and 0.1% naphthyl ethylenediamine dihydrochloride in 2.5% phosphoric acid). 100 µL of cell culture medium was mixed with 100 µL of Griess reagent. After incubation at room temperature for 10 min, the absorbance at 540 nm was measured in a microplate reader. The quantity of nitrite was determined from a sodium nitrite standard curve.

Reactive oxygen species measurement

RAW264.7 Macrophage (InvivoGen) cultured in complete media, were plated in 12-well plates at 1 x10^6 cells/mL and treated with agonist and agonist dimers for 16 h at 37 °C in a CO_2 incubator. The cells were released from the plate and centrifuged at 2500 RPM at room temperature for 10 min and the supernatant aspirated. The cells were then washed twice with PBS (200 uL) and the cell pellet resuspended in Hanks' Balanced Salt solution (HBSS) containing CM-H2DCFDA (1uM). Next, the cells were incubated for 30 min at 37 °C with 5 % CO_2. After incubation, the cells were washed twice with cold PBS. Fluorescence was measure using Flow Cytometry on FL-1 (fitc) channel.

Proliferation Assay

Proliferation assay was performed as previously reported.[2] Splenocytes were isolated from C57BL/6 mice and plated at 5×10^4 in 96-well plates. The splenocytes were then incubated with 3 μM of agonist and agonist dimers for 48 h at 37 °C in a CO_2 incubator. 3-[4,5-dimethylthiazol-2-yl]-2,5-diphenyltetrazolium bromide (MTT) (20 μl, 5 mg/ml in PBS) was added 4 h before the end of the incubation period. Purple crystals were dissolved in sterile DMSO and incubated for 5 minutes to ensure complete dissolution. The absorbance was measured at 590 nm using a Multiskan FC plate reader (Thermo Scientific). The proliferation rate was determined as follows: Abs(sample)/Abs (PBS)×100%.

Cell viability (MTT) assay

RAW264.7 Macrophage cells were incubated with agonist and agonist dimers for 16 h and subjected to cell viability assays. 3-(4,5-dimethylthiazol-2-yl)-2,5-diiphenyltetrazolium bromide (MTT) was dissolved in PBS to final concentration of 5 mg/mL and sterile-filtered. Treated cells were resuspended in fresh RPMI medium with 10 % FBS at concentration and plated in a 96-well plate at a concentration of 1 x 10^5 cell/mL. To these cells, 10 μL of MTT solution was added, then

incubated at 37 °C with 5 % CO_2 for 3 h. When purple crystals were visible, 75 μL of supernatant was removed. Purple crystals were dissolved in sterile DMSO and incubated for 5 minutes to ensure complete dissolution. The absorbance was measured at 590 nm using a Multiskan FC plate reader (Thermo Scientific). %Viability was calculated as follows: Abs(sample)-Abs(blank)/Abs (Rest cells)-Abs(blank) x 100%.

3.6 REFERENCES

1. Van Duin, D.; Medzhitov, R.; Shaw, A. C. Triggering TLR Signaling in Vaccination. *Trends in Immunology.* **2006**, *27* (1), 49-55

2. Duthie, M. S.; Windish, H. P.; Fox, C. B.; Reed, S. G. Use of Defined TLR Ligands as Adjuvants within Human Vaccines. *Immunol. Rev*. **2011**, *239* (1), 178-96

3. Steinhagen, F.; Kinjo, T.; Bode, C.; Klinman, D. M. TLR-Based Immune Adjuvants. *Vaccine*. **2011**, *29* (17), 3341-3355

4. Dunne, A.; Marshall, N. A.; Mills, K. H. G. TLR Based Therapeutics. *Current Opinion in Pharmacology*. **2011**, *11* (4), 404-411

5. Mifsud, E. J.; Tan, A. C. L.; Jackson, D. C. TLR Agonists as Modulators of the Innate Immune Response and Their Potential as Agents against Infectious Disease. *Frontiers in Immunology*. **2014**, *3* (5), 79

6. Mancini, R. J.; Stutts, L.; Ryu, K. A.; Tom, J. K.; Esser-Kahn, A. P. Directing the Immune System with Chemical Compounds. *ACS Chem. Biol*. **2014**, *9* (5), 1075–1085

7. Del Giudice, G.; Rappuoli, R.; Didierlaurent, A. M. Correlates of Adjuvanticity: A Review on Adjuvants in Licensed Vaccines. *Seminars in Immunology*. **2018**, *39*, 14-21

8. Flower, D. R. Systematic Identification of Small Molecule Adjuvants. *Expert Opin. Drug Discov*. **2012**, *7* (9), 807–817

9. Wu, T. Y.-H.; Singh, M.; Miller, A. T.; Gregorio, E. De; Doro, F.; Oro, U. D.; Skibinski, D. a. G.; Mbow, M. L.; Bufali, S.; Herman, A. E.; Cortez, A.; Li, Y.; Nayak, B. P.; Tritto, E.; Filippi, C. M.; Otten, G. R.; Brito, L. a.; Monaci, E.; Li, C.; Aprea, S.; Valentini, S.; Calabr, S.; Laera, D.; Brunelli, B.; Caproni, E.; Malyala, P.; Panchal, R. G.; De Gregorio, E.; Doro, F.; D'Oro, U.; Skibinski, D. a. G.; Mbow, M. L.; Bufali, S.; Herman, A. E.; Cortez, A.; Li, Y.; Nayak, B. P.; Tritto, E.; Filippi, C. M.; Otten, G. R.; Brito, L. a.; Monaci, E.; Li, C.; Aprea, S.; Valentini, S.; Calabro, S.; Laera, D.; Brunelli, B.; Caproni, E.; Malyala, P.; Panchal, R. G.; Warren, T.

K.; Bavari, S.; O'Hagan, D. T.; Cooke, M. P.; Valiante, N. M. Rational Design of Small Molecules as Vaccine Adjuvants. *Sci. Transl. Med.* **2014**, 6 (263), 263ra160

10. Tyring, S.; Conant, M.; Marini, M.; Van Der Meijden, W.; Washenik, K. Imiquimod; An International Update on Therapeutic Uses in Dermatology. *International Journal of Dermatology*. **2002**, *41* (11) 810-816

11. Meyer, T.; Stockfleth, E. Clinical Investigations of Toll-like Receptor Agonists. *Expert Opinion on Investigational Drugs.* **2008**, *17* (7) 1051-1065

12. Smith, A. J.; Li, Y.; Bazin, H. G.; St-Jean, J. R.; Larocque, D.; Evans, J. T.; Baldridge, J. R. Evaluation of Novel Synthetic TLR7/8 Agonists as Vaccine Adjuvants. *Vaccine* **2016**, *34* (36) 4304-4312

13. Ramakrishna, V.; Vasilakos, J. P.; Tario, J. D.; Berger, M. A.; Wallace, P. K.; Keler, T. Toll-like Receptor Activation Enhances Cell-Mediated Immunity Induced by an Antibody Vaccine Targeting Human Dendritic Cells. *J. Transl. Med*. **2007**. *5* (5)

14. Kim, W. G.; Choi, B.; Yang, H. J.; Han, J. A.; Jung, H.; Cho, H.; Kang, S.; Hong, S. Y. Covalent Conjugation of Small-Molecule Adjuvants to Nanoparticles Induces Robust Cytotoxic T Cell Responses via DC Activation. *Bioconjug. Chem*. **2016**, *27*, (9) 2007–2013

15. Kaczanowska, S.; Joseph, A. M.; Davila, E. TLR Agonists: Our Best Frenemy in Cancer Immunotherapy. *J. Leukoc. Biol*. **2013.** *93,* (6), 847-863

16. Caron, G.; Duluc, D.; Frémaux, I.; Jeannin, P.; David, C.; Gascan, H.; Delneste, Y. Direct Stimulation of Human T Cells via TLR5 and TLR7/8: Flagellin and R-848 Up-Regulate Proliferation and IFN-γ Production by Memory CD4 + T Cells. *J. Immunol*. **2005**. *175*, (3), 1551-1557

17. Li, Q.; Yan, Y.; Liu, J.; Huang, X.; Zhang, X.; Kirschning, C.; Xu, H. C.; Lang, P. A.; Dittmer, U.; Zhang, E.; Lu, M. Toll-Like Receptor 7 Activation Enhances CD8+ T Cell Effector Functions by Promoting Cellular Glycolysis. *Front. Immunol*. **2019**, *10*, 2191

18. Dowling, D. J. Recent Advances in the Discovery and Delivery of TLR7/8 Agonists as Vaccine Adjuvants. *ImmunoHorizons* **2018**, *2* (6) 185-197.

19. Lynn, G. M.; Sedlik, C.; Baharom, F.; Zhu, Y.; Ramirez-Valdez, R. A.; Coble, V. L.; Tobin, K.; Nichols, S. R.; Itzkowitz, Y.; Zaidi, N.; Gammon, J. M.; Blobel, N. J.; Denizeau, J.; de la Rochere, P.; Francica, B. J.; Decker, B.; Maciejewski, M.; Cheung, J.; Yamane, H.; Smelkinson, M. G.; Francica, J. R.; Laga, R.; Bernstock, J. D.; Seymour, L. W.; Drake, C. G.; Jewell, C. M.; Lantz, O.; Piaggio, E.; Ishizuka, A. S.; Seder, R. A. Peptide–TLR-7/8a Conjugate Vaccines Chemically Programmed for Nanoparticle Self-Assembly Enhance CD8 T-Cell Immunity to Tumor Antigens. *Nat. Biotechnol*. **2020**, *38*, 320–332

20. Moser, B. A.; Escalante-buendia, Y.; Steinhardt, R. C.; Rosenberger, M. G.; Cassaidy, B. J.; Naorem, N.; Chon, A. C.; Nguyen, M.; Tran, N.; Esser-Kahn, A. P. Small Molecule NF- κB Inhibitors as Immune Potentiators for Enhancement of Vaccine Adjuvants *Front Immunol*. **2020**, *11*, 511-513.

21. Shukla, N. M.; Malladi, S. S.; Mutz, C. A.; Balakrishna, R.; David, S. A. Structure-Activity Relationships in Human Toll-like Receptor 7-Active Imidazoquinoline Analogues. J. Med. Chem. **2010**, *53* (11), 4450–4465.

22. Murakami, Y.; Hirata, A.; Ito, S.; Shoji, M.; Tanaka, S.; Yasui, T.; Machino, M.; Fujisawa, S. Re-Evaluation of Cyclooxygenase-2-Inhibiting Activity of Vanillin and Guaiacol in Macrophages Stimulated with Lipopolysaccharide. *Anticancer Res*. **2007**, *27*, (2), 801

23. Zheng, L. T.; Ryu, G. M.; Kwon, B. M.; Lee, W. H.; Suk, K. Anti-Inflammatory Effects of Catechols in Lipopolysaccharide-Stimulated Microglia Cells: Inhibition of Microglial Neurotoxicity. *Eur. J. Pharmacol*. **2008**, *588* (1) 106-113

24. Gilmore, T. D.; Herscovitch, M. Inhibitors of NF-KB Signaling: 785 and Counting. *Oncogene* **2006** *25*, 6887–6899

25. Elgueta, R.; Benson, M. J.; De Vries, V. C.; Wasiuk, A.; Guo, Y.; Noelle, R. J. Molecular Mechanism and Function of CD40/CD40L Engagement in the Immune System. *Immunological Reviews* **2009** *229* (1) 152-172

26. Schmidt, S. T.; Khadke, S.; Korsholm, K. S.; Perrie, Y.; Rades, T.; Andersen, P.; Foged, C.; Christensen, D. The Administration Route Is Decisive for the Ability of the Vaccine Adjuvant CAF09 to Induce Antigen-Specific CD8(+) T-Cell Responses. *J. Control. Release* **2016**, 10 (239) 107-17

27. Vermaelen, K. Vaccine Strategies to Improve Anticancer Cellular Immune Responses. *Frontiers in Immunology*. **2019** 10, 8

28. Mullins, S. R.; Vasilakos, J. P.; Deschler, K.; Grigsby, I.; Gillis, P.; John, J.; Elder, M. J.; Swales, J.; Timosenko, E.; Cooper, Z.; Dovedi, S. J.; Leishman, A. J.; Luheshi, N.; Elvecrog, J.; Tilahun, A.; Goodwin, R.; Herbst, R.; Tomai, M. A.; Wilkinson, R. W. Intratumoral Immunotherapy with TLR7/8 Agonist MEDI9197 Modulates the Tumor Microenvironment Leading to Enhanced Activity When Combined with Other Immunotherapies. *J. Immunother. Cancer* **2019**, *7*, 244

4. Peptide-TLR7/8a-dopa conjugate enhances the immune response to antigens.

4.1 Summary

Synthetic vaccine adjuvants enhance immune response and induce undesirable levels of proinflammatory cytokines, including TNF-α and IL-6. Here, we present a synthetic peptide-TLR7/8a-dopa conjugate named p(TLR7/8a-dopa), which decreases reactogenicity and improves protective immune response. p(TLR7/8a-dopa) is an oligomeric peptide with repeating TLR7/8a and dopamine units. In this molecular construct, TLR7/8a units are the immunostimulant, and dopamine units are the immunomodulator. Our studies with ovalbumin demonstrate that p(TLR7/8a-dopa) generates greater humoral and similar cellular immunity than peptides lacking the immunomodulator: p(TLR7/8a). This work demonstrates a strategy to alter existing immune responses with immunomodulators, tailoring the activity to the desired level without the need to develop new agonists. We conclude that our p(TLR7/8a-dopa) adjuvant is a viable approach to enhancing the immunogenicity and tolerability of protein subunit vaccines.

4.2 Introduction

Vaccines often require external help to induce the desired immune stimulation through components known as adjuvants. However, a careful balance between stimulation and safety is vital as excess activation levels often result in systemic inflammation and undesirable effects. Developing safe and effective adjuvants has proved challenging. New approaches to modulate and tailor the innate immune activation are being investigated. Rather than search for entirely novel agonists, we modulated the immune response to existing ligands. Recently, we demonstrated that small-molecule NF-κB inhibitors could be used to modulate the activity of CpG (TLR 9 agonist)

in vaccine formulations[1,2]. However, we did not observe similar effects *in vivo* when a mixture of TLR7/8 agonist (R848) was used with small molecule modulators as the adjuvant. We believe this was due to the high diffusion rate of R848 and the immunomodulators from the injection site. Therefore, we synthesized dimeric molecules by covalently linking an imidazoquinolinone (TLR7/8a) derivative with a conjugatable amine handle to known immunomodulators such as vanilloid, catechol, and honokiol derivatives. [3, 1] We showed immune modulation via conjugation of selective immunomodulators to small molecule TLR7/8a to develop TLR7/8a-modulator dimers. [4] Such a construct would lead to cellular colocalization of the immunostimulant and immunomodulator. This would result in the coactivation of TLR 7/8 receptors and immunomodulation from the coupled NF-κB modulators. Using ovalbumin (OVA) as a model antigen, we demonstrated that the imidazoquinolinone-immunomodulator dimers significantly reduce systemic toxicity induced by the small molecule immunostimulant while maintaining the adjuvanticity in vaccine formulation. Despite these highly favorable features, these dimers suffered from two predicted liabilities: high bioavailability/ biodistribution and poor solubility. Furthermore, small-molecule TLR7/8a-dopa dimer may have lower avidity for binding receptors or result in suboptimal receptor clustering than natural agonists.

A variety of approaches have been developed to improve small molecule adjuvants' pharmacokinetic properties for use in vaccines. One strategy is to physically entrap the adjuvant within nano- and micro-sized particles[5–7]. As an alternative to physically trapping the adjuvant within particles, which can be limited by relatively low and variable adjuvant loading, the small molecule adjuvant can be covalently linked to macromolecular carriers [8–11]. Potential advantages of conjugating small molecule immunostimulant to macromolecular carriers are that loading can be controlled by the number of functional groups used for adjuvant attachment. The

macromolecular conjugate is a chemically defined single molecule that can be chemically programmed.

Here, we developed a multivalent approach to conjugate repeating units of TLR7/8a and an immunomodulator (dopamine) on a macromolecular scaffold to improve these results. This improved the pharmacokinetic property of the TLR7/8a-dopamine (TLR7/8-dopa) conjugate combination. Moreover, unlike small-molecule TLR7/8a-dopa dimer, which may have lower avidity for binding receptors, this multivalent scaffold presents the ligands as repeating macromolecular units like pathogen particles.

4.3 Results and Discussion

Previously we investigated combining small molecule NF-κB modulators with immunostimulants as adjuvants in vaccine formulations. We identified vanillin, catechol, and honokiol derivatives as the most effective small molecule modulators[4]. These molecules have been well studied for their innate immunity modulation by directly inhibiting the canonical NF-κB pathway or scavenging pro-inflammatory mediators such as nitric oxide and other ROIs.[12–14] However, these small molecules did not show the desired response with R848 in vaccine formulations. High levels of systemic cytokines 1 hour after vaccination were observed. To overcome that, we designed and synthesized dimers by conjugating a TLR 7/8 imidazoquinoline derivative with a conjugatable amine handle to vanillin, catechol, and honokiol derivatives to yield IMD-ferulic (**1**), IMD-vanillin (**2**), IMD-catechol (**3**), IMD-biphenyl (**4**) dimers[15]. These small-molecule dimers reduced systemic cytokine levels while maintaining the antibody response compared to when formulated as a soluble mixture. However, these dimers had high bioavailability

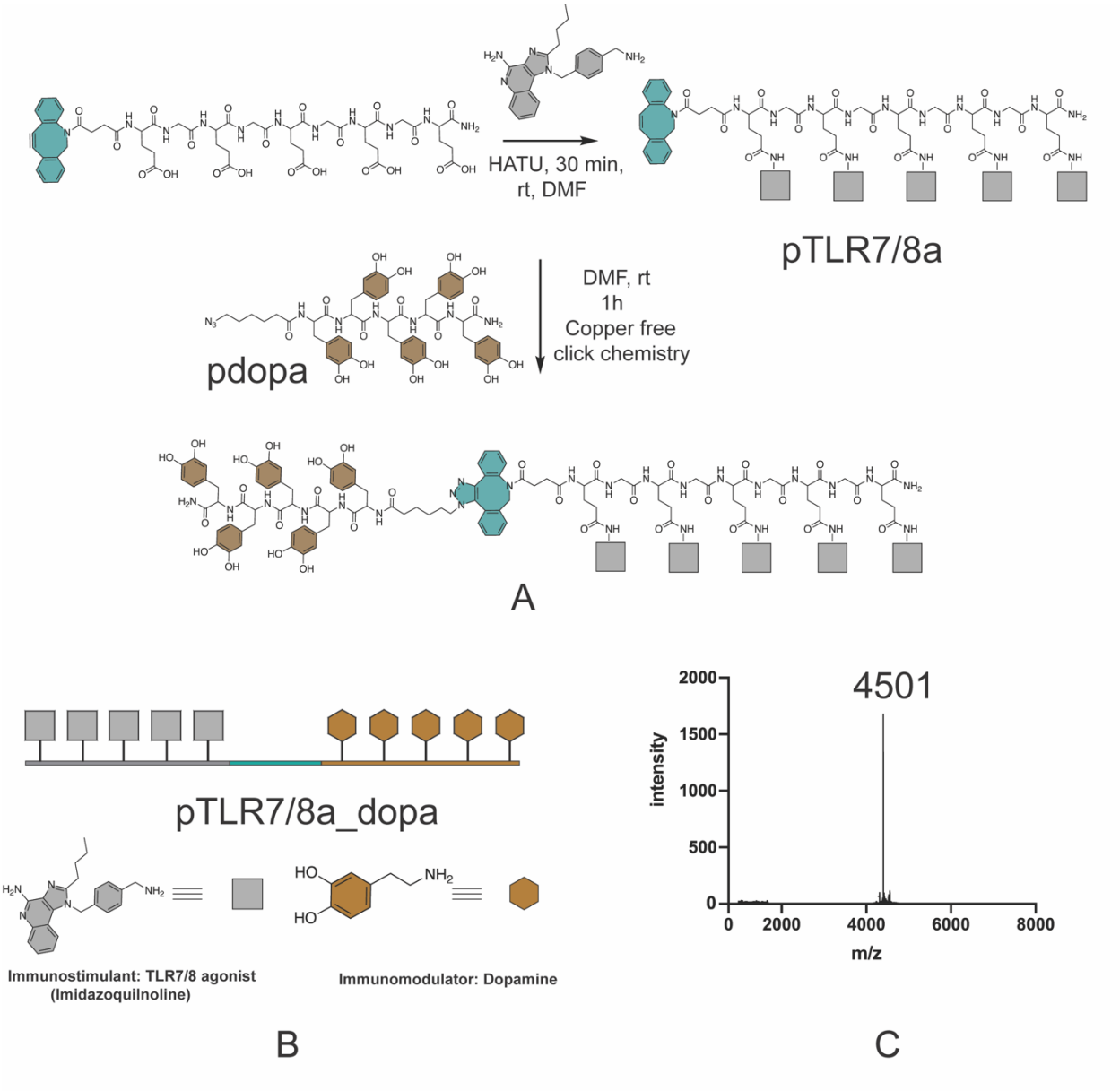

Figure 4.1. Synthesis of p(TLR7/8a_dopa). (A) Synthesis Scheme (B): Schematic presentation of the linked multivalent di-agonist. (C): MALDI trace of the linked multivalent di-agonist.

and biodistribution, which meant that excess compound was required to induce the desired level of the immune response. Also, due to pi-pi stacking, these compounds had limited solubility in aqueous media. Hence, we developed a macromolecular scaffold with repeating TLR7/8a and immunomodulator units (**Figure 4.1 B**)

4.3.1 Synthesis

The synthesis of the compound employed sequential conjugation chemistry used previously in the synthesis of PRR tri-agonists.[16,17] The synthesis started with the development of a peptide comprising five glutamic acids with glycine spacers (**Scheme S.4.3**). The N terminus of this peptide was modified with a DBCO handle via NHS chemistry (**Scheme S.4.3**). Following this, amine-functionalized imidazoquinoline (**2BXY_C6_NH2**) (**Figure 4.1 A**) was conjugated to the glutamic acid side chains using HATU coupling chemistry to give **pTLR7/8a**. Another peptide of five dopamine units was synthesized using solid-phase peptide synthesis. A hexane spacer with an azide handle was installed on the N terminus of this peptide, **pdopa (Scheme S.4.4)**. Following this, we conjugated **pTLR7/8** and **pdopa** using copper-free click chemistry to give **pTLR7/8a_dopa (Figure 4.1 A)**. The compound was purified using reverse-phase chromatography. Out of all the small molecule modulators, we chose dopamine because of solubility factors and the ease of incorporating it into a peptide. Amino acids with dopamine side chains are commercially available. Additionally, the hydroxy groups rendered the peptide scaffold soluble in water. It has been shown that particle formation is critical for enhancing the magnitude and duration of innate immune activation, especially TLR7/8 activating macromolecular carriers, in draining lymph nodes while reducing systemic distribution and toxicity.[18] So, we decided to formulate the compounds with Alum. Alum is extensively used in licensed vaccines for its adjuvanticity[19]. The mechanism of action of Alum is not well understood. However, a common explanation is the depot effect alum provides to vaccine components.[20,21]

4.3.2 In vitro experiment

Following synthesis, we next proceeded to analyze the immunological properties of the compound. Using a RAW macrophage NF-κB-SEAP (Secreted Alkaline Phosphatase) reporter cell line we measured the overall activity of the compounds. No reduction in the immune activity of the compound compared to the free imidazoquinolinone agonist was observed (**Figure 4.2A).** This implied that our multivalent scaffold did not hinder the

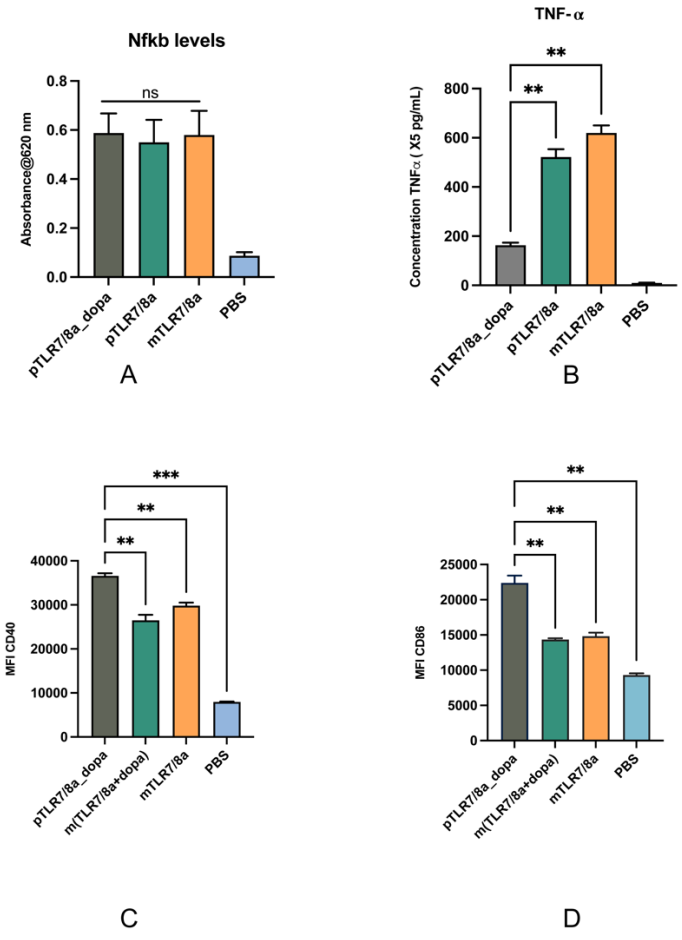

Figure 4.**2**. Immune activation as measured by (A): NF-κB in RAW-Blue 264.7 macrophage cell assay; (B): concentration of TNF-a in the supernatant of BMDMs after 18h of exposure to TLR7/8 ligand as either pTLR7/8a_dopa, pTLR7/8a, or mTLR7/8a; (C), (D): costimulatory molecules CD40 and CD86 on BMDMs. Error bars represent SD. Samples were run in triplicate. Statistical differences were determined via a two-tailed t-test (n= 3 per group). Each experiment was repeated thrice with similar results.

ligand-receptor interaction between imidazoquinoline units and TLR7/8 receptor. To further elucidate the immune activity of the compound we ran pro-inflammatory cytokine and cell surface protein expression assays on murine bone marrow-derived macrophages (BMDMs). After incubating BMDMs for 18 h with the compounds, we observed that **pTLR7/8a_dopa** reduced the expression of TNF-α three-fold (**Figure 4.2B)**. **pTLR7/8a** did not significantly change the TNF-a levels when compared to the parent ligand **(mTLR7/8a)**. This indicated that the multivalent scaffold was not hindering the ligand-receptor interaction. In a similar experiment, we stained the BMDMs for cell surface expression of CD40 and CD86, co-stimulatory molecules with important roles in adaptive immunity,[22] and quantified the expression levels using flow cytometry. Notably, we observed that the expression levels of CD40 and CD86 increased for **pTLR7/8a_dopa** (**Figure 4.2C, 4.2.D)**. This indicates that the chimeric molecule was modulating the immune response of the imidazoquinolinone as opposed to merely inhibiting the cytokine expression.

In addition to inhibition of the upstream events of NF-κB pathway, we hypothesize that our compound modulates the immune response by downstream inhibition of pro-inflammatory mediators such as nitric oxide and reactive oxygen species (ROS) similar to the small molecule dimers as shown before.[14] Previously we showed that the small molecule TLR7/8a-dopa dimer adjuvant reduced the NO levels to baseline levels compared to the parent TLR7/8a indicating that the dimer was a potent inhibitor of nitric oxide either through scavenging or direct inhibition of the enzymatic pathway. Additionally, using western blot analysis of RAW macrophage cell lysate we observed that the molecule inhibited inducible nitric oxide synthase (*i*NOS), a pathway precursor of NO.

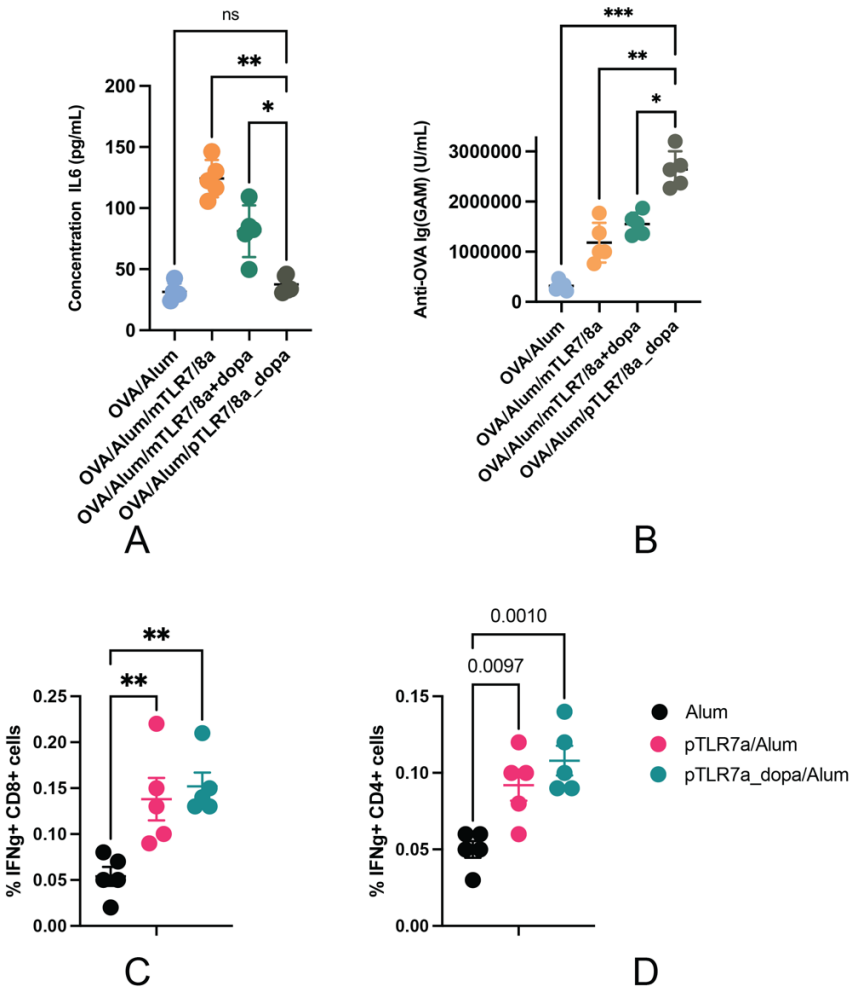

Figure 4.3. *In-vivo* vaccination studies. Mice (n=5) were vaccinated on day 0 with OVA (100 mg) adjuvanted with Alum (vehicle control), or 25 nmol of TLR7/8a formulated as m(TLR7/8a) + alum, p(TLR7/8a_dopa) + alum, m(TLR7/8a) + dopamine + alum. The final volume of each formulation was made 100 mL with PBS. Mice were given a vaccine boost on day 14. On days 1 and 21, sera were collected. Lymph nodes were collected from mice on day 28. Sera cytokine level (A) and antibody titer (B) were measured by ELISA. T cell response, (C) and (D) to OVA adjuvanted with just Alum, pTLR7/8+alum or pTLR7/8_dopa+alum was measured by intracellular cytokine staining. Statistical differences were determined via a two-tailed t-test.

4.3.3 In vivo analysis

With this promising *in vitro* analysis, we next set up *in vivo* experiments to see how this macromolecular scaffold would perform in a vaccine formulation. We chose to use alum to

formulate the vaccine components. Using ovalbumin as a model antigen we vaccinated mice. We performed subcutaneous injection (s.c) with 100 μg of OVA formulated with (1) just alum, (2) 25 nmoles of TLR7/8 agonist as a free small molecule with alum, (3) equimolar mixtures of imidazoquinolinone and NF-κB modulators in alum or (4) **p(TLR7/8a_dopa).** At the 1-hour mark post-injection, we collected sera from the mice and quantified systemic levels of TNF-α and IL-6 (**Figure 4.3**). We observed that formulation with **p(TLR7/8a_dopa)** resulted in the lowest level of systemic cytokines comparable to the alum/OVA formulation. On day 14 we performed a boost injection, then on day 28, we sacrificed the mice, collected sera, and analyzed anti-OVA antibodies. Notably, compound **p(TLR7/8a_dopa)** induced the highest levels of anti-OVA Ig (A+G+M).

Because activation of TLR 7/8 has been previously associated with increased CD8+ T cell function[23] we were interested in investigating if **p(TLR7/8a_dopa)** enhanced T cell activity compared to **pTLR7/8** agonist. On day 28 post the OVA vaccination experiment we harvested the lymph node of the mice and performed intracellular cytokine staining and analyzed the cells using Flow cytometry. We did not observe increased activity with **p(TL7/8a_dopa)** compared to **pTLR7/8a (Figure 4.3)**. Nevertheless, **p(TLR7/8a_dopa)** stimulated T cells to a similar level as **pTLR7/8a**. In summary, the attachment of the modulator increased the humoral response while maintaining T-cell response and decreasing systemic inflammation.

4.4 Conclusion

Agonists that activate TLR7/8 receptors are an attractive target as vaccine adjuvants. Small molecules activating TLR 7/8 such as the imidazoquinolinone family are potent immunostimulant whose major downside is their reactogenicity limiting their use. In this study, we show that by conjugating these small molecules with NF-κB modulating small molecules on a macromolecular

scaffold, we can modulate the immune response enhancing the adjuvanticity. Due to the large availability of molecules that modulate the NF-κB, IRF, and MAPK inflammatory pathways, we believe this strategy is a viable approach to formulating small molecule immunostimulants and immunomodulators as adjuvants in vaccines.

4.5 Materials and Methods

BMDC activation studies: Bone marrow derived dendritic cells (BMDCs) were harvested from the femurs of 6-week-old C57BL/6 mice (Jackson Laboratory). BMDCs were cultured in BMDC primary medium: RPMI 1640 (Life Technologies), 10% heat inactivated fetal bovine serum (FBS), 20 ng/mL granulocyte-macrophage colony-stimulating factor (GM-CSF), 2 mM L-glutamine (Life Technologies), antibioticantimycotic (1×) (Life Technologies), and 50 μM betamercaptoethanol (all components were 0.2 μM sterile filtered together before use). For BMDC activation studies, 2×10^5 cells per well were seeded in round-bottom 48-well plates and treated with various concentrations of linked PRR tri-agonist or 1:1:1(molar ratio) mixture of the analogous unlinked PRR agonists or various linked di-agonist combination, then incubated at 37 °C. The supernatants were collected after 6 h or 24 h. Cytokine concentration in the media were measured either by mouse inflammation kit CBA (BD Biosciences) or ELISA kits (BioLegend) following manufacturer's instructions.

***In-vitro* cytokine analysis by cytometric bead array (CBA).** CBA mouse inflammation kit was purchased from BD Biosciences. BMDCs were plated in 48 well plates (4×10^5 cells in 400 μL) and stimulated with indicated sample for 6 h. The supernatant was transferred to Eppendorf tubes and centrifuged at 1000 x g for 10 minutes. The supernatant was removed and diluted by a factor

of 2.5. The assay was then performed following manufacturers protocol and analyzed by a Novocyte flow cytometer. Data were analyzed using Graphpad Prism software.

***In-vitro* cytokine analysis by ELISA.** BMDCs were plated in 48 well plates (4 x 10^5 cells in 400 µL) and stimulated with indicated sample at 37 ^oC for 24 h. The supernatants were assessed by ELISA for IL-6 and TNF-a. ELISA kits were purchased from Biolegend and used according to instruction manual. Samples were diluted 100X.

***In-vivo* studies.** All animal experiments were approved by Institutional Animal Care and Use Committee (IACUC), University of Chicago (72517). Mice (n=5) were vaccinated on day 0 with OVA (100 ug) adjuvanted with alum (vehicle control), 25 nmole each of unconjugated agonist, equimolar mix of immunostimulant and immunomodulator (25 nmole), or 5 nmole of conjugated agonists in alum. The final volume of each formulation was made 100 uL with PBS. Mice were given a vaccine boost on day 14. On day 24, sera and spleens were collected from mice. Antibody titer was measured by ELISA and T cell response was measured by intracellular cytokine staining.

T-cell recall assays: Spleens were collected from mice on day 24 and incubated in ice-cold RPMI until processing. Spleens were processed into a single-cell suspension via mechanical disruption and passaged through a 70 µm strainer. The splenocytes were washed with PBS and then treated with RBC lysis buffer for 3 min at room temperature. The single-cell suspension was washed with PBS and resuspended in RPMI. These single cell suspensions were then plated at a density of 10^7 cells/mL and treated with respective peptide epitopes (20 mg/mL). Following two hours of incubation, golgi plug (Brefeldin A) was added and the cells were additionally stimulated for 6 h more. Following incubation, cells were stained with viability stain and for appropriate cell surface markers (CD4, CD8) and intracellular cytokine staining was performed for IFN-g. Samples were analyzed on a NovoCyte 3000 flow using the NovoExpress software. Total numbers of spleen/LN

lymphocytes were back-calculated from the number of marker-positive cells read and the total volume of sample processed by the NovoCyte 3000 flow cytometer.

Measurement of the anti-OVA IgG response: Blood was collected by cardiac puncture from mice on day 24 and serum was separated by centrifugation and stored at −20 °C. Sera was assayed for antibody levels against OVA using ELISA kit (Alpha Diagnostics) following manufacturer's protocol. The absorbance was measured at 450 nm in a microtiter-plate spectrophotometer using a blank measurement at 620 nm.

4. 6 REFERENCES

1. Moser, B. A.; Escalante-Buendia, Y.; Steinhardt, R. C.; Rosenberger, M. G.; Cassaidy, B. J.; Naorem, N.; Chon, A. C.; Nguyen, M. H.; Tran, N. T.; Esser-Kahn, A. P. Small Molecule NF-KB Inhibitors as Immune Potentiators for Enhancement of Vaccine Adjuvants. *Frontiers in Immunology* **2020**, *11*.

2. Moser, B. A.; Steinhardt, R. C.; Escalante-Buendia, Y.; Boltz, D. A.; Barker, K. M.; Cassaidy, B. J.; Rosenberger, M. G.; Yoo, S.; McGonnigal, B. G.; Esser-Kahn, A. P. Increased Vaccine Tolerability and Protection via NF-KB Modulation. *Science Advances 6* (37), eaaz8700.

3. Wu, Y.; Hu, Y.; Wang, B.; Li, S.; Ma, C.; Liu, X.; Moynagh, P. N.; Zhou, J.; Yang, S. Dopamine Uses the DRD5-ARRB2-PP2A Signaling Axis to Block the TRAF6-Mediated NF-KB Pathway and Suppress Systemic Inflammation. *Molecular Cell* **2020**, *78* (1), 42-56. e6.

4. Kimani, F. W.; Manna, S.; Moser, B.; Shen, J.; Nihesh, N.; Esser-Kahn, A. P. Improving the Adjuvanticity of Small Molecule Immune Potentiators Using Covalently Linked NF-KB Modulators. *ACS Med. Chem. Lett.* **2021**, *12* (9), 1441–1448.

5. Kasturi, S. P.; Skountzou, I.; Albrecht, R. A.; Koutsonanos, D.; Hua, T.; Nakaya, H. I.; Ravindran, R.; Stewart, S.; Alam, M.; Kwissa, M.; Villinger, F.; Murthy, N.; Steel, J.; Jacob, J.; Hogan, R. J.; García-Sastre, A.; Compans, R.; Pulendran, B. Programming the Magnitude and Persistence of Antibody Responses with Innate Immunity. *Nature* **2011**, *470* (7335), 543–547.

6. Kasturi, S. P.; Rasheed, M. A. U.; Havenar-Daughton, C.; Pham, M.; Legere, T.; Sher, Z. J.; Kovalenkov, Y.; Gumber, S.; Huang, J. Y.; Gottardo, R.; Fulp, W.; Sato, A.; Sawant, S.; Stanfield-Oakley, S.; Yates, N.; LaBranche, C.; Alam, S. M.; Tomaras, G.; Ferrari, G.; Montefiori, D.; Wrammert, J.; Villinger, F.; Tomai, M.; Vasilakos, J.; Fox, C. B.; Reed, S. G.; Haynes, B. F.; Crotty, S.; Ahmed, R.; Pulendran, B. 3M-052, a Synthetic TLR-7/8 Agonist, Induces Durable HIV-1 Envelope-Specific Plasma Cells and Humoral Immunity in Nonhuman Primates. *Sci Immunol* **2020**, *5* (48), eabb1025.

7. Madan-Lala, R.; Pradhan, P.; Roy, K. Combinatorial Delivery of Dual and Triple TLR Agonists via Polymeric Pathogen-like Particles Synergistically Enhances Innate and Adaptive Immune Responses. *Sci Rep* **2017**, *7* (1), 2530.

8. Lynn, G. M.; Laga, R.; Darrah, P. A.; Ishizuka, A. S.; Balaci, A. J.; Dulcey, A. E.; Pechar, M.; Pola, R.; Gerner, M. Y.; Yamamoto, A.; Buechler, C. R.; Quinn, K. M.; Smelkinson, M. G.; Vanek, O.; Cawood, R.; Hills, T.; Vasalatiy, O.; Kastenmüller, K.; Francica, J. R.; Stutts, L.; Tom, J. K.; Ryu, K. A.; Esser-Kahn, A. P.; Etrych, T.; Fisher, K. D.; Seymour, L. W.; Seder, R. A. In Vivo Characterization of the Physicochemical Properties of Polymer-Linked TLR Agonists That Enhance Vaccine Immunogenicity. *Nat Biotechnol* **2015**, *33* (11), 1201–1210.

9. Kuai, R.; Sun, X.; Yuan, W.; Ochyl, L. J.; Xu, Y.; Hassani Najafabadi, A.; Scheetz, L.; Yu, M.-Z.; Balwani, I.; Schwendeman, A.; Moon, J. J. Dual TLR Agonist Nanodiscs as a Strong Adjuvant System for Vaccines and Immunotherapy. *J Control Release* **2018**, *282*, 131–139.

10. Wilson, D. S.; Hirosue, S.; Raczy, M. M.; Bonilla-Ramirez, L.; Jeanbart, L.; Wang, R.; Kwissa, M.; Franetich, J.-F.; Broggi, M. A. S.; Diaceri, G.; Quaglia-Thermes, X.; Mazier, D.; Swartz, M. A.; Hubbell, J. A. Antigens Reversibly Conjugated to a Polymeric Glyco-Adjuvant Induce Protective Humoral and Cellular Immunity. *Nature Materials* **2019**, *18* (2), 175–185.

11. Ali, O. A.; Verbeke, C.; Johnson, C.; Sands, R. W.; Lewin, S. A.; White, D.; Doherty, E.; Dranoff, G.; Mooney, D. J. Identification of Immune Factors Regulating Antitumor Immunity Using Polymeric Vaccines with Multiple Adjuvants. *Cancer Res* **2014**, *74* (6), 1670–1681.
12. Murakami, Y.; Hirata, A.; Ito, S.; Shoji, M.; Tanaka, S.; Yasui, T.; Machino, M.; Fujisawa, S. Re-Evaluation of Cyclooxygenase-2-Inhibiting Activity of Vanillin and Guaiacol in Macrophages Stimulated with Lipopolysaccharide. *Anticancer Research* **2007**.

13. Zheng, L. T.; Ryu, G. M.; Kwon, B. M.; Lee, W. H.; Suk, K. Anti-Inflammatory Effects of Catechols in Lipopolysaccharide-Stimulated Microglia Cells: Inhibition of Microglial Neurotoxicity. *European Journal of Pharmacology* **2008**.

14. Gilmore, T. D.; Herscovitch, M. Inhibitors of NF-KB Signaling: 785 and Counting. *Oncogene*. 2006.

15. Shukla, N. M.; Malladi, S. S.; Mutz, C. A.; Balakrishna, R.; David, S. A. Structure-Activity Relationships in Human Toll-like Receptor 7-Active Imidazoquinoline Analogues. *Journal of Medicinal Chemistry* **2010**, *53* (11), 4450–4465.

16. Nihesh, N.; Manna, S.; Studnitzer, B.; Shen, J.; Esser-Kahn, A. P. A Synthetic Pathogen Mimetic Molecule Induces a Highly Amplified Synergistic Immune Response via Activation of Multiple Signaling Pathways. *Chem. Sci.* **2021**, *12* (19), 6646–6651.

17. Albin, T. J.; Tom, J. K.; Manna, S.; Gilkes, A. P.; Stetkevich, S. A.; Katz, B. B.; Supnet, M.; Felgner, J.; Jain, A.; Nakajima, R.; Jasinskas, A.; Zlotnik, A.; Pearlman, E.; Davies, D. H.; Felgner, P. L.; Burkhardt, A. M.; Esser-Kahn, A. P. Linked Toll-Like Receptor Triagonists Stimulate Distinct, Combination-Dependent Innate Immune Responses. *ACS Cent. Sci.* **2019**, *5* (7), 1137–1145.

18. Lynn, G. M.; Chytil, P.; Francica, J. R.; Lagová, A.; Kueberuwa, G.; Ishizuka, A. S.; Zaidi, N.; Ramirez-Valdez, R. A.; Blobel, N. J.; Baharom, F.; Leal, J.; Wang, A. Q.; Gerner, M. Y.; Etrych, T.; Ulbrich, K.; Seymour, L. W.; Seder, R. A.; Laga, R. Impact of Polymer-TLR-7/8 Agonist (Adjuvant) Morphology on the Potency and Mechanism of CD8 T Cell Induction. *Biomacromolecules* **2019**, *20* (2), 854–870.

19. Djurisic, S.; Jakobsen, J. C.; Petersen, S. B.; Kenfelt, M.; Klingenberg, S. L.; Gluud, C. Aluminium Adjuvants Used in Vaccines. *Cochrane Database Syst Rev* **2018**, *2018* (7), CD013086.

20. HogenEsch, H.; O'Hagan, D. T.; Fox, C. B. Optimizing the Utilization of Aluminum Adjuvants in Vaccines: You Might Just Get What You Want. *npj Vaccines* **2018**, *3* (1), 1–11.

21. Moyer, T. J.; Kato, Y.; Abraham, W.; Chang, J. Y. H.; Kulp, D. W.; Watson, N.; Turner, H. L.; Menis, S.; Abbott, R. K.; Bhiman, J. N.; Melo, M. B.; Simon, H. A.; Herrera-De la Mata, S.; Liang, S.; Seumois, G.; Agarwal, Y.; Li, N.; Burton, D. R.; Ward, A. B.; Schief, W. R.; Crotty, S.; Irvine, D. J. Engineered Immunogen Binding to Alum Adjuvant Enhances Humoral Immunity. *Nat Med* **2020**, *26* (3), 430–440.

22. Elgueta, R.; Benson, M. J.; De Vries, V. C.; Wasiuk, A.; Guo, Y.; Noelle, R. J. Molecular Mechanism and Function of CD40/CD40L Engagement in the Immune System. *Immunological Reviews*. 2009.

23. Li, Q.; Yan, Y.; Liu, J.; Huang, X.; Zhang, X.; Kirschning, C.; Xu, H. C.; Lang, P. A.; Dittmer, U.; Zhang, E.; Lu, M. Toll-Like Receptor 7 Activation Enhances CD8+ T Cell Effector Functions by Promoting Cellular Glycolysis. *Frontiers in Immunology* **2019**.

Appendix A: Supplementary Data for Chapter 2

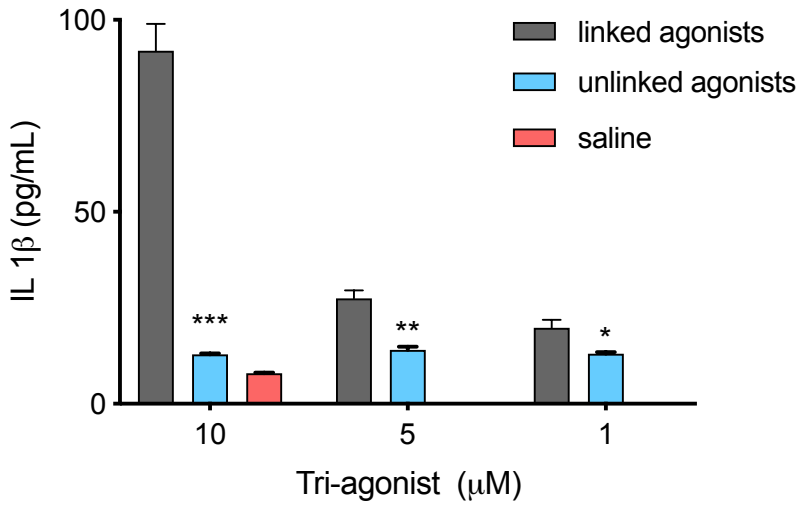

Figure S2.1: In vitro cytokine expression from BMDCs as measured by ELISA (IL-1b). Cells were incubated with PRR triagonist (100 nM, 1 μM or 10 μM) or a 1:1:1 (molar ratio) mixture of the analogous unlinked TLR agonists for 24 h at 37 °C. Error bars represent standard deviation of the mean. Samples were run in triplicate, where * $p < 0.05$; ** $p < 0.01$, *** $p < 0.001$. Statistical analysis is between the linked tri-agonist and the unlinked mixture, performed using ANOVA by the Turkey's multiple comparison test.

Peptide synthesis: Peptides were synthesized on an automated microwave peptide synthesizer by Fmoc solid phase peptide synthesis. A low-loading Rink Amide resin (Sigma Aldrich, 0.34 $meqg^{-1}$) was used for all peptide synthesis. Peptide couplings were performed using DIC, Oxyma at 90 °C for 3 minutes per coupling except for the coupling of Arginine, in which case the coupling reaction went up to 10 minutes at 90 °C for two cycles. The Fmoc group was deprotected with 20 % piperidine in DMF (v/v) at 75 °C for 5 minutes. Azido hexanoic acid was used to modify the N

terminus of the TAT-GWWWG peptide. A PEG_6 spacer was installed between the TAT peptide and the GWWWG sequence. Peptides were cleaved in 95% trifluoroacetic acid, 2.5% H2O and 2.5% triisopropylsilane, for 4 h at 25 °C. After precipitation in ice-cold diethyl ether, peptides were dried, resuspended in 0.1 % TFA in 50:50 water/acetonitrile mixture and purified by HPLC on a C8 or C18 column using a gradient of 0.1% TFA in acetonitrile. Peptide masses were confirmed by matrix-assisted laser desorption/ionization–time of flight mass spectrometry (MALDI-TOF).

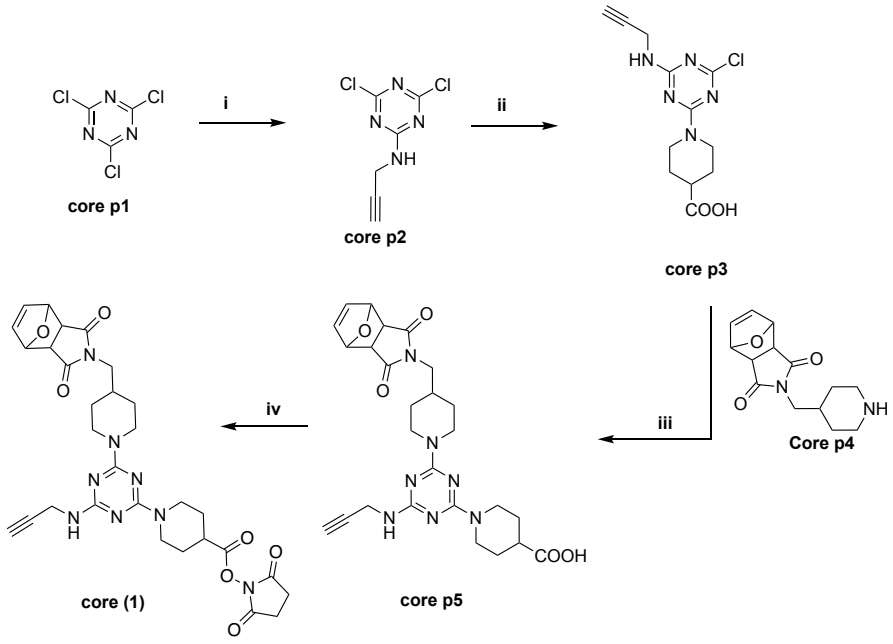

Scheme S2.1: Synthetic route of **core (1)**. Reagents and conditions: (i) propargyl amine, DIPEA, THF, 0 °C, 3 h 80%; (ii) isonipecotic acid, DIPEA, H_2O: DMF (20:80), 80 °C, 12 h, 70%; (iii) DIPEA, DMF, 60 °C, 6 h, 50%; (iv) N'-Dissuccinimidyl carbonate, DMAP, DMF, rt, 6 h, 87%.

core p3: core p2[1] (200 mg, 1 mmol) was dissolved in DMF (10 mL). DIPEA (200 uL, 1.1 mmol) and isonipecotic acid (150 mg, 1.15 mmol) were added to the solution. The mixture was heated at 80 °C for 12 h. The reaction was monitored by mass spectrometry. The reaction was then

concentrated and purified by column chromatography (1% MeOH/ EtOAc with 1% NH_4OH). The product was a white powder (170 mg, 70%). ^{1}H NMR (400 MHz, DMSO-d_6) δ 12.29 (br s, 1H), 4.07 – 3.98 (m, 2H), 3.09 (s, 2H), 2.61 – 2.50 (m, 1H), 1.87 (m, 2H), 1.46 (m, 2H), 1.25 (m, 3H). ^{13}C NMR (101 MHz, DMSO) δ 175.50, 168.44, 164.99, 163.63, 80.76, 72.90, 53.55, 42.39, 29.72, 27.67, 18.06, 16.72. ESI-MS: m/z calc'd for $C_{12}H_{14}ClN_5O_2$ $[M+H]^+$ 296.3, observed 296.1.

core p5: **core p3** (100 mg, 0.33 mmol), **core p4**[3] (110 mg, 0.4 mmol) and DIPEA (100uL, 0.55 mmol) were dissolved in DMF (5 mL) and heated to 60 °C for 6 h. The reaction was monitored by mass spectrometry. The reaction was then concentrated and purified by column chromatography (1% MeOH/EtOAc with 1% NH_4OH). The product was a white powder (60 mg, 0.11 mmol, 35%). ^{1}H NMR (400 MHz, DMSO-d_6) δ 11.94 (br s, 1H), 6.55 (s, 2H), 5.13 (s, 2H), 4.52 (br s, 2H), 4.12 (s, 2H), 3.27 (d, J = 7.2 Hz, 2H), 3.09(m, 3H), 2.93 (s, 2H), 2.89 (br s, 1H), 2.55 (m, 1H), 2.01 – 1.80 (m, 3H), 1.62 (d, J = 12.8 Hz, 2H), 1.57 – 1.36 (br s, 2H), 1.25(m, 3H), 1.17 – 0.92 (br s, 2H). ^{13}C NMR (101 MHz, DMSO) δ 176.76, 175.47, 161.47, 158.90, 158.55, 136.48, 80.44, 73.34, 53.56, 47.13, 43.56, 43.20, 42.88, 41.82, 33.96, 29.86, 28.66, 27.76, 18.04, 16.72. ESI-MS: m/z calc'd for $C_{26}H_{31}N_7O_5$ M+H]$^+$ 522.3, observed 522.2.

core (1): core p5 (20 mg, 0.038 mmol) was dissolve in DMF (5 mL). DMAP (1 mg, 0.007 mmol) and N'-Dissuccinimidyl carbonate (20 mg, 0.08 mmol) were added to the solution. The solution was stirred at rt for 6 h. The reaction was monitored by mass spectrometry. After HPLC purification (Solvent A: 0.1 % TFA in water, solvent B: 0.1% TFA in acetonitrile. Gradient: t 0-20 min, ramp 10% B to 90% B), fractions containing **core** were pooled and concentrated to give 65 % yield. ESI-MS: m/z calc'd for $C_{30}H_{34}N_8O_7$ $[M+H]^+$ 619.2, observed 618.9.

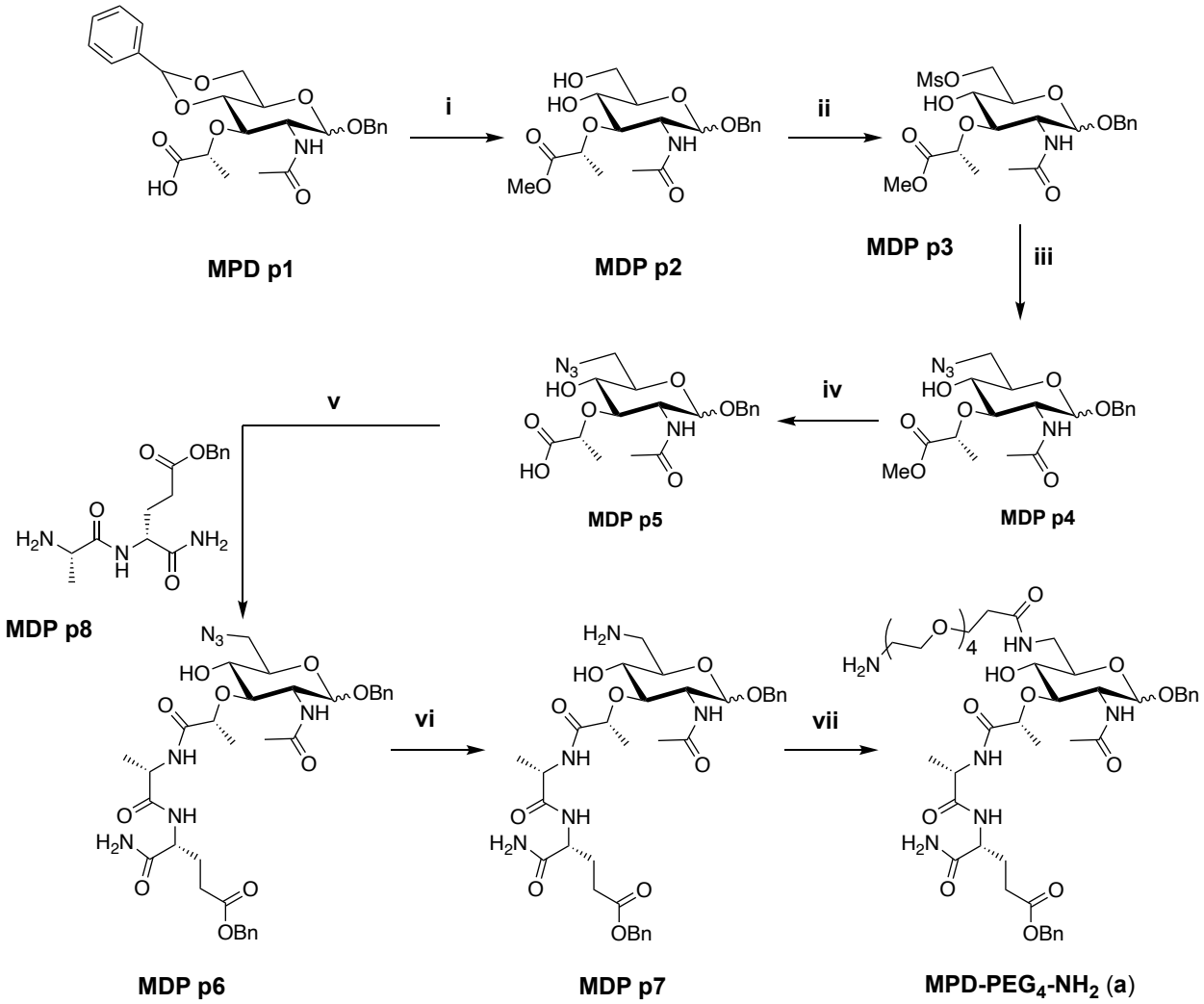

Scheme S2.2[2]: Synthetic route of MDP-PEG_4-NH_2 (a). Reagents and conditions: (i) IRA H^+ Resin, MeOH, reflux, 4 h, quantitative; (ii) p-toluene sulfonic acid, methyl sulfonyl chloride, pyridine, -10 °C, 78% 4 h; (iii) sodium azide, DMF, 70 °C, 16 h, 77%; (iv) potassium hydroxide; (v) HATU, DIPEA, DMF, rt, 3 h 63%; (vi) TCEP, MeOH, 60 °C, 5 h, 82%; (vii) (1) azido-PEG_4-NHS ester, DIPEA, DMF, 45 °C 3 h; (2) TCEP, MeOH, 60 °C, 2 h, 87%.

MDP p7: MDP p6 (25 mg, 0.035 mmol) was dissolved in methanol (10mL) and 1 M TCEP solution in water (2 mL) was added. The solution was heated to 60 °C for 5 h. The reaction was monitored by mass spectrometry and was stopped when **MDP p6** could no longer be detected.

The solvent was removed, and the residue was dissolved in 0.1% TFA/H_20 (1 mL). **MDP p7** was purified by HPLC (Solvent A: 0.1 % TFA in water, solvent B: 0.1% TFA in acetonitrile. Gradient: t 0-20 min, ramp 10% B to 90% B). Desired fractions were pooled and concentrated to give **MDP p7** (0. 020 g, 0.029 mmol, 82%)**.**

^{1}H NMR (400 MHz, DMSO-d_6) δ 8.14 (d, J = 8.2 Hz, 1H), 8.09 (d, J = 8.2 Hz, 1H), 7.57 (d, J = 6.9 Hz, 1H), 7.40-7.31 (m, 10H), 7.08 (s, 1H), 5.30 (d, J = 6.9 Hz, 2H), 5.07 (s, 2H), 4.74 (d, J = 3.5 Hz, 1H), 4.67 (d, J = 12.5 Hz, 1H), 4.44 (d, J = 12.5 Hz, 1H), 4.27 (m, 1H), 4.19 (m, 1H), 4.10 (m, 1H), 3.81 (m, 1H), 3.66 (m, 1H), 3.57 – 3.45 (m, 3H), 3.17 (d, J = 5.0 Hz, 2H), 2.35 (t, J = 7.9 Hz, 2H), 2.01 (m, 1H), 1.78 (s, 4H), 1.24 (d, J = 6.7 Hz, 3H), 1.21 (d, J = 6.9 Hz, 3H). ^{13}C NMR (101 MHz, DMSO) δ 171.28, 171.02, 170.48, 170.46, 167.89, 136.08, 134.52, 126.78, 126.56, 126.34, 126.24, 125.92, 125.84, 94.29, 77.48, 74.81, 71.58, 67.99, 66.21, 63.84, 60.43, 58.94, 51.27, 49.81, 46.95, 46.54, 28.37, 25.37, 20.96, 17.37, 16.70. ESI-MS: m/z calc'd for $C_{33}H_{45}N_5O_{10}$ $[M+H]^+$ 673.2, observed 673.4.

MDP-PEG$_4$-NH2: MDP p7 (20 mg, 0.029 mmol)**,** azido-PEG$_4$-NHS ester (22mg, 0.060 mmol) and DIPEA (6 uL, 0.035 mmol) were dissolved in DMF (5 mL) and heated to 45 ^{o}C for 3 h. The reaction was monitored by mass spectrometry and stopped when **MDP p7** could no longer be detected. 1 M TCEP solution in water (2 mL) was added and the temperature was increased to 60 ^{o}C and maintained for 2 h. The reaction was monitored by mass spectrometry. **MDP-PEG$_4$-NH2** was purified by HPLC (Solvent A: 0.1 % TFA in water, solvent B: 0.1% TFA in acetonitrile. Gradient: t 0-20 min, ramp 10% B to 90% B). Fractions containing **MDP-PEG$_4$-NH2** were pooled and concentrated to give a yield of 55%**.**

^{1}H NMR (400 MHz, DMSO-d_6) δ 8.17 (d, J = 8.2 Hz, 1H), 8.12 (d, J = 8.2 Hz, 1H), 7.58 (d, J = 6.8 Hz, 1H), 7.40 – 7.31 (m, 10H), 7.09 (s, 1H), 5.08 (s, 2H), 4.75 (d, J = 3.5 Hz, 1H), 4.64 (d, J = 12.4 Hz, 1H), 4.42 (d, J = 12.4 Hz, 1H), 4.27 (m, 2H), 4.19 (m, 1H), 3.64 – 3.41 (m, 29 H), 3.23 – 3.13 (m, 2H), 2.36 (t, J = 7.9 Hz, 2H), 2.07 – 1.92 (m, 1H), 1.79 (s, 4H), 1.24 (d, J = 6.6 Hz, 3H), 1.22 (d, J = 6.9 Hz, 3H). ^{13}C NMR (101 MHz, DMSO) δ 173.77, 173.08, 172.70, 172.24, 170.99, 169.78, 137.65, 136.24, 128.53, 128.32, 128.10, 127.97, 127.76, 127.67, 95.95, 78.76, 76.58, 70.92, 69.79, 68.04, 66.71, 65.59, 52.99, 51.60, 48.30, 38.72, 35.98, 30.11, 27.06, 22.67, 19.04, 18.42. ESI-MS: m/z calc'd for $C_{44}H_{66}N_6O_{15}$ [M+H] $^{+}$ 919.4, observed 919.3.

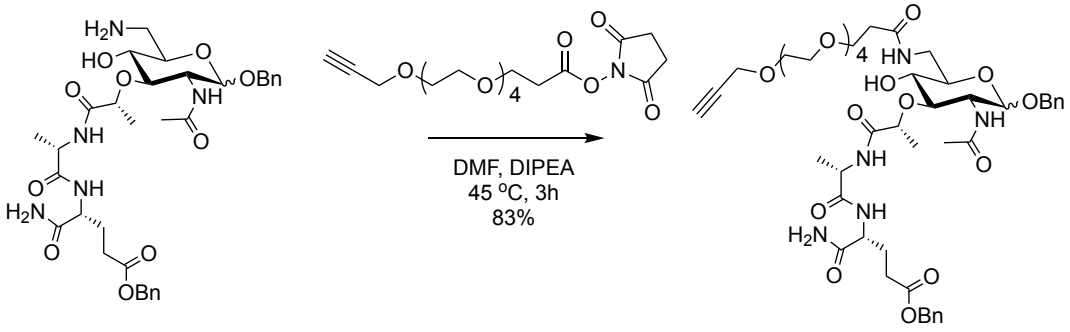

MDP p7 **MPD-Peg$_4$-alkyne (d)**

MDP-PEG$_4$-alkyne: MDP p7 (20 mg, 0.029 mmol)**,** alkyne-PEG$_4$-NHS ester (25 mg, 0.060 mmol) and DIPEA (6 uL, 0.035 mmol) were dissolved in DMF (5 mL) and heated to 45 °C for 3 h. The reaction was monitored by mass spectrometry and stopped when **MDP p7** could no longer be detected. **MDP-PEG$_4$-alkyne** was purified by HPLC (Solvent A: 0.1 % TFA in water, solvent B: 0.1% TFA in acetonitrile. Gradient: t 0-20 min, ramp 10% B to 90% B). Fractions containing **MDP-PEG$_4$-alkyne** were pooled and concentrated to give a yield of 83%. ESI-MS: m/z calc'd for $C_{47}H_{67}N_5O_{16}$ [M+H] $^{+}$ 958.5, observed 958.3.

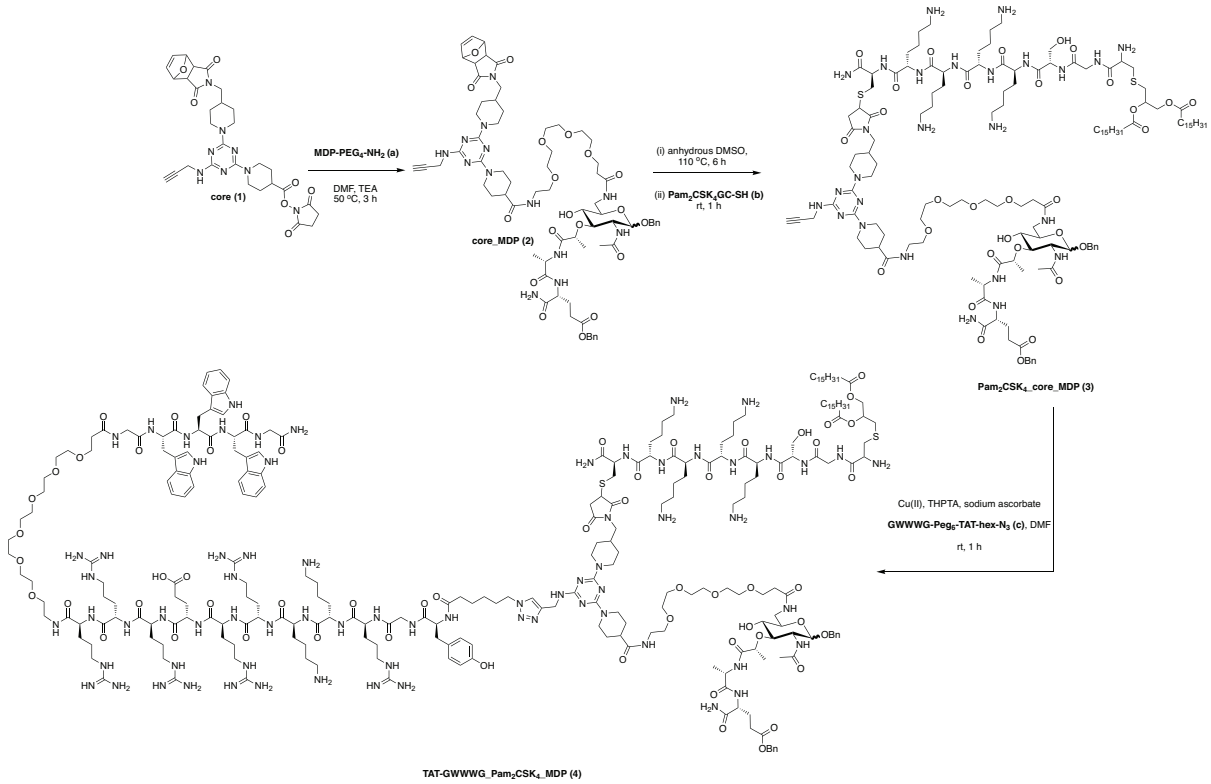

Scheme S2.3: Synthetic route of **TAT-GWWW_Pam$_2$CSK$_4$_MDP (4)** tri-agonist.

core_MDP (2): MDP-PEG$_4$-NH2 (a) (10 mg, 0.01 mmol)**, core (1)** (9 mg, 0.013 mmol) and TEA (5µL) were dissolved in DMF (5 mL). The mixture was stirred at 50 °C for 3 h. The reaction was monitored by mass spectrometry and was stopped when **MDP-PEG$_4$-NH2 (a)** could no longer be detected. The solvent was removed, and the residue was dissolved in 0.1% TFA/H_20 (1 mL). The compound was purified by HPLC (Solvent A: 0.1 % TFA in water, solvent B: 0.1% TFA in acetonitrile. Gradient: t 0-20 min, ramp 10% B to 90% B). Desired fractions were pooled and concentrated to give **core_MDP (2)**. (11 mg, 0.008 mmol, 77%). ESI-MS: m/z calc'd for $[M+H]^+$ 1422.7 observed 1422.5.

Pam_2CSK_4_core_MDP (3): Furan protected **core_MDP (2)** (10 mg, 0.007 mmol) was dissolved in anhydrous DMSO (3 mL) and stirred for 6 h at 110 °C to expose the maleimide. The reaction was monitored by mass spectrometry. When furan was completely deprotected, the solution was cooled to room temperature. **Pam_2CSK_4GC (b)** (10 mg, 0.007 mmol) and DIPEA (500 uL) were added to the solution and stirred for 1 h. The reaction was monitored by mass spectrometry. **Pam_2CSK_4_core_MDP (3)** was purified by HPLC (Solvent A: 0.1 % TFA in water, solvent B: 0.1% TFA in acetonitrile. Gradient: t 0-20 min, ramp 10% B to 90% B) to give a yield of 52%. ESI-MS: m/z calc'd for $[M+H]^+$ 2784.6 observed 2784.8

TAT-GWWWG_ Pam_2CSK_4_MDP (4): Pam_2CSK_4_core_MDP (3) (5 mg, 0.002 mmol) was dissolved in DMF (200 µL). **GWWWG-peg_6-TAT-hex-N_3 (c)** (5 mg, 0.002 mmol) dissolved in DMF (200 µL) were added to the solution. 200 µL of $CuSO4•5H_2O$ (20 mM) solution and 400 µL of THPTA (50 mM) solution were mixed and added to the mixture. 200 µL of sodium ascorbate (100 mM) was then added to the reaction mixture. The reaction was monitored by mass spectrometry. **TAT-GWWWG_ Pam_2CSK_4_MDP (4)** was purified by HPLC (Solvent A: 0.1 % TFA in water, solvent B: 0.1% TFA in acetonitrile. Gradient: t 0-20 min, ramp 10% B to 90% B) to give a yield of 30%. MALDI-TOF: m/z calc'd for $[M+H]^+$ 5490.14 observed $[M+H]^+$ 5490.94

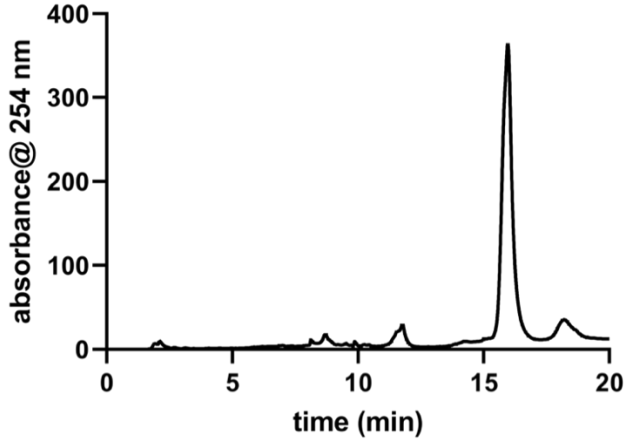

Figure S2.2: HPLC trace of **TAT-GWWWG_ Pam$_2$CSK$_4$_MDP** measured at 254 nm on a C8 analytical column. Solvent A: 0.1 % TFA in HPLC grade water, solvent B: 0.1% TFA in HPLC grade acetonitrile. Gradient: ramp 10% B to 90% over 20 min.

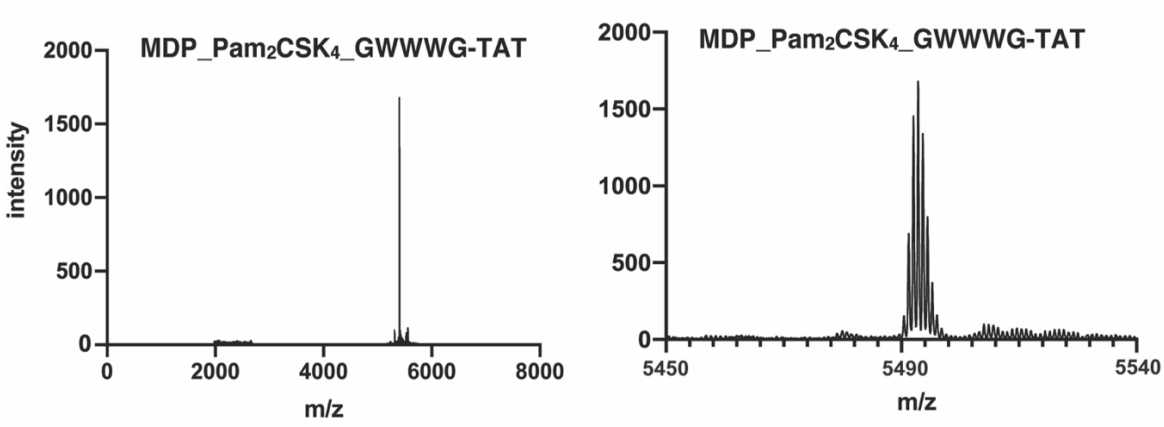

Figure S2.3: MALDI trace of **TAT-GWWWG_ Pam$_2$CSK$_4$_MDP** tri-agonist (left) and enlarged view of the major peak (right). Sample acquired in positive reflector mode using dihydroxybenzoic acid matrix.

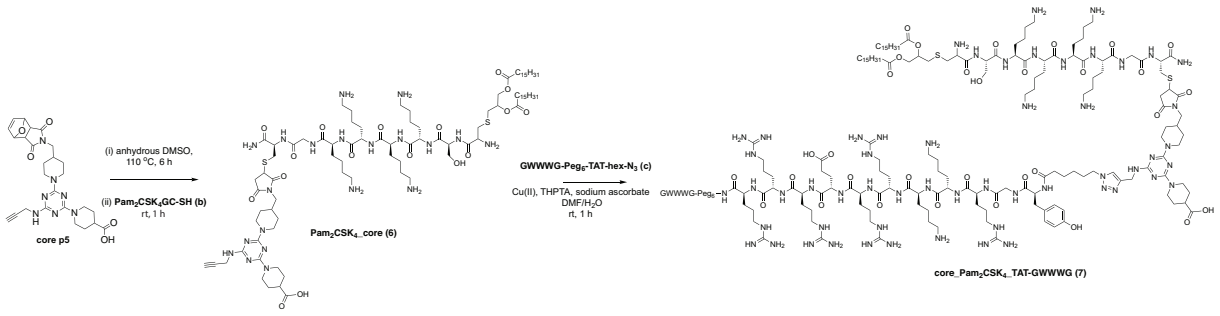

Scheme S2.4: Synthetic route to di-agonist **core_Pam$_2$CSK$_4$_TAT-GWWWG (7)**.

core_MDP_TAT-GWWWG (**8**): **core_MDP (2)** (5 mg, 0.035 mmol) was dissolved in DMF (200 µL). **GWWWG-Peg$_6$-TAT-hex-N$_3$ (c)** (10 mg, 0.004 mmol) dissolved in DMF (200 µL) were added to the solution. 200 µL of CuSO4•5H$_2$O (20 mM) solution and 400 µL of THPTA (50 mM) solution were mixed and added to the mixture. 200 µL of sodium ascorbate (100 mM) was then added to the reaction mixture. The reaction was monitored by mass spectrometry. **core_MDP_TAT-GWWWG (8)** was purified by HPLC (Solvent A: 0.1 % TFA in water, solvent B: 0.1% TFA in acetonitrile. Gradient: t 0-20 min, ramp 10% B to 90% B) to give a yield of 30%. MALDI-TOF: m/z calc'd for $[M+H]^+$ 4128.19, observed $[M+H]^+$ 4128.11

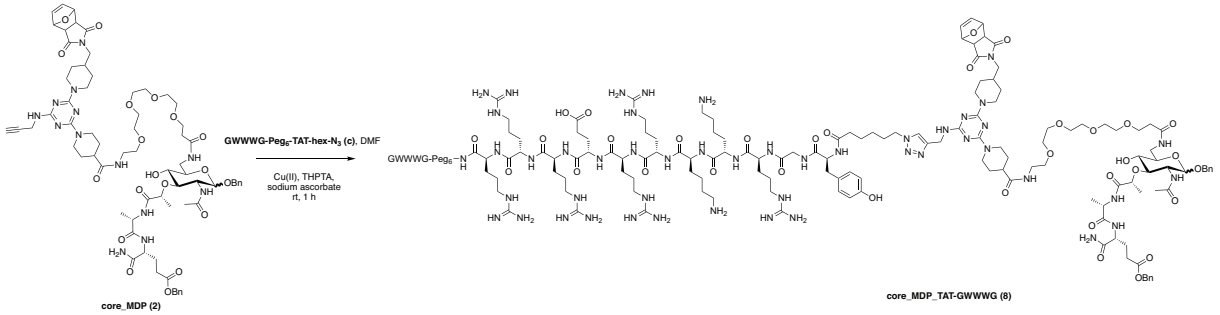

Scheme S2.5: Synthetic route to di-agonist **core_MDP_TAT-GWWWG (8)**.

Pam_2CSK_4_core (6): Furan protected **core p5** (4mg, 0.007 mmol) was dissolved in anhydrous DMSO (3 mL) and stirred for 6 h at 110 °C to expose the maleimide. The reaction was monitored by mass spectrometry. When furan was completely deprotected, the solution was cooled to room temperature. **Pam_2CSK_4GC (b)** (10 mg, 0.007 mmol) and DIPEA (500 uL) were added to the solution and stirred for 1 h. The reaction was monitored by mass spectrometry. **Pam_2CSK_4_core** (**6**) was purified by HPLC (Solvent A: 0.1 % TFA in water, solvent B: 0.1% TFA in acetonitrile. Gradient: t 0-20 min, ramp 10% B to 90% B) to give a yield of 82%. MALDI-TOF: m/z calc'd for [M+H] 1884.19, observed $[M+H]^+$ 1883.99.

core_Pam_2CSK_4_TAT-GWWWG (**7**): **Pam_2CSK_4_core** (**6**) (5 mg, 0.003 mmol) was dissolved in DMF (200 µL). **GWWWG-Peg_6-TAT-hex-N_3 (c)** (5 mg, 0.002 mmol) dissolved in DMF (200 µL) were added to the solution. 200 µL of $CuSO4•5H_2O$ (20 mM) solution and 400 µL of THPTA (50 mM) solution were mixed and added to the mixture. 200 µL of sodium ascorbate (100 mM) was then added to the reaction mixture. The reaction was monitored by mass spectrometry. **core_Pam_2CSK_4_TAT-GWWWG** (**7**) was purified by HPLC (Solvent A: 0.1 % TFA in water, solvent B: 0.1% TFA in acetonitrile. Gradient: t 0-20 min, ramp 10% B to 90% B) to give a yield of 30%. MALDI-TOF: m/z calc'd for $[M+H]^+$ 4589.69, observed $[M+H]^+$ 4590.10

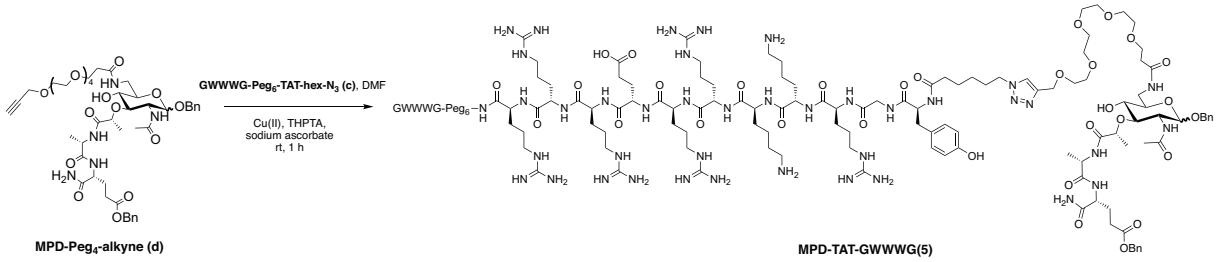

Scheme S2.6: Synthetic route to di-agonist **MDP_TAT-GWWWG (5)**.

MDP_TAT-GWWWG (**5**): **MDP-Peg$_4$-alkyne** (**d**) (5 mg, 0.005mmol) was dissolved in DMF (200 μL). **GWWWG-Peg$_6$-TAT-hex-N$_3$ (c)** (5 mg, 0.002 mmol) dissolved in DMF (200 μL) were added to the solution. 200 μL of CuSO4•5H$_2$O (20 mM) solution and 400 μL of THPTA (50 mM) solution were mixed and added to the mixture. 200 μL of sodium ascorbate (100 mM) was then added to the reaction mixture. The reaction was monitored by mass spectrometry. **MDP_ TAT-GWWWG (5)** was purified by HPLC (Solvent A: 0.1 % TFA in water, solvent B: 0.1% TFA in acetonitrile. Gradient: t 0-20 min, ramp 10% B to 90% B) to give a yield of 30%. MALDI-TOF: m/z calc'd for $[M+H]^+$ 3663.96, observed $[M+H]^+$ 3664.16

REFERENCES

1. 1 R. Banerjee, N. J. Pace, D. R. Brown, E. Weerapana, *J. Am. Chem. Soc.*, 2013, **135**, 2497–2500.

2. C. L. Grimes, D. K. Podolsky, E. K. O'Shea, *Bioorg. Med. Chem. Lett.*, 2010, **20**, 6061–6063.

3. T. J. Albin, J. K. Tom, S. Manna, A. P. Gilkes, S. A. Stetkevich, B. B. Katz, M. Supnet, J. Felgner, A. Jain, R. Nakajima, A. Jasinskas, A. Zlotnik, E. Pearlman, D. H. Davies, P. L. Felgner, A. M. Burkhardt, A. P. Esser-Kahn, *ACS Cent. Sci.*, 2019, **5**, 1137–1145.

Appendix B: Supplementary Data for Chapter 3

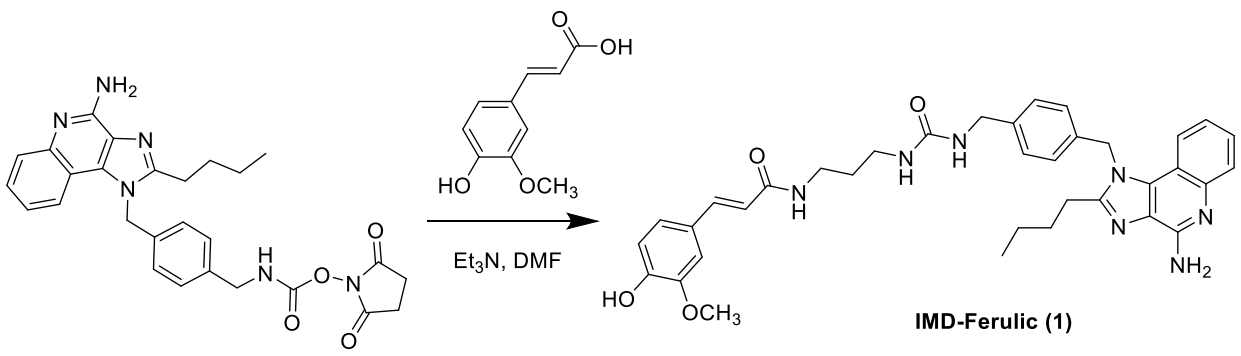

IMD-Ferulic (1)

Compound **1** was synthesized as follows. To a solution of **7** (19 mg, 0.078 mmol) and triethylamine (0.01 mL, 0.078 mmol) was added **12** (26 mg, 0.052 mmol) in 1 mL DMF. The mixture was stirred at room temperature under argon for 12 h. The reaction mixture purified using preparative HPLC to give the product as a white solid (15 mg, 40% yield)

^{1}H NMR (400 MHz, DMSO) δ 13.47 (s, 1H), 7.95 (t, *J* = 8.3 Hz, 2H), 7.80 (d, *J* = 8.0 Hz, 1H), 7.62 (t, *J* = 7.4 Hz, 1H), 7.38 (t, *J* = 7.3 Hz, 1H), 7.30 (d, *J* = 15.7 Hz, 1H), 7.20 (t, *J* = 7.6 Hz, 2H), 7.12 (d, *J* = 1.7 Hz, 1H), 7.05 – 6.95 (m, 3H), 6.79 (d, *J* = 8.1 Hz, 1H), 6.42 (d, *J* = 15.7 Hz, 1H), 6.37 (s, 1H), 5.96 (d, *J* = 11.2 Hz, 1H), 5.93 (s, 2H), 4.15 (s, 2H), 3.80 (s, 3H), 3.14 (dd, *J* = 12.6, 6.5 Hz, 2H), 2.98 (dd, *J* = 16.6, 9.0 Hz, 4H), 1.73 (dt, *J* = 15.3, 7.6 Hz, 2H), 1.58 – 1.45 (m, 2H), 1.39 (dq, *J* = 14.7, 7.4 Hz, 2H), 0.87 (t, *J* = 7.4 Hz, 3H).(not observed NH_2) ^{13}C NMR (100 MHz, DMSO) δ 165.8, 158.9, 158.6, 158.5, 157.4, 149.2, 148.7, 148.3, 141.2, 139.3, 135.8, 134.3, 134.1, 129.9, 128.0, 126.9, 125.9, 125.2, 125.1, 122.0, 119.4, 119.0, 116.0, 114.9, 112.9, 111.1, 55.9, 43.9, 36.7, 30.7, 29.7, 29.4, 26.6, 22.9, 22.2, 14.1. HRMS (ESI) m/z calcd for $(C_{36}H_{41}N_7O_4)+H^+$: 636.3298 $[M + H]^+$; found: 636.3294

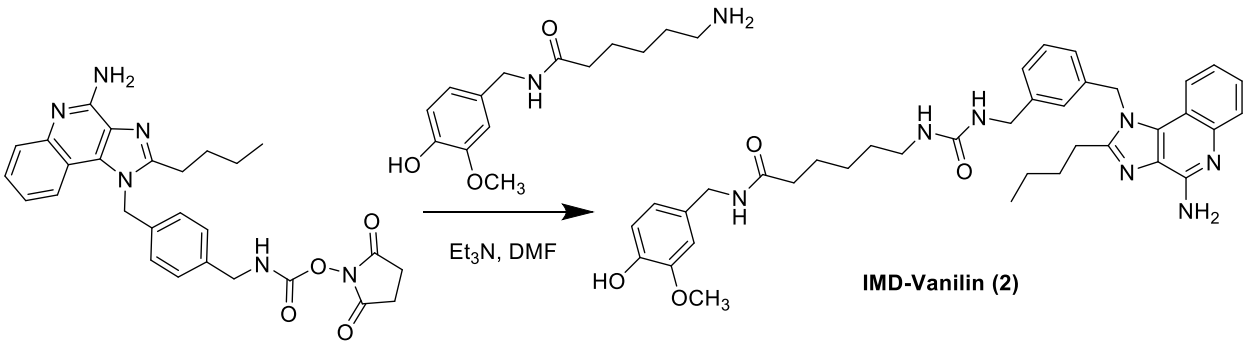

Compound **2** was synthesized as follows. To a solution of **8** (20 mg, 0.066 mmol) and triethylamine (0.01 mL, 0.078 mmol) was added **12** (26 mg, 0.052 mmol) in 1 mL DMF. The mixture was stirred at room temperature for 12 h. The reaction mixture purified using preparative HPLC to give the product as a white solid (18 mg, 54% yield) ^{1}H NMR (400 MHz, DMSO) δ 13.51 (s, 1H), 8.15 (t, *J* = 5.8 Hz, 1H), 7.95 (d, *J* = 8.2 Hz, 1H), 7.79 (d, *J* = 8.0 Hz, 1H), 7.62 (t, *J* = 7.4 Hz, 1H), 7.37 (t, *J* = 7.4 Hz, 1H), 7.18 (t, *J* = 7.3 Hz, 2H), 7.01 (d, *J* = 8.1 Hz, 2H), 6.79 (d, *J* = 1.7 Hz, 1H), 6.69 (d, *J* = 8.0 Hz, 1H), 6.62 (dd, *J* = 8.0, 1.8 Hz, 1H), 6.24 (s, 1H), 5.93 (s, 2H), 5.89 (s, 1H), 4.13 (d, *J* = 5.5 Hz, 4H), 3.72 (s, 4H), 2.95 (dd, *J* = 15.7, 8.0 Hz, 4H), 2.08 (dd, *J* = 9.4, 5.3 Hz, 2H), 1.72 (dt, *J* = 15.3, 7.6 Hz, 2H), 1.49 (dt, *J* = 15.0, 7.5 Hz, 2H), 1.36 (qd, *J* = 14.9, 7.2 Hz, 4H), 1.20 (dt, *J* = 14.7, 7.3 Hz, 2H), 0.87 (t, *J* = 7.4 Hz, 3H).(not observed NH) ^{13}C NMR (100 MHz, DMSO) δ 172.3, 159.0, 158.7, 158.4, 157.4, 149.3, 147.9, 145.8, 141.2, 135.8, 134.4, 134.1, 130.9, 129.8, 128.0, 125.8, 125.2, 125.1, 122.0, 120.1, 118.9, 115.6, 112.9, 112.1, 55.9, 48.6, 42.9, 42.3, 35.8, 30.2, 29.7, 26.7, 26.5, 25.6, 22.2, 14.1. HRMS (ESI) m/z calcd for $(C_{37}H_{46}N_7O_4)^+$: 652.3611 [M + H]$^+$; found: 652.3610

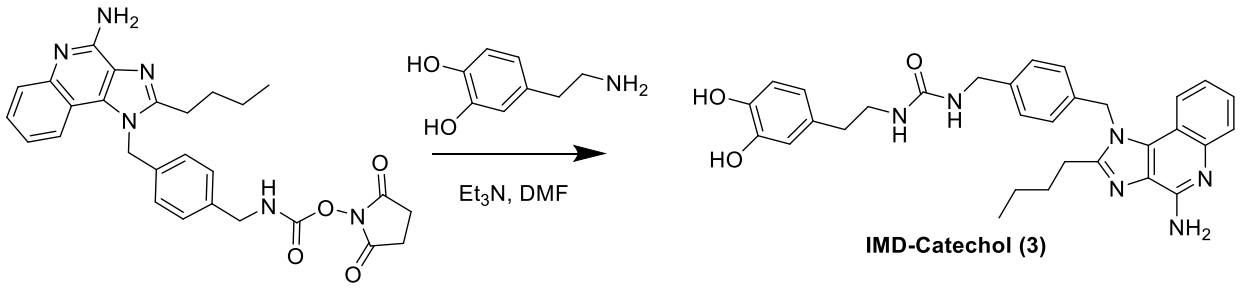

IMD-Catechol (3)

Compound **3** was synthesized as follows. To a solution of dopamine hydrochloride (20 mg, 0.105mmol) and triethylamine (0.027 mL, 0.105 mmol) was added **12** (26 mg, 0.052 mmol) in 1 mL DMF. The mixture was stirred at room temperature for 12 h. The reaction mixture purified using preparative HPLC to give the product as a white solid (9.3 mg, 33% yield) ^{1}H NMR (400 MHz, DMSO) δ 13.53 (s, 1H), 7.95 (d, *J* = 8.3 Hz, 1H), 7.79 (d, *J* = 8.0 Hz, 1H), 7.62 (t, *J* = 7.8 Hz, 1H), 7.37 (t, *J* = 7.4 Hz, 1H), 7.18 (t, *J* = 6.6 Hz, 2H), 7.01 (d, *J* = 8.1 Hz, 2H), 6.61 (d, *J* = 7.9 Hz, 1H), 6.55 (d, *J* = 1.9 Hz, 1H), 6.40 (dd, *J* = 8.0, 1.9 Hz, 1H), 6.34 (s, 1H), 5.93 (s, 2H), 5.84 (s, 1H), 4.13 (s, 2H), 3.11 (t, *J* = 7.0 Hz, 2H), 3.00 – 2.89 (m, 2H), 2.46 (t, *J* = 7.3 Hz, 2H), 1.73 (dt, *J* = 15.3, 7.6 Hz, 2H), 1.37 (dt, *J* = 14.6, 7.4 Hz, 2H), 0.87 (t, *J* = 7.3 Hz, 3H).(not observed -OH and NH_2) ^{13}C NMR (100 MHz, DMSO) δ 159.1, 158.7, 158.3, 157.4, 149.3, 145.5, 143.9, 141.1, 136.3, 135.8, 134.3, 134.06, 132.28, 130.83, 129.89, 128.06, 125.90, 125.23, 125.13, 122.96, 122.04, 119.67, 118.96, 117.83, 116.4, 115.9, 114.9, 112.9, 48.7, 42.8, 41.7, 36.0, 29.7, 26.7, 22.2, 14.2. HRMS (ESI) m/z calcd for ($C_{31}H_{34}N_6O_4$,): 554.2642 $[M]^+$; found: 554.2648

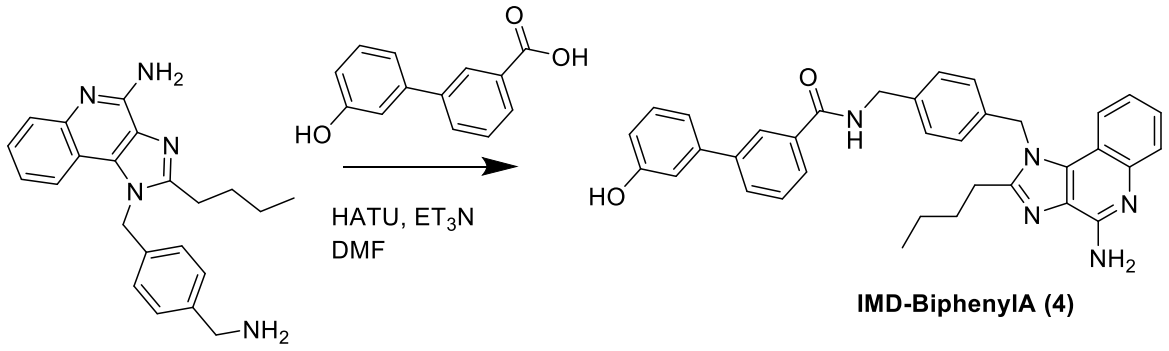

IMD-BiphenylA (4)

Compound **4** was synthesized as follows. To a solution of the imidazoquinoline[3] (30 mg, 0.084 mmol) and **9** (20 mg, 0.093 mmol) in 5 mL DMF stirred at room temperature under argon was added triethylamine (0.015 mL, 1.5 equiv., 0.15 mmol) and 1-[Bis(dimethylamino)methylene]-1H-1,2,3-triazolo[4,5-b] pyridinium 3-oxide hexafluorophosphate (HATU) (41 mg, 1.1 equiv, 0.12 mmol in 0.2 mL DMF). The mixture was stirred at room temperature for 12 h. The reaction mixture was loaded on a silica column and purified by using column chromatography using DCM/MeOH 9:1 to yield an off-white powder. (30 mg, 55% yield) ^{1}H NMR (400 MHz, DMSO) δ 13.55 (s, 1H), 9.57 (s, 1H), 9.15 (t, J = 5.9 Hz, 1H), 8.09 (s, 1H), 7.97 (d, J = 8.3 Hz, 1H), 7.86 – 7.72 (m, 3H), 7.62 (t, J = 7.7 Hz, 1H), 7.53 (t, J = 7.7 Hz, 1H), 7.37 (t, J = 7.7 Hz, 1H), 7.31 (d, J = 8.4 Hz, 2H), 7.26 (d, J = 7.9 Hz, 1H), 7.12 (d, J = 7.8 Hz, 1H), 7.07 (dd, J = 11.9, 5.1 Hz, 3H), 6.80 (dd, J = 8.0, 2.1 Hz, 1H), 5.95 (s, 2H), 4.47 (d, J = 5.7 Hz, 2H), 3.01 – 2.90 (m, 2H), 1.79 – 1.64 (m, 2H), 1.44 – 1.31 (m, 2H), 0.87 (t, J = 7.3 Hz, 3H). ^{13}C NMR (100 MHz, DMSO) δ 166.5, 158.7, 158.4, 157.8, 149.5, 141.4, 140.8, 139.7, 135.8, 135.2, 134.4, 130.4, 129.8, 129.4, 128.9, 126.8, 126.4, 125.7, 125.1, 122.2, 119.4, 118.3, 115.2, 114.1, 112.9, 48.7, 42.6, 35.5, 32.3, 29.7, 26.6, 22.2, 14.1. HRMS (ESI) m/z calcd for ($C_{35}H_{33}N_5O_2$) $+H^+$: 556.2713, $[M + H]^+$; found: 556.2718

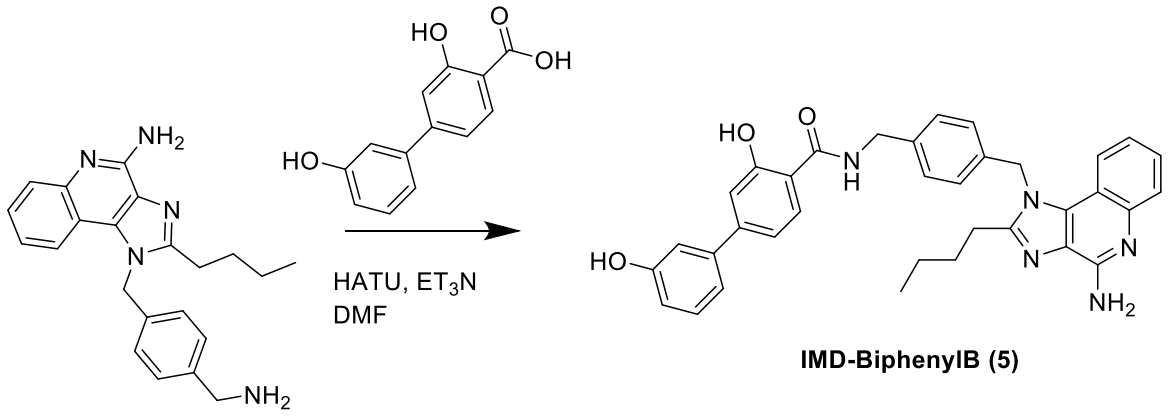

Compound **5** was synthesized as follows. To a solution of the imidazoquinoline[3] (30 mg, 0.083 mmol) and **10** (35 mg, 0.15 mmol) in 5 mL DMF stirred at room temperature under argon was added triethylamine (0.015 mL, 1.5 equiv., 0.15 mmol) and HATU (50 mg, 1.1 equiv, 0.13 mmol in 0.2 mL DMF). The mixture was stirred at room temperature for 12 h. The reaction mixture was loaded on a silica column and purified by using column chromatography using DCM/MeOH 9:1 to yield an off-white powder. The product was further purified using preparative HPLC (20 mg, 55% yield) ^{1}H NMR (400 MHz, DMSO) δ 13.89 (s, 1H), 12.55 (s, 1H), 9.35 (t, *J* = 6.0 Hz, 1H), 9.05 (s, 2H), 8.01 – 7.87 (m, 2H), 7.84 – 7.73 (m, 1H), 7.67 – 7.57 (m, 1H), 7.40 – 7.20 (m, 4H), 7.16 – 6.96 (m, 6H), 6.82 – 6.77 (m, 1H), 5.95 (s, 2H), 4.49 (d, *J* = 5.8 Hz, 2H), 3.00 – 2.93 (m, 2H), 1.78 – 1.65 (m, 2H), 1.38 (dq, *J* = 14.7, 7.4 Hz, 2H), 0.90 – 0.82 (m, 3H). ^{13}C NMR (100 MHz, DMSO) δ 169.4, 161.0, 158.4, 157.4, 149.4, 145.9, 139.2, 135.8, 135.0, 134.6, 134.8, 129.9, 129.8, 128.6, 128.5, 128.6, 126.3, 126.1, 125.2, 125.1, 122.0, 118.9, 118.3, 116.8, 116.2, 115.4, 114.4, 113.4, 112.9, 48.7, 42.4, 29.7, 26.7, 22.2, 14.1 HRMS (ESI) m/z calcd for ($C_{35}H_{33}N_5O_3$) + H^+: 572.2662 $[M + H]^+$; found: 572.2659

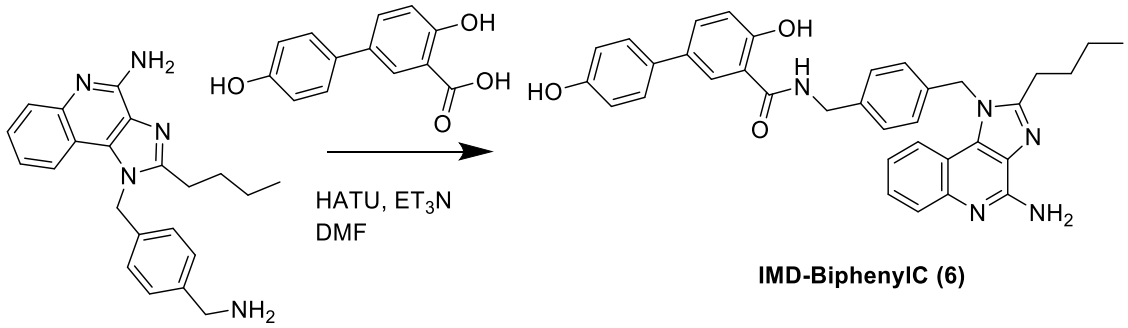

IMD-BiphenylC (6)

Compound **6** was synthesized as follows. To a solution of the imidazoquinoline (ref) (30 mg, 0.084 mmol) and **11** (20 mg, 0.093 mmol) in 5 mL DMF stirred at room temperature under argon was added triethylamine (0.015 mL, 1.5 equiv., 0.15 mmol) and HATU (41 mg, 1.1 equiv, 0.12 mmol in 0.2 mL DMF). The mixture was stirred at room temperature for 12 h. The reaction mixture was loaded on a silica column and purified by using column chromatography using DCM/MeOH 9:1 to yield an off-white powder. The product was further purified using preparative HPLC (33.3 mg, 75 % yield) ^{1}H NMR (400 MHz, DMSO) δ 13.82 (s, 1H), 12.52 (s, 1H), 9.25 (t, *J* = 6.0 Hz, 1H), 8.97 (s, 2H), 7.90 (d, *J* = 8.3 Hz, 1H), 7.81 (d, *J* = 8.4 Hz, 1H), 7.74 – 7.68 (m, 1H), 7.58 – 7.52 (m, 1H), 7.49 – 7.43 (m, 2H), 7.29 (dd, *J* = 11.4, 4.1 Hz, 1H), 7.23 (d, *J* = 8.2 Hz, 2H), 7.05 (dd, *J* = 8.4, 1.8 Hz, 1H), 7.02 – 6.95 (m, 3H), 6.82 – 6.72 (m, 2H), 5.84 (d, *J* = 27.7 Hz, 2H), 4.40 (d, *J* = 5.7 Hz, 2H), 2.95 – 2.85 (m, 2H), 1.65 (dt, *J* = 15.3, 7.5 Hz, 2H), 1.39 – 1.23 (m, 2H), 0.79 (t, *J* = 7.3 Hz, 3H).^{13}C NMR (100 MHz, DMSO) δ 169.1, 160.7, 158.3, 157.4, 149.4, 146.0, 140.7, 139.1, 135.8, 134.6, 134.8, 130.5, 129.9, 128.9, 128.4, 126.1, 125.2, 125.1, 122.0, 118.9, 118.3, 117.9, 117.6, 115.8, 115.8, 114.6, 113.9, 112.9, 48.7, 42.4, 29.7, 26.7, 22.2, 14.1 HRMS (ESI) m/z calcd for $(C_{35}H_{33}N_5O_3)+H^+$: 572.2662 $[M + H]^+$ found: 572.2659

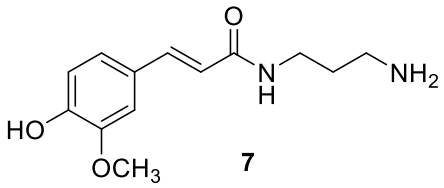

7

Compound **7** was synthesized as follows. To a solution of trans-ferulic acid (200 mg, 1.03 mmol, 1.0 equiv.) and 3-azidopropylamine (0.15 mL, 1.5 mmol, 1.5 equiv.) in 5 mL DMF, was added triethylamine (0.14 mL, 1.02 mmol, 1.0 equiv.) and HATU (390 mg, 1.02 mmol, 1.0 equiv.) and the solution stirred for 12 h at RT under argon. The reaction mixture was extracted into ethyl acetate (10 mL X 3) and the solvent evaporated in vacuo. The crude product obtained from the organic layer was dissolved in 5 mL MeOH/H2O 4:1 and to this solution Tris(2-carboxyethyl) phosphine hydrochloride (295 mg, 1.03 mmol) was added and the mixture stirred for 12 h at RT. The reaction mixture was loaded on a silica column and purified by using column chromatography using DCM/MeOH 9:1 to yield an amorphous solid (80 mg, 67 % yield). ^{1}H NMR (400 MHz, DMSO) δ 8.20 (t, *J* = 5.8 Hz, 1H), 7.77 (d, *J* = 39.7 Hz, 2H), 7.33 (d, *J* = 15.7 Hz, 1H), 7.13 (d, *J* = 1.7 Hz, 1H), 6.99 (dd, *J* = 8.2, 1.7 Hz, 1H), 6.79 (d, *J* = 8.1 Hz, 1H), 6.45 (d, *J* = 15.7 Hz, 1H), 3.80 (s, 3H), 3.24 (q, *J* = 6.5 Hz, 2H), 2.81 (dt, *J* = 12.4, 6.1 Hz, 2H), 1.78 – 1.68 (m, 2H). (not observed OH)^{13}C NMR (100 MHz, DMSO) δ 166.4, 148.8, 148.3, 139.7, 126.7, 122.10, 119.0, 116.1, 111.2, 55.9, 37.3, 36.2, 28.0. HRMS (ESI) m/z calcd for $(C_{13}H_{18}N_2O_3)+Na^+$: 273.1215 $[M + Na]^+$; found: 273.1209

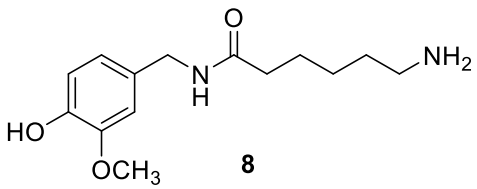

8

Compound **8** was synthesized as follows. To a solution of 4-hydroxy-3-methoxybenzylamine hydrochloride (75 mg, 0.40 mmol, 1.0 equiv.) and 6-Azidohexanoic Acid NHS ester (100 mg, 0.40 mmol, 1.0 equiv.) in 1 mL DMF was added triethylamine (0.06 mL, 0.43 mmol, 1.2 equiv.) and the solution stirred for 12 h at RT under argon. The reaction mixture was dissolved in 5 mL MeOH/H2O 4:1 and to this solution Tris(2-carboxyethyl) phosphine

hydrochloride (120 mg, 0.40 mmol) was added and the mixture stirred for 12 h at RT. The reaction mixture was loaded on a silica column and purified by using column chromatography using DCM/MeOH 9:1 to yield an amorphous solid (58 mg, 50 % yield). ^{1}H NMR (400 MHz, DMSO) δ 8.84 (s, 1H), 8.19 (t, *J* = 5.7 Hz, 1H), 7.68 (s, 2H), 6.81 (d, *J* = 1.7 Hz, 1H), 6.70 (d, *J* = 8.0 Hz, 1H), 6.63 (dd, *J* = 8.0, 1.8 Hz, 1H), 4.15 (d, *J* = 5.8 Hz, 2H), 3.74 (s, 3H), 2.84 – 2.70 (m, 2H), 2.17 – 2.06 (m, 2H), 1.59 – 1.44 (m, 4H), 1.36 – 1.23 (m, 2H).^{13}C NMR (100 MHz, DMSO) δ 172.2, 147.9, 145.8, 130.9, 120.2, 115.6, 112.2, 56.0, 42.3, 35.6, 27.3, 25.9, 25.3. HRMS (ESI) m/z calcd for $(C_{14}H_{22}N_2O_3)+Na^+$: 289.1528 $[M + Na]^+$; found: 289.1521

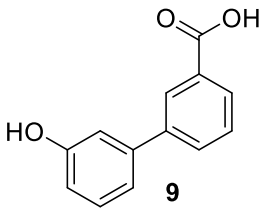

9

Compound **9** was synthesized as follows. A mixture of 3-hydroxyphenylboronic acid (220 mg, 1.59 mmol) 3-iodobenzoic acid (200 mg, 0.81 mmol) potassium carbonate (400 mg, 2.89 mmol) and Pd/C (10%) in 20 mL H2O was refluxed at 80 °C for 4 h. Solution was acidified with 1M HCl and extracted with ethylacetate and washed with brine. Solvent evaporated in vacuo. Compound was purified by column chromatography to yield product as white powder (120 mg, 69% yield) ^{1}H NMR (400 MHz, DMSO) δ 8.13 (t, J = 1.6 Hz, 1H), 7.96 – 7.91 (m, 1H), 7.88 – 7.82 (m, 1H), 7.58 (dd, J = 9.6, 5.8 Hz, 1H), 7.28 (t, J = 7.9 Hz, 1H), 7.13 – 7.05 (m, 2H), 6.81 (dd, J = 7.8, 2.0 Hz, 1H).(not observed OH, COOH) ^{13}C NMR (100 MHz, DMSO) δ 167.7, 158.4, 141.1, 141.1, 131.9, 131.4, 130.6, 129.8, 128.6, 127.6, 117.9, 115.4, 113.9. HRMS (ESI) m/z calcd for $(C_{13}H_{10}O_3)$: 214.0630 $[M]^+$; found: 214.0673

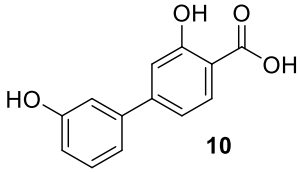

10

Compound **10** was synthesized as follows. A mixture of 3-hydroxyphenylboronic acid (220 mg, 1.59 mmol) 2-hydroxy-4-iodobenzoic acid (210 mg, 0.79 mmol) potassium carbonate (400 mg,

2.89 mmol) and Pd/C (10%) in 20 mL H2O was refluxed at 80 °C for 4 h. Solution was acidified with 1M HCl and extracted with ethylacetate and washed with brine. Solvent evaporated in vacuo. Compound was purified by column chromatography to yield product as white powder (126 mg, 68%) ^{1}H NMR (400 MHz, DMSO) δ 13.97 (s, 1H), 11.33 (s, 1H), 9.56 (d, *J* = 40.7 Hz, 1H), 7.83 (dd, *J* = 20.0, 8.2 Hz, 1H), 7.28 (t, *J* = 7.9 Hz, 1H), 7.15 (ddd, *J* = 14.2, 10.4, 5.0 Hz, 3H), 7.05 (dd, *J* = 5.2, 3.2 Hz, 1H), 6.86 – 6.80 (m, 1H).^{13}C NMR (100 MHz, DMSO) δ 172.2, 161.8, 158.3, 158.1, 147.8, 140.5, 131.3, 130.5, 118.1, 116.0, 115.0, 114.1, 112.3. HRMS (ESI) m/z calcd for ($C_{13}H_{10}O_4$): 230.0579 $[M]^+$; found: 230.0551

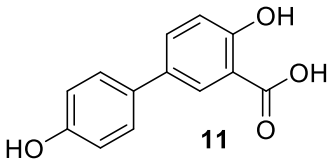

11

A mixture of 4-hydroxyphenylboronic acid (220 mg, 1.59 mmol) 3-iodobenzoic acid (200 mg, 0.79 mmol) potassium carbonate (400 mg, 2.89 mmol) and Pd/C (10%) in 20 mL H2O was refluxed at 80 °C for 4 h. Solution was acidified with 1M HCl and extracted with ethylacetate and washed with brine. Solvent evaporated in vacuo. Compound was purified by column chromatography to yield product as white powder (75 mg, 41% yield) ^{1}H NMR (400 MHz, DMSO) δ 11.19 (s, 1H), 9.51 (s, 1H), 7.93 (t, *J* = 5.3 Hz, 1H), 7.74 (dd, *J* = 8.6, 2.5 Hz, 1H), 7.43 (ddd, *J* = 7.7, 4.8, 2.4 Hz, 3H), 7.01 (d, *J* = 8.6 Hz, 1H), 6.86 – 6.81 (m, 2H). ^{13}C NMR (100 MHz, DMSO) δ 172.3, 160.2, 157.2, 133.8, 132.0, 130.3, 127.7, 127.6, 127.5, 118.1, 116.2, 116.2, 113.6. HRMS (ESI) m/z calcd for ($C_{13}H_{10}O_4$)+H^+: 231.0657 $[M + H]^+$ found: 231.0473

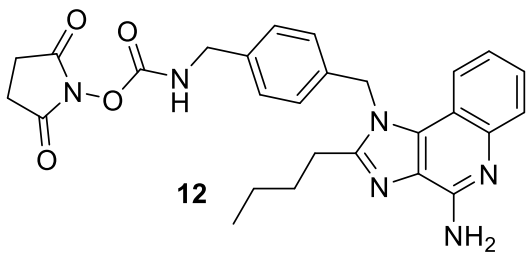

12

Compound **12** was synthesized as follows. To a solution of imidazoquinoline[3] (60 mg, 0.167mmol) and triethylamine (0.023, 0.167 mmol) was added N, N′-Disuccinimidyl carbonate (60 mg, 0.235 mmol) was added. The reaction mixture was stirred at room temperature for 6 h. The reaction mixture was loaded on a silica column and purified by using column chromatography using DCM/MeOH 9:1 to yield a low melting clear solid (40 mg, 60 % yield) ^{1}H NMR (500 MHz, DMSO) δ 8.85 (t, J = 6.0 Hz, 1H), 7.96 (d, J = 8.3 Hz, 1H), 7.79 (d, J = 8.3 Hz, 1H), 7.69 – 7.55 (m, 1H), 7.36 (dd, J = 21.9, 14.0 Hz, 1H), 7.22 (dd, J = 16.2, 8.0 Hz, 2H), 7.05 (dd, J = 22.6, 7.6 Hz, 2H), 5.95 (s, 2H), 4.23 (d, J = 3.6 Hz, 2H), 2.96 (t, J = 7.7 Hz, 2H), 2.75 (s, 4H), 1.73 (m, J = 15.2, 7.7 Hz, 2H), 1.38 (m, J = 14.6, 7.4 Hz, 2H), 0.87 (dd, J = 7.8, 6.9 Hz, 3H).(not observed NH_2)^{13}C NMR (125 MHz, DMSO) δ 171.3, 157.5, 152.6, 148.7, 146.0, 138.3, 135.9, 134.9, 129.9, 128.2, 126.2, 125.2, 125.1, 122.5, 118.9, 112.8, 48.7, 44.4, 29.6, 26.6, 25.7, 22.2, 14.1.HRMS (ESI) m/z calcd for $(C_{27}H_{28}N_6O_4)+H^+$: 501.2250 $[M + H]^+$ found: 501.2261

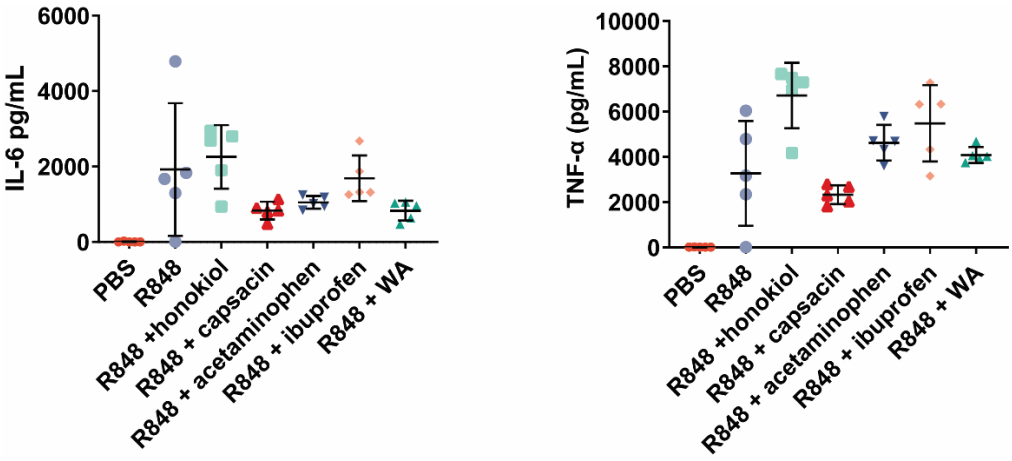

Figure S3.1. In vivo assays with R848 and NF-κB inhibitor. Serum levels of cytokines assayed 1h after injection. IL-6 and TNF- α levels are not significantly reduced when compared with R848.

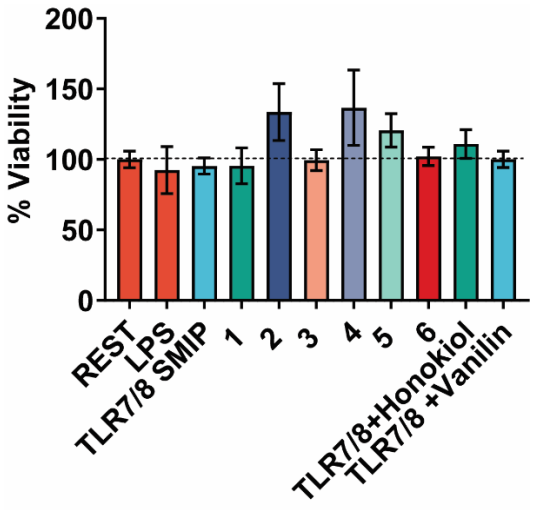

Figure S3.2. MTT assay showing the viability of agonist and agonist dimer treated cells. At the assayed concentrations the cells have comparable viability to resting cells.

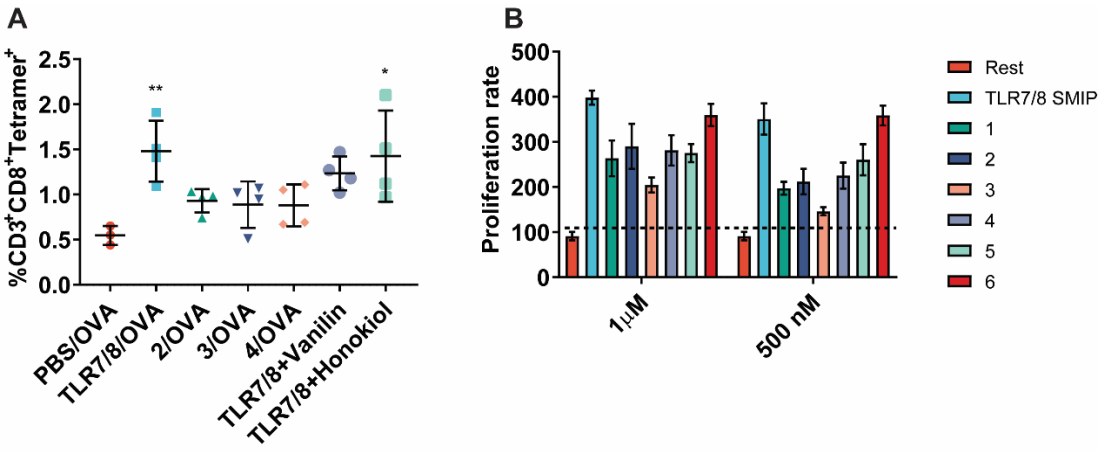

Figure S3.3. A) SINFEKL MHC-specific tetramer on day 28 post-vaccination isolated spleens. B) Proliferation assay on naïve spleenocytes

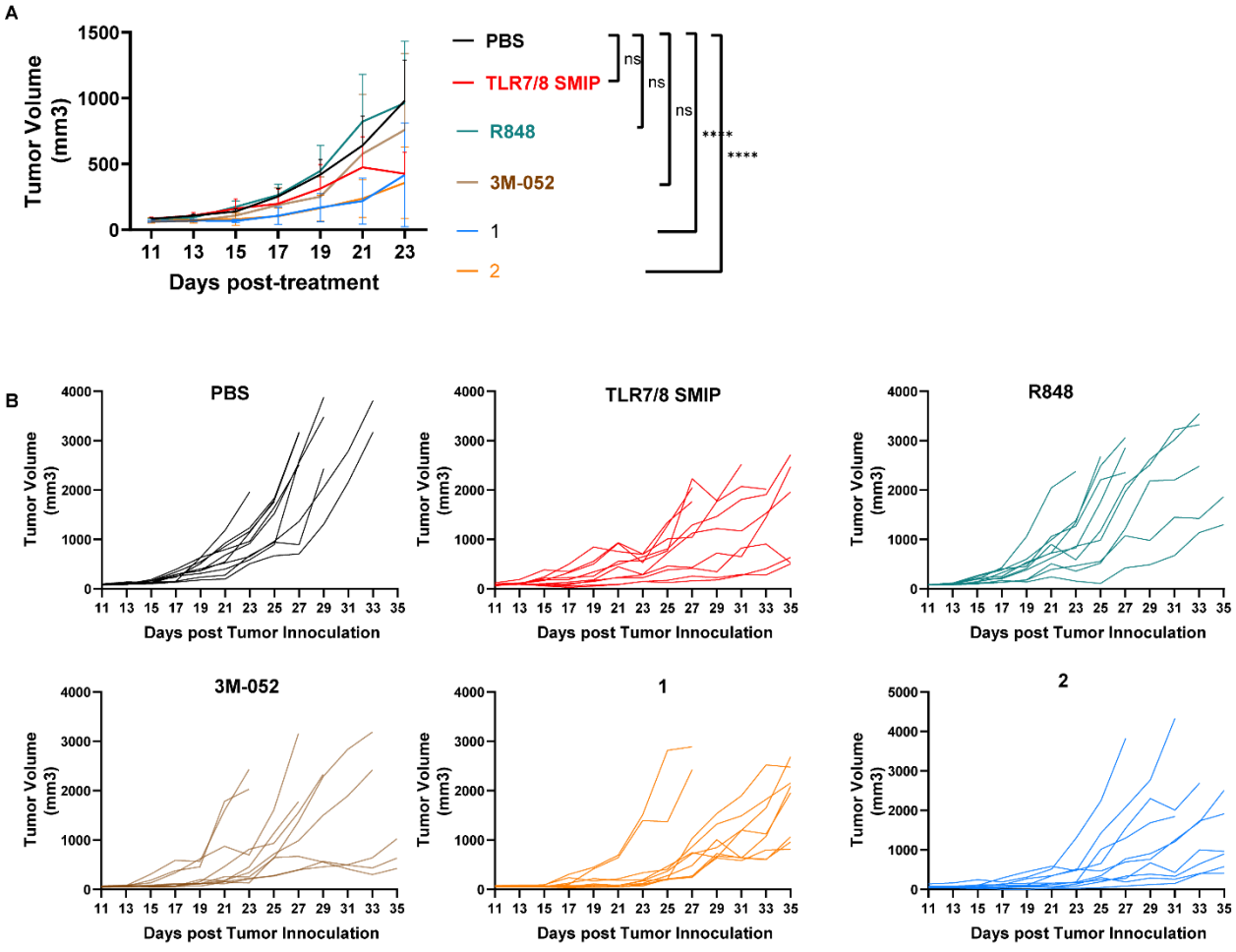

Figure S3.4. *In vivo* tumor model experiment using SMIP-modulator dimers with peritumoral injection into subcutaneous CT-26 tumor model. Agonists were injected when tumors were about 75 cc in size followed by three additional injections every four days.

REFERENCES

1. Tom, J. K.; Dotsey, E. Y.; Wong, H. Y.; Stutts, L.; Moore, T.; Davies, D. H.; Felgner, P. L.; Esser-Kahn, A. P. Modulation of Innate Immune Responses via Covalently Linked TLR Agonists. *ACS Cent. Sci*. **2015**, *1* (8), 439–448

2. Ma, F.; Zhang, J.; Zhang, J.; Zhang, C. The TLR7 Agonists Imiquimod and Gardiquimod Improve DC-Based Immunotherapy for Melanoma in Mice. *Cell. Mol. Immunol.* **2010**, *7*, 381–388

3. Shukla, N. M.; Malladi, S. S.; Mutz, C. A.; Balakrishna, R.; David, S. A. Structure-Activity Relationships in Human Toll-like Receptor 7-Active Imidazoquinoline Analogues. *J. Med. Chem.* **2010**, *53* (11), 4450–4465

Appendix C: Supplementary Data for Chapter 4

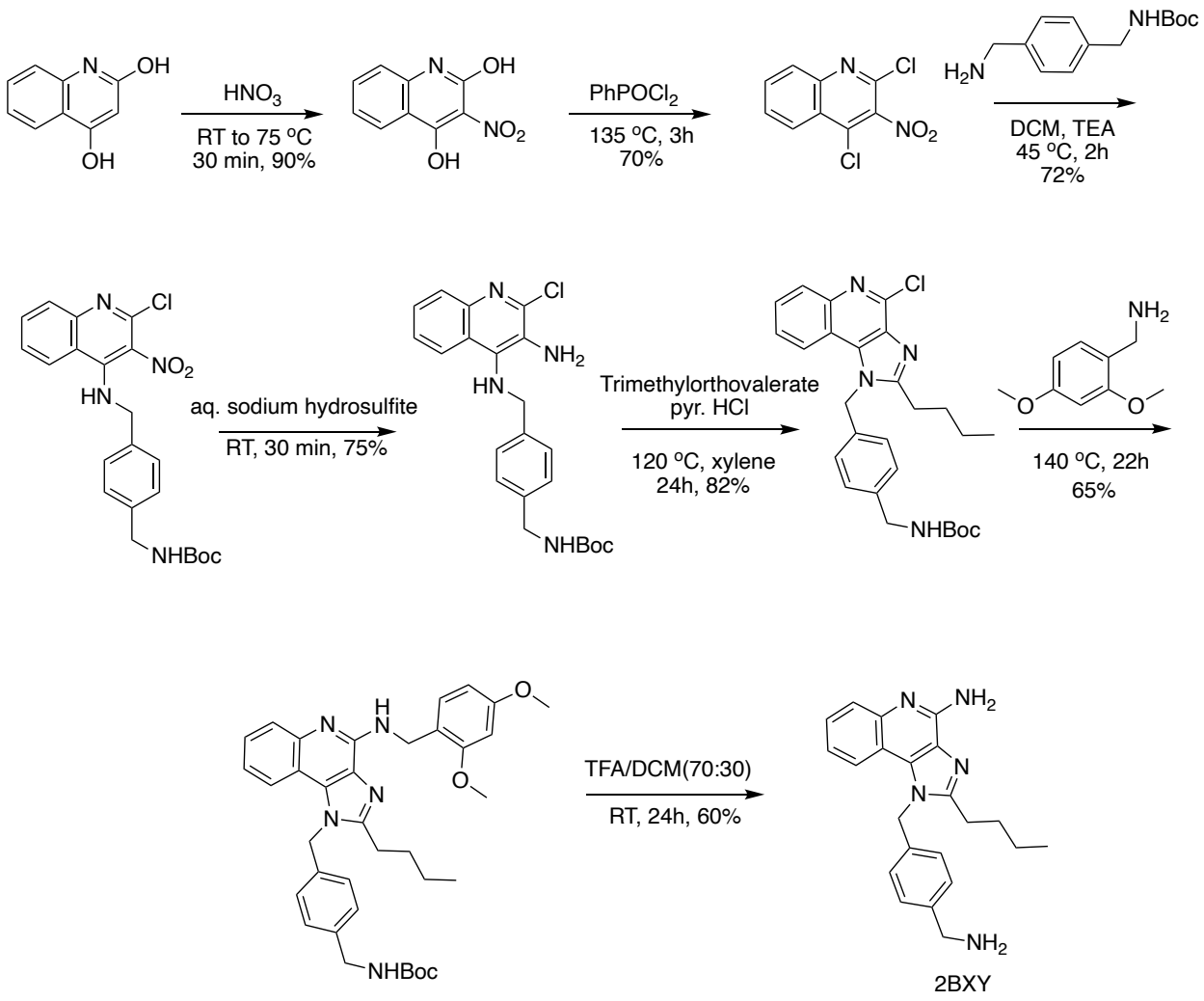

Scheme S4.1: Synthesis of 2BXY.

2BXY was synthesized according to literature procedures reported by Shukla, *et al.*[1]

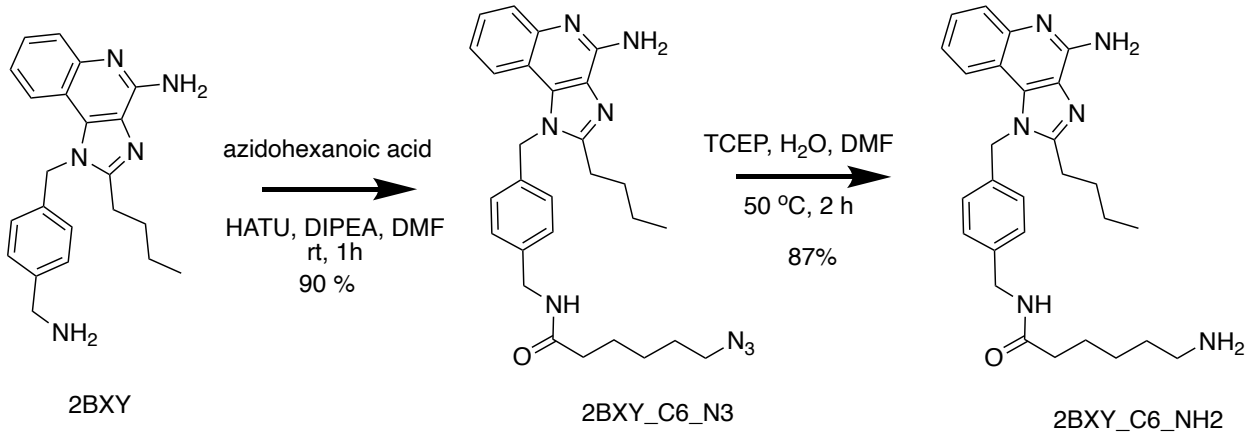

Scheme S4.2: Synthesis of 2BXY_C6_NH2

2BXY (75 mg, 0.21 mmol) and azidohexanoic acid (32 mg, 0.21 mmol) were dissolved in DMF (5mL). DIPEA (66 µL, 0.38 mmol) and subsequently HATU (80 mg, 0.21 mmol) were added. The reaction was allowed to stir at RT for 1 h. The crude solution was purified by reverse phase HPLC using a C8 preparatory column, where the solvent system was A: water + 0.1% TFA, B: acetonitrile + 0.1% TFA (10-90% acetonitrile/water + 0.1% TFA gradient, 0-19 minutes). The HPLC fractions were lyophilized to afford the desired product as an of white solid (90% yield). 2BXY_C6_N3(50 mg, 0.1 mmol) was dissolved in DMF (5mL). TCEP (250 mg, 1 mmol) was dissolved in water(5mL). TCEP solution was added, and the reaction was allowed to stir at 50 °C for 2h. The crude solution was purified by reverse phase HPLC, and the fractions were lyophilized to give the desired product (87% yield). ESI-MS: m/z calc'd for $C_{29}H_{38}N_6O$ $[M+H]^+$ 473.6, observed 473.2.

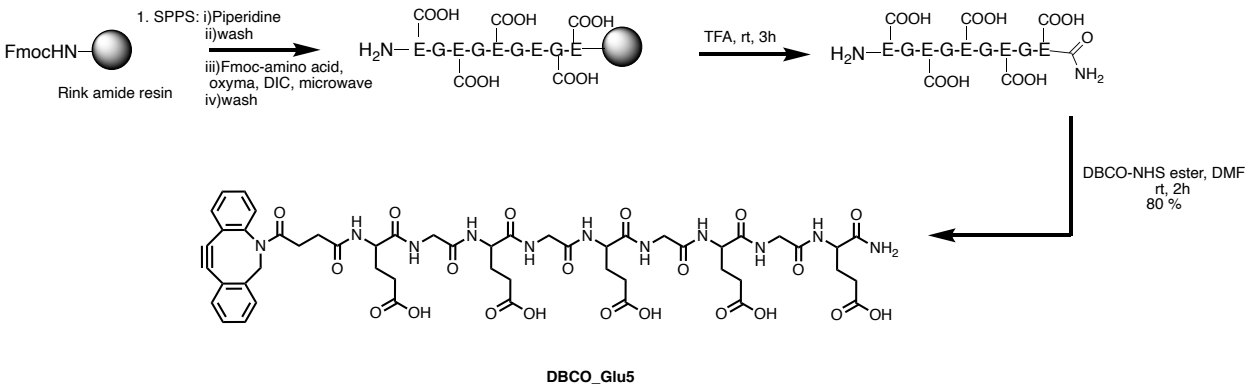

Scheme S4.3: Synthesis of DBCO_Glu5

Peptide was synthesized on an automated microwave peptide synthesizer by Fmoc solid phase peptide synthesis. A low-loading Rink Amide resin (Sigma Aldrich, 0.34 meqg^{-1}) was used for all peptide synthesis. Peptide couplings were performed using DIC, Oxyma at 90 ^{o}C for 3 minutes per cyle. The Fmoc group was deprotected with 20 % piperidine in DMF (v/v) at 75 ^{o}C for 5 minutes. Peptides were cleaved in 95% trifluoroacetic acid, 2.5% H2O and 2.5% triisopropylsilane, for 3 h at 25 °C. After precipitation in ice-cold diethyl ether, peptides were dried. The N terminus was modified with DBCO handle using NHS ester chemistry. The peptide was purified by HPLC on a C8 or C18 column using a gradient of 0.1% TFA in acetonitrile. Peptide masses were confirmed by matrix-assisted laser desorption/ionization–time of flight mass spectrometry (MALDI-TOF). Fractions were pooled and lyophilized.

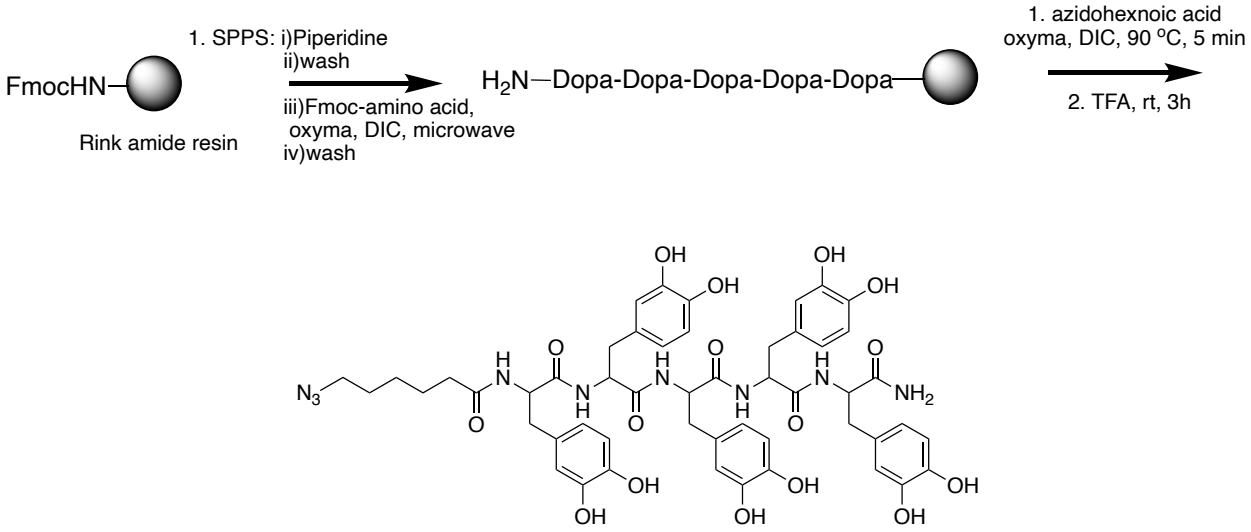

Scheme S4.4: Synthesis of dopa5_az

Peptide was synthesized on an automated microwave peptide synthesizer by Fmoc solid phase peptide synthesis. A low-loading Rink Amide resin (Sigma Aldrich, 0.34 meqg^{-1}) was used for all peptide synthesis. Peptide couplings were performed using DIC, Oxyma at 90 °C for 3 minutes per cyle. The Fmoc group was deprotected with 20 % piperidine in DMF (v/v) at 75 °C for 5 minutes. Peptides were cleaved in 95% trifluoroacetic acid, 2.5% H2O and 2.5% triisopropylsilane, for 3 h at 25 °C. After precipitation in ice-cold diethyl ether, peptides were dried. The peptide was purified by HPLC on a C8 or C18 column using a gradient of 0.1% TFA in acetonitrile. Peptide masses were confirmed by matrix-assisted laser desorption/ionization–time of flight mass spectrometry (MALDI-TOF). Fractions were pooled and lyophilized.

REFERENCES

1. Shukla, N. M.; Malladi, S. S.; Mutz, C. A.; Balakrishna, R.; David, S. A. Structure−Activity Relationships in Human Toll-Like Receptor 7-Active Imidazoquinoline Analogues. *J. Med. Chem.* **2010**, *53* (11), 4450–4465.